Tampere University

Juuso Puutio

ELECTROMECHANICAL CHARACTERIZATION FOR WEARABLE ELECTRONICS

Master's thesis
Faculty of Information Technology and Communication Sciences
Examiners: Professor Matti Mäntysalo
PhD Karem Lozano Montero
January 2025

ABSTRACT

Juuso Puutio: ELECTROMECHANICAL CHARACTERIZATION FOR WEARABLE ELECTRONICS
Master's thesis
Tampere University
Master's Programme in Electrical Engineering
January 2025

The modernization of electronics production demands intensive research to create environmentally friendly and sustainable electronics. In addition to reducing the environmental burden, electronics manufactured using printing technologies pave the way for flexible electronics. Unlike traditional electronics, which rely on rigid fiberglass substrates that cannot adapt to mechanical stress, flexible electronics use substrates and inks that are bendable and stretchable, allowing them to conform to new shapes. This flexibility opens up a range of applications that were previously impossible with rigid bodies.

This work investigates the electromechanical behavior of screen-printed tracks made from silver and carbon inks on various substrates, including PET, PLA, and paper substrates. Bending tests were conducted under various conditions to assess the electromechanical durability of each material combination.

Two different bending setups were utilized. The primary device featured two plates: a stationary bottom plate and a top plate that moved horizontally, bending the sample positioned between them. Resistance was continuously measured across each of the seven tracks on the sample, providing valuable information about the increase in resistance as a function of the bending cycles. To complement these findings, the secondary setup was employed to subject samples to varying bending radii. Furthermore, tests were conducted under both compressive and tensile stresses to assess durability more comprehensively.

A threshold of 1.7 times the initial resistance was used to define failure, and with at least eight replicates, the most durable material combinations were identified. The results showed that within all tested combinations, the print was consistently more durable under tensile stress compared to compressive stress. The effect of bending radius was as expected: larger radii resulted in less stress and longer lifespans. Notably, none of the combinations printed with carbon inks exhibited any signs of degradation, even under the most extreme bending condition, where the radius was reduced from 9 mm to 3 mm. Thus, the carbon-based samples were ranked as the most durable under bending. Additionally, substrates such as smooth, thin paper and cellulose-based alternatives to plastic films demonstrated high durability, withstanding thousands of cycles, whereas thicker, rougher substrates failed within tens or hundreds of cycles.

Several factors influencing the bending reliability of screen-printed tracks were analyzed. The findings revealed how specific substrate-ink combinations behaved under mechanical stress, providing valuable insights into their potential usage in sustainable electronics.

Keywords: Sustainable electronics, Printed electronics, Flexible electronics, Electromechanical Durability

TIIVISTELMÄ

Juuso Puutio: PUETTAVAN ELEKTRONIIKAN ELEKTROMEKAANINEN KARAKTERISOINTI
Diplomityö
Tampereen yliopisto
Sähkötekniikan DI-ohjelma
Tammikuu 2025

Elektroniikan valmistuksen modernisoiminen ympäristön kannalta kestäväksi vaatii merkittäviä panostuksia tutkimukseen. Alhaisemman ympäristökuormituksen lisäksi painettavan elektroniikan teknologiat edistävät joustavan elektroniikan kehitystä. Perinteinen elektroniikka perustuu jäykkään lasikuituun, joka ei pysty mukautumaan mekaanisen rasituksen seurauksena. Joustava elektroniikka sen sijaan hyödyntää substraatteja ja musteita, jotka kykenevät taipumaan ja venymään, mahdollistaen uuden ulottuvuuden elektroniikan sovelluksia, jotka eivät aiemmin olleet mahdollisia jäykillä materiaaleilla.

Tässä työssä tutkitaan silkkipainomenetelmällä valmistettujen johtimien elektromekaanista käyttäytymistä. Näytteitä valmistettiin useilla eri materiaaliyhdistelmillä, kuten esimerkiksi PET-, PLA- ja paperisubstraateilla sekä hopea- ja hiilimusteilla. Kunkin materiaaliyhdistelmän elektromekaanista kestävyyttä arvioitiin suorittamalla erilaisia taivutustestejä.

Testeissä hyödynnettiin kahta erilaista taivutuslaitteistoa. Ensimmäinen laite koostui kahdesta horisontaalisesta levystä, joista alempi pysyi paikallaan ja ylempää liikuteltiin edestakaisin niin, että levyjen väliin asetettu näyte pääsi taipumaan. Testin aikana näytteen resistanssia mitattiin keskeytyksettä kustakin näytteen seitsemästä johdinrakenteesta saaden arvokasta tietoa resistanssin kasvusta suhteessa taivutussykleihin. Tämän lisäksi käytettiin toista taivutuslaitetta, jolla näytteitä pystyttiin testaamaan pienemmällä säteellä. Testeissä näytteitä altistettiin joko puristavaan tai venyttävään voimaan tuottaen kattavaa dataa niiden elektromekaanisesta kestävyydestä.

Näytteiden vikaantumiskriteeriksi valittiin resistanssin kasvaminen 1,7-kertaiseksi alkuperäiseen arvoon verrattuna. Kustakin materiaaliyhdistelmästä testattiin vähintään kahdeksan näytettä kestävimmän yhdistelmän määrittämiseksi. Saadut tulokset osoittivat, että kaikilla testatuilla yhdistelmillä näyte kesti paremmin kun se altistettiin venyttävälle voimalle puristavan voiman sijaan. Taivutussäteen kasvatus odotetusti vähensi rasitusta pidentäen näytteiden kestävyyttä. Yllätykseksi mikään hiilimusteita sisältävä yhdistelmä ei alkanut hajoamaan, edes äärimmäisessä testissä, jossa säteenä käytettiin 3 mm aiemman 9 mm sijaan. Näin ollen hiilipohjaiset näytteet määritettiin kaikista kestävimmiksi kyseisissä taivutustesteissä. Näiden lisäksi substraatit kuten sileä ja ohut paperi sekä selluloosapohjainen vaihtoehto muovikalvolle osoittivat merkittävää elektromekaanista kestävyyttä, selviten tuhansia taivutussyklejä. Sen sijaan paksut ja karkeapintaiset substraatit hajosivat jo kymmenien tai satojen syklien jälkeen.

Työssä analysoitiin useita tekijoita, jotka vaikuttavat taivuksessa olevian silkkipainettujen johtimien luotettavuuteen. Tulokset osoittivat, miten tietyt substraatti-musteyhdistelmät käyttäytyvät mekaanisessa rasituksessa. Tätä arvokasta tietoa voidaan hyödyntää mahdollisissa kestävän elektroniikan sovelluksissa.

Avainsanat: Kestävästi tuotettu elektroniikka, Painettava eletroniikka, Joustava elektroniikka, Elektromekaaninen kestävyys

USE OF AI IN THESIS

I have utilised AI tools in my thesis:

☐ No
☒ Yes

The AI tools utilised in my thesis and their purposes are described below.

Names and versions of AI tools: OpenAI's GPT-4 with a knowledge cutoff in September 2023.

Purpose of using AI tools: AI tools have been used to enhance the quality of my thesis by checking for grammar, vocabulary, and overall language refinement.

Sections where AI tools were used: AI tools have been applied throughout the entire thesis to check and refine the language.

I acknowledge that I am fully responsible for the entire content of my thesis, including the parts generated by AI, and accept accountability for any violations of ethical standards in publications.

PREFACE

This Master's thesis was conducted as part of the Sustronics project, co-funded by the European Union under Grant Agreement 101112109. The project consortium consists of 46 partners–comprising research organizations, universities, SMEs, and large enterprises–across 11 countries. Sustronics' primary goal is to revolutionize the European electronics industry by integrating sustainable materials, sustainable manufacturing, eco-design, and circular business models. The project aims to meet with the Green Deal objectives across the sector, while enhancing electronics industry's competitiveness. This thesis was carried out at Tampere University's Laboratory for Future Electronics under the guidance of Professor Matti Mäntysalo and Dr. Karem Lozano.

I want to thank my supervisors, Matti and Karem, for providing me with this incredible opportunity and the freedom to explore and apply my knowledge. I am deeply grateful to the entire team at the Laboratory for Future Electronics for creating such an amazing environment to work and solve problems with. Special thanks go to MSc Timo Punkari for his engaging coffee and lunch breaks filled with discussions on current hot topics and debates, providing me with much-needed break from science and engineering.

I also want to thank my friends for sharing their own academic experiences and struggles, broadening my perspective and lightening the academic burden. Just as importantly I want to show my gratitude to my parents and family for supporting and encouraging me throughout all my studies.

Tampere, 2nd January 2025

Juuso Puutio

CONTENTS

LIST OF FIGURES

LIST OF TABLES

LIST OF SYMBOLS AND ABBREVIATIONS

α	scale parameter
A	area
β	shape parameter
χ	elastic modulus ratio
d_{dry}	dry thickness
d_{wet}	wet thickness
E	Young's modulus
E_p	print's elastic modulus
E_s	substrate's elastic modulus
ϵ	strain
η	thickness ratio
F	force
L	length
ΔL	change in length
L_0	original length
ν	Poisson's ratio
R_a	average surface roughness
R	resistance
R_{sh}	sheet resistance
ρ	density
ϱ_{bulk}	bulk resistivity
$\rho_{solid-\%}$	solid material concentration
σ	stress
t	thickness
V_{AI}	analog-input voltage
V_{sup}	supply voltage
w	width

0D	zero-dimensional
1D	one-dimensional
2D	two-dimensional
ADC	analog-to-digital converter
AgNP	silver nanoparticle
AgNW	silver nanowire
CAGR	compound annual growth rate
CC	creative commons
CDF	cumulative distribution function
CI	confidence interval
CIJ	continuous inkjet
CuNP	copper nanoparticle
DOD	drop on demand
ECG	electrocardiogram
FET	field-effect transistor
HCF	high-cycle fatigue
INL	integral non-linearity
IPA	isopropyl alcohol
IQR	interquartile range
LCF	low-cycle fatigue
LCP	liquid-crystal polymer
LSB	least-significant bit
MSA	measurement system analysis
NI	National Instruments
OLED	organic light-emitting diode
OPV	organic photovoltaic
PCB	printed circuit board

PDF	probability density function
PDMS	polydimethyl-siloxane
PE	printed electronics
PEN	polyethylene naphthalate
PET	plyethylene terephthalate
PI	polyimide
PLA	polylactic acid
R2R	roll-to-roll
SC	supercapacitor
SPM	sustainable packing material
TPU	thermoplastic polyurethane
VCO	volatile organic compound
ZIF	zero insertion force

1. INTRODUCTION

Electronics as a field covers a vast range of topics such as power electronics, radio frequency electronics, optoelectronics and so on. Electronic device composed of an electronic board and components is typically perceived as rigid and hard structure. This traditional circuitry has enormous amount of different applications and is used virtually everywhere in modern society. However, this hard-lined and stiff architecture has its drawbacks and limitations in specific applications, such as wearable devices, where flexibility and conformability are essential features. This brings up another field along traditional electronics called flexible electronics, which has drawn significant interest in recent years. [1]

For instance, different flexible displays and wearable electronic devices have emerged in the past years, and this trend of development is likely to continue. This is further accelerated by modern manufacturing technologies where electronics can be mass-produced with lower cost. In particular, printed electronics (PE) are being developed alongside flexible electronics. PE is based on additive manufacturing, which differs significantly from the subtractive nature of conventional manufacturing. Advantages such as cost-effectiveness and material versatility drive the research of PE forward, let alone it being more environmentally friendly, due to reduced material and energy consumption. This helps tackling yet another problem: electronic waste, also known as e-waste. [2]

E-waste is one of many challenges that the modern society encounters. The reduction of e-waste and modernization of the current electronic production are the key motivations behind this thesis, which aim is to analyse electromechanical behavior of screen printed flexible wiring boards made from different material combinations.

Nassajfar et al. [3] investigated the environmental impacts of four-layer printed circuit board (PCB) and compared conventional PCB production with an additive approach using printed silver. They found that the environmental burden of manufacturing could be reduced by 86 % using printing methods. Välimäki et al. [4] studied roll-to-roll (R2R) printed organic photovoltaics (OPVs). They demonstrated the feasibility of producing printed OPV modules using R2R gravure and screen printing processes. While their study primarily focused on the technical aspects of these methods, the use of printing aligns with sustainable manufacturing principles by enabling efficient, large-scale production with potentially

lower energy consumption and material waste.

This master's thesis research was conducted as part of the Sustronics project, which is co-funded by the European Union. The primary goal of Sustronics is to develop the European electronics industry towards a more sustainable future. This is achieved by implementing sustainable materials, sustainable manufacturing, Eco-design, energy efficient products, and circular business models. [5] Within this framework, this thesis addresses the need for affordable and environmentally friendly wiring and medical electrodes for electrocardiogram (ECG) monitoring. The goal is to identify and test other materials, replacing the currently used ones with more sustainable alternatives (for instance, replacing silver with copper or carbon, and PET with paper).

As the aim of this thesis is to study the electromechanical behavior of alternative materials by examining the bending durability of screen-printed tracks, durability is assessed by measuring the tracks' resistances in relation to the number of bending cycles. This thesis seeks to identify the most durable material combination among the selected options while also investigating the effects of bending radius and the differences between compressive and tensile stress during bending. To achieve the set goals, the following research questions are addressed:

1. How do sustainable material combinations perform under bending-induced stress?
2. What factors affect electromechanical durability?
3. How do stress type and bending radius influence the observed degradation?

To investigate these research questions and fulfill the objectives of this thesis, the following chapters are structured to provide a comprehensive overview of the relevant concepts, methods, and findings. Chapter 2 introduces a theory of flexible electronics along strategies to achieve stretchable electronic structures. Chapter 3 presents printed electronics technologies with its advantages and challenges. Chapter 4 introduces the materials and methods used within this thesis. Chapter 5 describes the manufacturing of the samples as well as their characterization. Chapter 6 presents and discusses the obtained results and observations. Finally, chapter 7 concludes the results and discusses how well different objectives set for this thesis have been achieved and what could be researched in the future.

2. FLEXIBLE AND STRETCHABLE ELECTRONICS

Traditionally, electronic circuits are viewed as rigid structures, consisting of a PCB made from fiberglass, which makes the circuit unable to reform under a mechanical stress. [6] However, in a non-conventional approach, electronic circuits are seen as bendable and stretchable and therefore capable of adapting to new shapes under a mechanical strain. In this chapter a theory regarding stretching and bending of an electronic conductor is presented, along with some basic strategies to achieve these types of conductors, and how to evaluate their reliability and to detect their failure mechanisms.

2.1 Mechanical properties

When talking about materials under applied strain, one useful property regarding material's stiffness is called Young's modulus *E*, also known as elastic modulus. It describes the linear relationship between stress and strain within material's elastic region, as expressed by one-dimensional Hooke's law

$$\sigma = E\varepsilon, \tag{2.1}$$

where ε and σ are stress and strain respectively. [7] Stress is either tensile or compressive stress depending on whether the object is being stretched or compressed. It can be calculated as force *F* per unit area *A* [7]

$$\sigma = \frac{F}{A}. \tag{2.2}$$

Strain's definition consists of a change in length ΔL and the original length L_0 and is given by [7]

$$\varepsilon = \frac{\Delta L}{L_0}, \tag{2.3}$$

If the object is compressed, the change in length is negative and thus the strain becomes negative. Here defined strain is one-dimensional normal strain. Both stress and strain can be expanded into general three-dimensional form, but to avoid extra complexity, in

the scope of this thesis only uniaxial stress and strain are considered.

Under minor stress and deformation, many materials exhibit linear stress-strain behavior validating Hooke's law. While in elastic region, the object returns to its original length when the stress is removed. When stress and strain increase over material's elastic limit, the material will have some permanent plastic deformations. This happens in so called plastic region of the strain-stress curve, where the linear behavior does not apply anymore. [7]

A typical stress-strain behavior can be seen in figure 2.1. Stress-strain curve is a simple way to visualize material's mechanical behavior. The slope of the curve in elastic region is equal to Young's modulus.

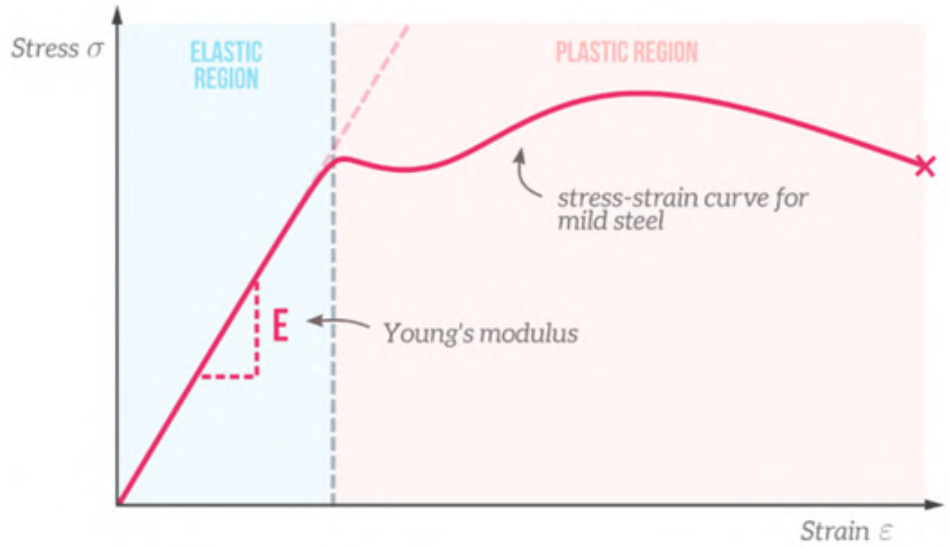

Figure 2.1. *Stress-strain curve for mild steel. Material goes through plastic deformation until it fractures under maximum strain [8].*

Typical Young's modulus values are for example steel at 207 GPa, aluminum at 68.9 GPa and rubber at 0.0019 GPa. [7] Based on these values, it becomes evident that steel would require 100,000 times more stress than rubber for the same amount of stretch. Conversely, under equivalent stress, rubber would stretch 100,000 times more than steel, provided we remain within material's elastic limits.

Another useful material property is called Poisson's ratio ν, which describes how a material deforms in the lateral direction when stress is applies in the longitudinal direction. It is calculated by the following equation [9]

$$\nu = -\frac{\varepsilon_{lateral}}{\varepsilon_{longitudinal}}. \tag{2.4}$$

Nearly all materials have a positive Poisson's ratio, and to be more precise, its value falls between 0.25 and 0.35 for most of commonly used solid materials such as metals and

polymers. In some rare cases, Poisson's ratio can have a negative value which results into counter intuitive mechanical behavior, where material stretches simultaneously in both lateral and longitudinal direction. [9] Figure 2.2 illustrates material's behavior when a longitudinal strain is applied.

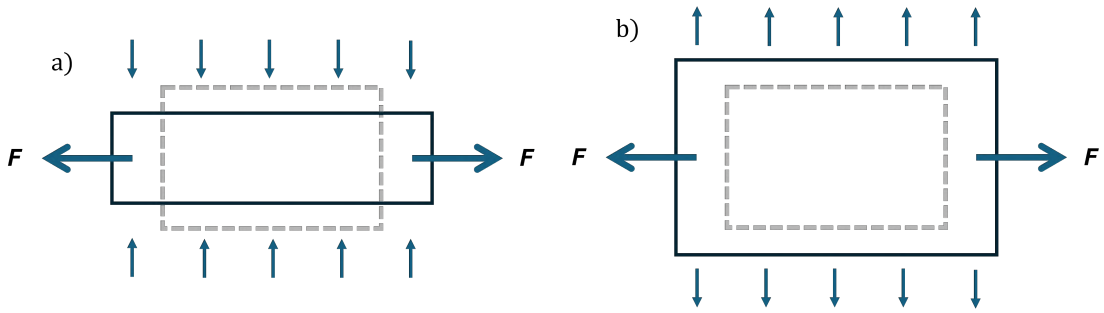

Figure 2.2. *Material under a longitudinal strain when Poisson's ration is a) positive b) negative. Adapted from [10].*

Another important aspect is the material's bending theory, which relates to the stretching of the material, as bending causes one section to stretch while another section compresses. The bending theory can be approached using a simple analytical method, where a beam is defined as a structural element. Its other dimensions are negligible compared to its length, and the loads produce deflections perpendicular to the beam's longitudinal axis. According to the Euler-Bernoulli beam theory, the beam has a neutral axis, which experiences no longitudinal stresses or strains when the beam is bent. Based on this assumption, an infinitesimal length dl of a beam element on the neutral axis can be assumed to deform into an arc while maintaining its original length. [11][12][13] This is illustrated in Figure 2.3.

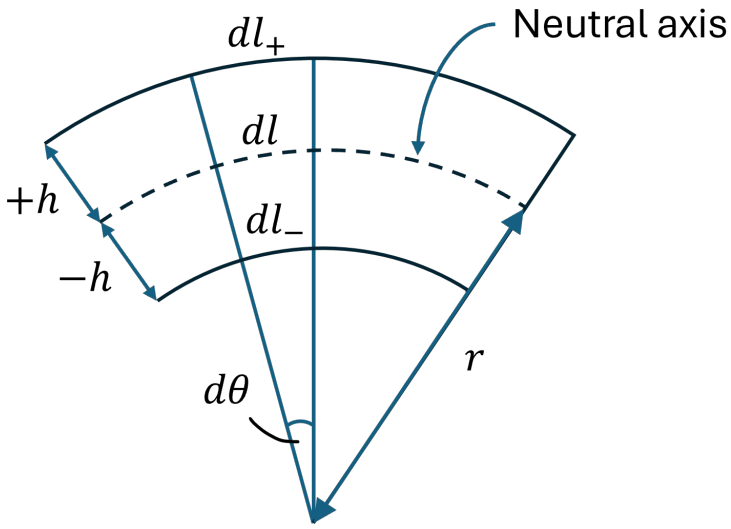

Figure 2.3. *A beam under bending. Neutral axis does not experience stress. Adapted from [11].*

The bending radius is denoted as *r* and thus $dl = rd\theta$, where θ is the arcs infinitesimal angle. When moving further from the neutral axis, at the distance $\pm h$ the arcs' have infinitesimal lengths $dl_{\pm} = (r \pm h)d\theta$. Now, the strain of the beam element at a distance $\pm h$ from the neutral axis is calculated as

$$\varepsilon = \frac{dl_{\pm} - dl}{dl} = \frac{(r \pm h)d\theta - rd\theta}{rd\theta} = \pm\frac{h}{r}, \tag{2.5}$$

where positive ε corresponds to tensile strain, and negative ε for compressive strain. Equation 2.5 can be straightforwardly applied in the context of printed electronics since the substrate material's thickness is usually significantly larger than the printed conductor's layer thickness. Hence, the bending behavior is assumed to be primarily influenced by the substrate properties. By ignoring the print thickness, the equation simplifies to

$$\varepsilon = \pm\frac{h}{r} = \pm\frac{\frac{d_s}{2} + t}{r} \approx \pm\frac{d_s}{2r}, \tag{2.6}$$

where d_s and *t* are the substrate thickness and print thickness respectively. [11] This simplified analysis doesn't take into account e.g. material properties. In order to accurately calculate the strain under bending, a more complex approach should be used. Suo et al. have presented a formula where the elasticity of material used is considered [14]

$$\varepsilon = \pm\left(\frac{d_s + t}{2r}\right)\frac{(1 + 2\eta + \chi\eta^2)}{(1 + \eta)(1 + \chi\eta)}, \tag{2.7}$$

where η = t/d_s and χ = E_p/E_s, in which E_p and E_s correspond to the elastic modulus of the print and substrate respectively. When the materials exhibit similar elasticity (χ = 1), Equation 2.7 simplifies to Equation 2.6. However, When the materials differ in their elastic moduli, for example in a case of flexible substrate (E_p>E_s), the neutral axis shifts towards the printed layer, reducing strain on the top surface. The strain in a circuit can be further minimized by sandwiching the circuit between the substrate and an encapsulation layer, that has a suitable thickness and elastic modulus. [14]

As explained with Equation 2.5, the type of stress and strain is different, depending on whether the printed conductor is located on the inner or outer side of the bent substrate. On the inside, the conductor experiences compressive forces, which drive the material together. On the contrary, the conductor is subjected to tensile forces when placed on the outside curve; hence, the material is stretched or elongated. In both cases, a smaller bending radius, while having sharper curvature, leads to increased localized stress and possibly premature failure. The comparison of compressive and tensile strain, as well as the effect of the radius, will be presented later when different substrates and inks are subjected to bending.

2.2 Electrical properties

Resistance *R* can be calculated from bulk resistivity ϱ_{bulk} by

$$R = \varrho_{bulk}\frac{L}{wt}, \tag{2.8}$$

where *L*, *w* and *t* are object's length, width and thickness respectively [15]. Thus, the bulk resistivity is independent of the object's geometry. When talking of thin conductive layers, a more common approach is to use sheet resistance R_{sh} which can be easily derived from the bulk resistivity as

$$R_{sh} = \frac{\varrho_{bulk}}{t}, \tag{2.9}$$

where the film is either assumed to be uniform, or an average thickness is used. This is a convenient way to get a conductor's resistance from number of squares as the sheet resistance's unit is $\Omega/\square$. Hence, Equation 2.8 can be rewritten as

$$R = R_{sh}\frac{L}{w}, \tag{2.10}$$

where the ratio *L/w* describes how many squares are included within the conductor. [15]

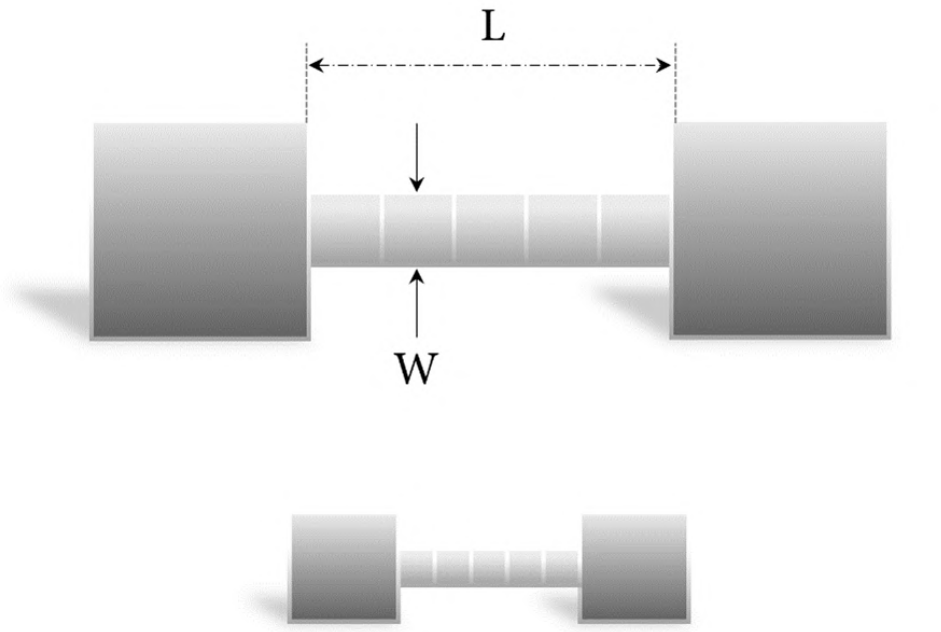

Figure 2.4. *Two conductors having a same resistance but with different length and width.*

Figure 2.4 demonstrate how conductor's resistance can be obtained with sheet resistance. Although, both conductors have the same number of squares and thus the same resistance value, they might differ in other important aspects which are not covered by sheet resistance. For instance, their high-frequency performance and power handling capability are most likely different.

When a conductor is stretched, presumably its resistance changes. This is apparent when looked at the Equation 2.8. Stretching a conductor, increases its length, hence increasing its resistance. Furthermore, as discussed above for positive Poisson's ratio, applying a longitudinal strain shrinks the conductor in lateral direction, thus reducing its thickness and/or width and increasing its resistance. One can reach a similar conclusion with Equation 2.10. When the conductor is stretched, due to the increase of length and the decrease of width, the number of squares increases which has a direct impact on the resistance. More on the change in resistance under deformation is discussed in the next section. Different structures are introduced, along with the loss of percolation, which occurs when the conductive path becomes discontinuous, in this case due to bending or stretching of the material.

2.3 Making stretchable structures

With the goal of developing flexible electronic devices, the substrates used must be mechanically flexible, enabling them to adapt to irregular shapes. Every electronic device or application also necessitates some conductive pathways to make its functions possible. The need for flexible conductors inspires the concept of intrinsic and extrinsic stretchability, which will be introduced in this chapter.

2.3.1 Flexible substrates

Regarding flexible and stretchable electronics, the most commonly used substrates are Polyethylene Terephthalate (PET), Polylactic Acid (PLA), Thermoplastic Polyurethane (TPU), Polyimide (PI), Polydimethyl-Siloxane (PDMS), Polyethylene Naphthalate (PEN) and Liquid-Crystal Polymer (LCP) [16]. Another approach involves using clothes and fabrics as flexible substrates creating e-textiles, where devices seamlessly conform to the irregular and soft surface of the human body, providing an integration between humans and electronics. E-textiles hold the potential to revolutionize various multidisciplinary fields. However, they currently face significant challenges, including stability and washability, ensuring safety and biocompatibility, and achieving sustainability. [17]

PET is a linear semicrystalline polymer obtained by polycondensation reaction of monomers. It has various good properties such as, smooth morphology, high strength and stiffness, lightweight, good gas and moisture barrier and electrical insulation, broad range of use

temperatures and high visible light transmittance [18]. PET has also shown significant mechanical flexibility, stability, and reliability in bending tests. While it is one of the most common substrate materials in printed electronics, it was selected as a reference for this thesis. [19] [20].

TPU is an elastomer which has the characteristics of both plastic and rubber. It has low Young's modulus, excellent elasticity and flexibility, and has typical maximum strains in the order of 200%. These attributes make it a great material for flexible and wearable electronics. [21] [22]

PLA is an aliphatic polyester made from lactic acid building blocks. Its mechanical and barrier behavior are comparable to PET [23]. PLA is a biodegradable and compostable polymer that can be derived from renewable plant sources, such as starch and sugar. Due to this feature, it is considered a potential alternative to petroleum-based substrates, while also helping to alleviate waste disposal problems. [24] [25] Consequently, it was selected as one of the substrates in this thesis.

In addition to the aforementioned polymers, paper-based materials have demonstrated their suitability as substrate materials in flexible electronics. Jansson et al. tested several commercial paper-based substrates using both flexography and screen printing, and compared their performance with plastic foils. They found that certain levels of surface roughness and porosity are advantageous for improved ink transfer and can decrease the printed metal conductor's resistance. [26] Considering the recyclability and sustainability of paper-based substrates, they have a promising future in the field of printable and flexible electronics. Therefore, paper-based substrates were also a key focus of this thesis.

2.3.2 Intrinsic stretchability

Making electronics both stretchable and bendable through intrinsic measures comes down to the material's micro-properties. These micro-properties, including crystallinity, intermolecular forces, molecular structure, morphology of the material, and mechanical properties, play a crucial role in determining how well a material can deform without breaking or losing its functionality. [27] One effective approach to optimizing mechanical durability under strain is through the use of conductive inks containing composite nanomaterials.

Composite nanomaterials, also called nanocomposites, usually consist of a polymer matrix and conductive solid particles. The purpose of the polymer matrix is to bind the particles together and act as a stretchable component. When used in printing, nanocomposites are typically in the form of a solution or ink to deposit them onto the substrate. Generally, these printable inks also include non-functional components, such as solvents

and surfactants, which control the viscosity and surface tension of the ink, among other properties. [28] Printing techniques are covered more profoundly in Chapter 3.

Nanomaterials are categorized into different groups based on their dimensions. Zero-dimensional (0D) material includes a nanoparticle, which is on the nanometer scale in all dimensions. One-dimensional (1D) nanoparticle exceeds the nanometer scale in one dimension, and two-dimensional (2D) material exceeds the nanometer scale in two dimensions. Illustrating these categories, a silver nanoparticle (AgNP), a silver nanowire (AgNW), and a silver flake are examples of each group in respective order. [28]

Nanoparticles, such as AgNPs, have a large contact area between particles due to the sintering process, where the particles are fused together. This results in a good conductivity. Additionally, NPs can be deposited with ease onto the substrate due to their nanometer scale and are, therefore, widely used as a conductive ink in printing technologies. However, they possess low stretchability, as the conductivity of nanoparticle-based conductors decreases rapidly when stretched. This is due to the rapid loss of conductive paths within the ink as the nanoparticles are pulled apart, which occurs because the particles have formed a dense structure during sintering that tends to break under mechanical stress. [28] [29]

Nanowires are less conductive compared to nanoparticles due to the smaller density and contact area of the conductive material. The conductive path is composed of crisscrossing nanowires, as illustrated in Figure 2.5. This kind of structure exhibits high stretchability, where the NWs can slide and rotate with respect to each other. [28]

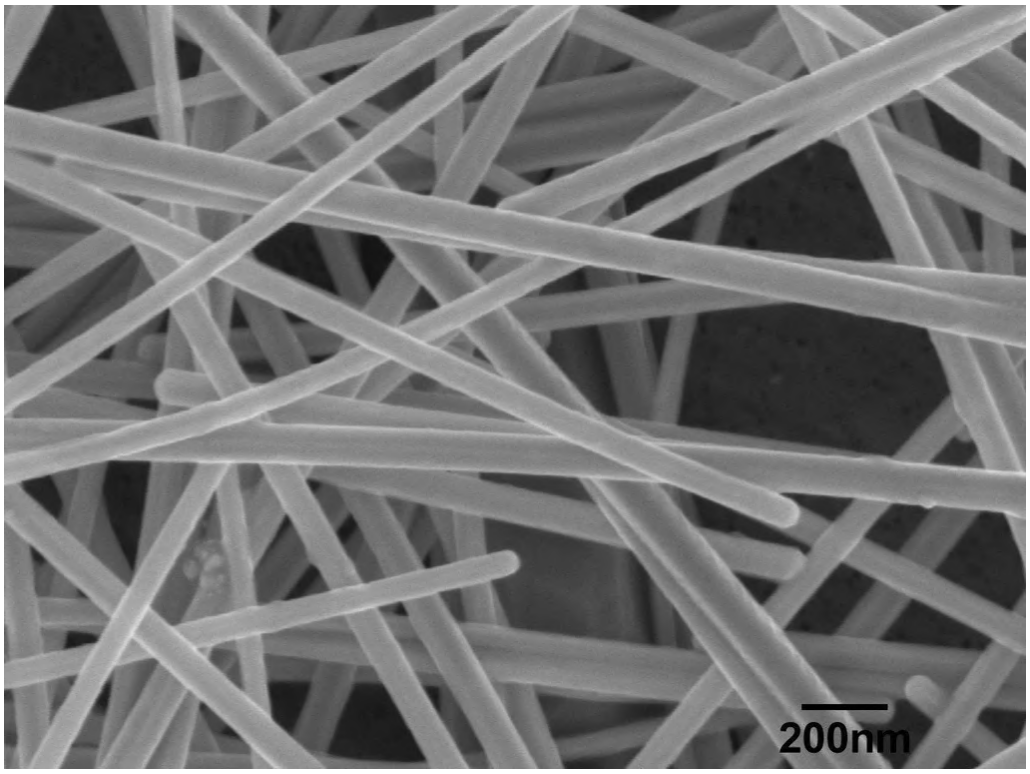

Figure 2.5. *SEM image of silver nanowires (average diameter = 70 nm, average length = 50 μm). Reprinted with permission from Novarials [30].*

2D nanomaterials, like silver flakes, possess good conductivity due to their large surface area as well as the contact area between the flakes. The large surface area allows the flakes to maintain their conductive path when stretched, which is why inks with silver flakes exhibit superior flexibility compared to inks with NPs, but not as good as those with NWs. However, the large surface area can prevent the fabrication of transparent conductors, which might be crucial in some wearable electronics applications. [28]

Although silver is the most commonly used, it is important to note that the nanomaterials presented are not limited to silver. For instance, inks containing copper nanoparticles have also attracted attention, as copper is 1,000 times more abundant than silver, its price is 1% of silver's, and its conductivity is within the same order of magnitude. However, copper-based inks face some challenges due to the copper oxidation and, therefore, a decrease in conductivity. [31] Graphene-based inks have also demonstrated their place in printed flexible electronics. This arises from their potential for low cost and environmentally friendly production. [32]

Additionally, there is a relatively new family of 2D materials known as MXenes, which are a group of metal carbides, nitrides, and carbonitrides, derived from their parent MAX phases by selective etching. MXenes exhibit unique properties such as high electrical conductivity and high mechanical strength. While they have a highly customizable surface chemistry, some MXenes have shown promise for biological applications. Their

hydrophilicity, biocompatibility, and, in some cases, non-toxicity and sustainability make them attractive for applications in bio-sensing and other medical devices. [33]

2.3.3 Extrinsic stretchability

This section regarding extrinsic stretchability covers patterning strategies that may either improve the stretchability of intrinsically stretchable conductors, or make stretching possible for conventional bulk metal conductors that were not originally flexible. Extrinsic stretchability is based on geometric design, and it is important to note how improvements in stretchability allow the device to bend more easily, as both stretching and compression occur along its curved path.

Moving the atoms with respect to each other in the material's crystal lattice is difficult due to the strong interatomic bonds. In order to make the conductive structure stretchable, a different approach is used. By shaping the material into a certain pattern, the system can be stretched even when the material itself is only bent. [28] Bending can be done with relatively small effort when the material is thin enough, as can be observed from the equation

$$S = \frac{Et^3}{12}, \tag{2.11}$$

where S represents the bending stiffness of a monolayer film, E is the elastic modulus, and t is the thickness of the monolayer film. [13] By decreasing the film's thickness, the stiffness decreases drastically, hence making it more bendable.

One widely used strategy to achieve geometrically rendered stretchability is to use wavy or serpentine shapes. When these patterns are stretched, the structure becomes straighter, ideally leaving the conductor free of strain. An out-of-plane wavy structure, or buckled film, can be fabricated by pre-straining the substrate before the deposition of the conductive material. [34] The behavior of the buckled film is illustrated in Figure 2.6.

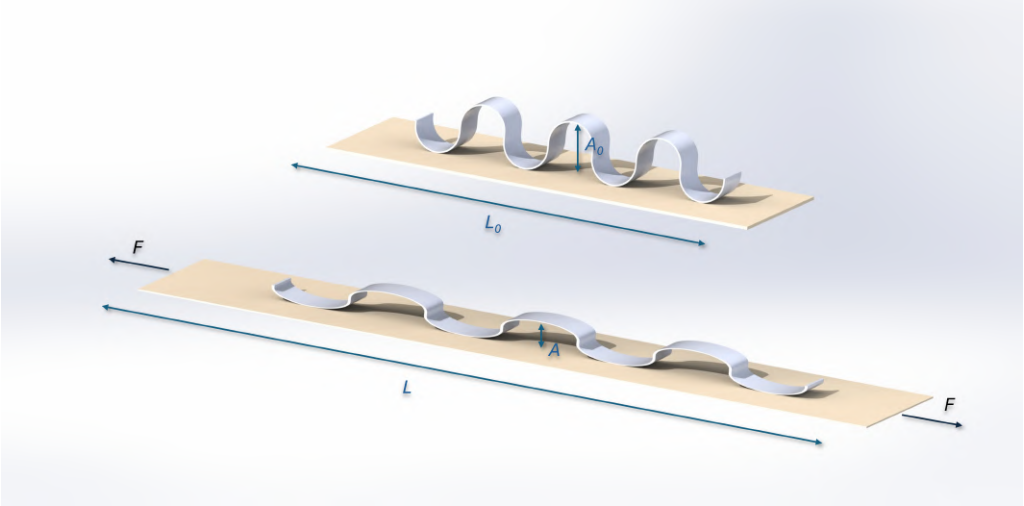

Figure 2.6. *Geometrically rendered stretchability achieved using a buckled film. When the substrate is exposed to longitudinal strain, the buckle straightens out.*

When the substrate is stretched ($L > L_0$), the serpentine pattern deposited on it straightens up. The pattern's amplitude decreases ($A < A_0$), but its total length remains unaffected; therefore, it doesn't stretch. There are several different designs that similarly aim to render systems, that can stretch by utilizing the pattern's geometry. Figure 2.7 portrays various types of methods along with their achievable stretchability and size scale. It is important to note that while a complex structure adds more stretchability to the system, it increases its nominal resistance. Serpentine, or any other non-straight structure, undoubtedly always has lower conductivity than a direct path. This might be an important trade-off from application to application.

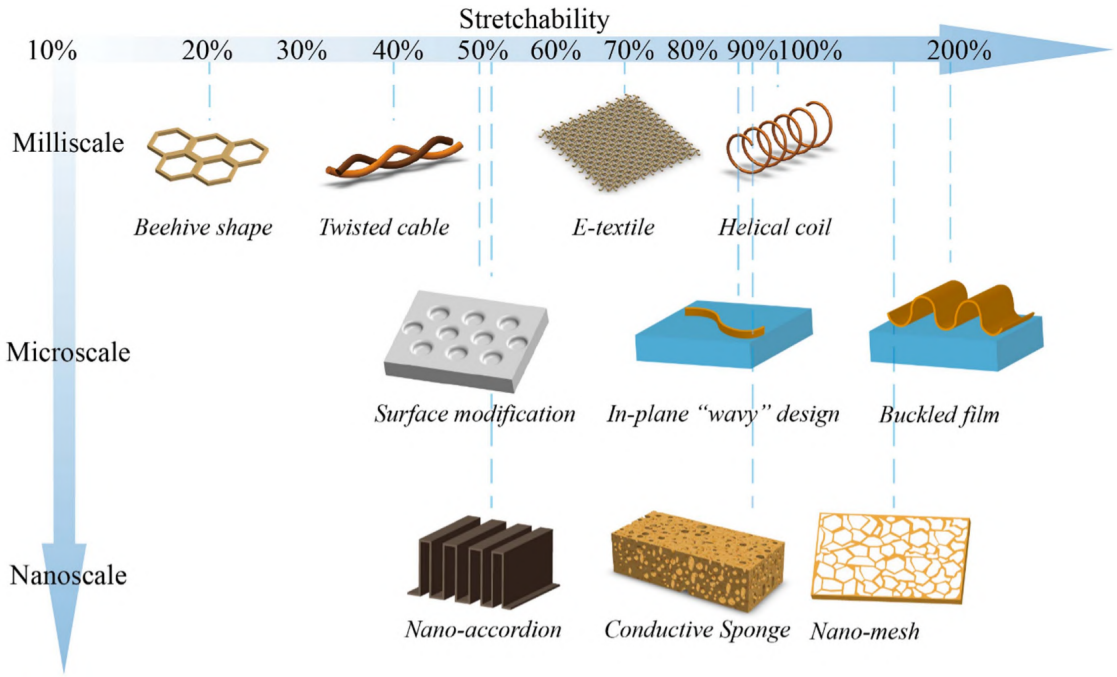

Figure 2.7. *Various design patterns to achieve geometrically rendered stretchability. The patterns are categorized by their achievable elongation and size scale. [34]*

2.4 Reliability, fatigue & failure mechanisms

The durability of conductors under bending can be evaluated using statistical methods. In engineering, a generally applied tool is so-called Weibull distribution which gives a means of analysing the specimen's lifetime. By adjusting the distribution's parameters, it can be a great fit for a wide range of experimental data, such as dielectric breakdown, fracture in ceramics, and capacitor failure. While Weibull's probability density function (PDF) provides insight how the probabilities are distributed over the range of possible values, its integral, Weibull's cumulative distribution function (CDF), shows the probability of the event with the given *x* value. [35] CDF of the Weibull distribution is

$$F(x) = 1 - e^{-(\frac{x}{\alpha})^{\beta}}, \quad for \quad x \geq 0, \tag{2.12}$$

where α, β > 0 are scale and shape parameters respectively [35]. The scale parameter describes the lifetime of the test population and indicates where 63.2 % of the specimens have failed. It can be seen to shift the distribution in horizontal axis as demonstrated in Figure 2.8a. Furthermore, the shape parameter derived from the Weibull analysis indicates the uniformity of the population. [11] The slope of the distribution grows steep with a greater β, as shown in the Figure 2.8b.

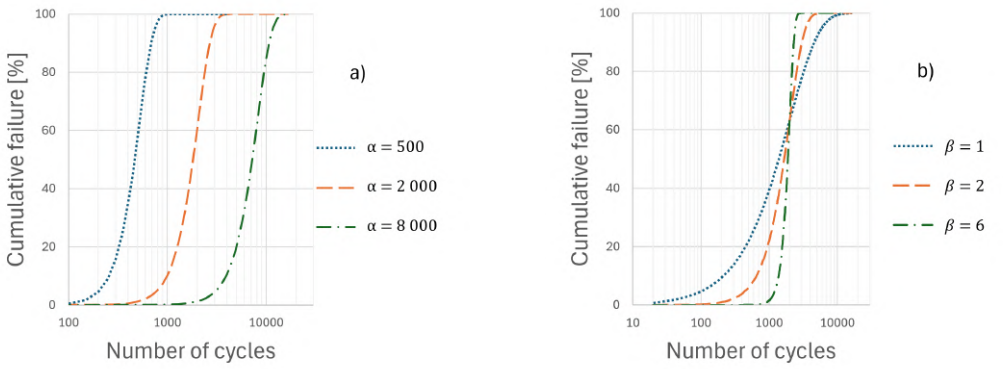

Figure 2.8. *Example of Weibull's cumulative distribution function a) varying scale parameter (β = 3) and b) varying shape parameter (α = 2 000). Inspired by [11].*

Depending on the shape parameter, different failure types can be identified. If β < 1, the failure rate decreases over time, which depicts samples known as infant mortalities. If β = 1, the failure rate is constant and indicates the useful life of a system or device. Lastly, if β > 1, the failure rate increases over time implying a wear-out type failure i.e. fatigue. [11]

Fatigue can be understood as a material's response to repeated loading. The failure process due to fatigue involves multiple stages: initiated by the formation of cracks, followed by their propagation until the specimen becomes structurally damaged. Several factors are known to affect specimen's fatigue life stemming from external geometry as well as microstructures. Notches and joints, which act as geometric discontinuities, are typical sites for crack initiation due to having stress and strain concentrations. [36]

Repeated loading, also known as cyclic loading divides into two regimes depending on the number of cycles to reach the failure. High-cycle fatigue (HCF) refers to a situation where the cycle number is relatively high while the stress remains low. Conversely, the term low-cycle fatigue (LCF) is used when the lifetime is short under high loading. The transition from LCF to HCF occurs between 10^4 and 10^5 cycles. [37] Thinner films tend to have longer lifetimes under HCF-conditions compared to thicker films [38].

Dai et al. researched thin films on a flexible substrates under bending and concluded four different failure mechanisms: cracking, which occurs in a form of ruptures of the thin film on the flexible substrate, slipping, delamination, and delamination in the slipping zone, which all three occur at the interface between the substrate and the thin film. [39] For instance, cracking has been identified to be a contributor to increased resistance of screen-printed silver conductors, when they were subjected to mechanical stress. The applied strain creates partial breakage of the conductive network, as well as, reduces the contact area between the electrically conductive particles, and further decreases the volume ratio of conductive particles within the ink. [40]

Although the structure subjected to bending experiences different stresses depending on the location on the substrate (tensile stress on the convex surface and compressive stress on the concave surface), the underlying mechanisms are alike. Generally occurring in brittle materials, fatigue damage originates from repetitive mechanical deformation, which causes dislocations in the material's structure. Accumulated dislocations lead to surface extrusions (bumps) and intrusions (dents), leading to stress concentrations, which result in crack evolution, an increase in resistance, and finally, total failure. [38]

It is important to note that in real-life scenarios, the device is most likely exposed to several factors affecting its lifetime all at once. Despite the fact that tests with just one impact are easier to implement, a hybrid reliability test would be necessary to realistically simulate the various conditions that an actual application might encounter. Such a comprehensive test could, for instance, involve stretching in multiple axes while simultaneously exposing the specimen to high temperatures and high humidity. Additionally, integrating other factors such as mechanical vibrations, chemical exposure, and thermal cycling could further enhance the realism of the test. This approach would help to identify potential failure modes that may not be evident under single-factor testing conditions, thereby improving the reliability and longevity of the device in practical use.

3. PRINTED ELECTRONICS

Printed electronics have drawn significant interest in recent years. In this chapter, the drivers behind this growth are explained, along with the advantages and challenges of printed electronics. The chapter covers the most important printing technologies, comparing them to each other and to conventional electronics production. Additionally, the chapter delves more deeply into screen printing technology, as it is the method used to process the samples in this thesis.

3.1 Key benefits and potential

Looking at the market size of flexible electronics, it is expected to grow at 10.5% compound annual growth rate (CAGR) from 2023 to 2030. The global market size was valued at USD 24.9 billion in 2022 and is forecasted to reach USD 54.1 billion by 2030. The growth stems from multiple sources, such as flexible and curved OLED displays, medical devices and diagnostic tools, to headsets for immersive gaming experiences and wearable devices. [41]

Although printed electronics have acquired more foothold in research and development, as well as on the global market, it is not a completely new technology. Its roots trace back to as early as 1950, when researchers at Nippon Telegraph and Telephone applied gravure printing technology into the printed circuit boards' (PCBs) manufacturing (Nagatsu, 1959, as cited in [42]). They discovered that this technology could be used to achieve mass production, and as the matter of fact, a large number of products produced by the means of printed electronics technologies have appeared in our daily lives. For instance, the electronic circuit corresponding to the keys on keyboards are often fabricated by screen printing technology. [43] It is also worth noting that printing technologies have been widely utilized in other fields, from a regular inkjet printers found at home to gravure-printed milk cartons in packaging industry. Figure 3.1 illustrates the analogy between traditional color printing inks and those used in the production of printed electronics.

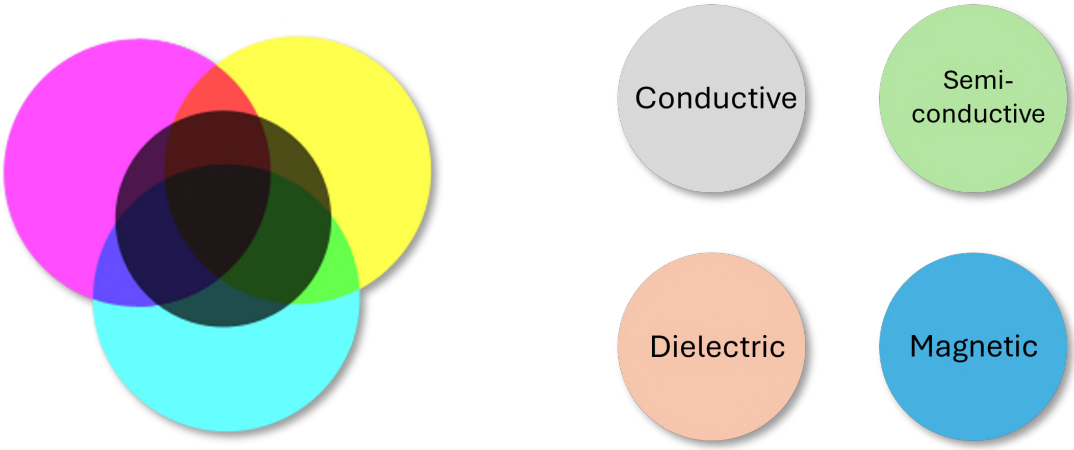

Figure 3.1. *An analogy between color printing and electronic printing. Color printer uses magenta, cyan, yellow and black to achieve a color image. In electronic printing, the traditional colors are replaced by functional inks – conductive, semi-conductive, dielectric, and magnetic – to manufacture electronic devices.*

Producing electronics through printing processes offers various advantages over the traditional manufacturing methods which typically consist of lithography. Generally these traditional methods include several process steps, which make the production line longer and more complex; hence, the production speed and volume are more challenging to increase. Printing processes, on the contrary, can be very high-speed and high-volume, allowing large-scale flexible electronics to be produced with comprehensive automation. Large-scale in this context can refer to device arrays spanning tens centimeters or even meters, being far larger than the focus of traditional technology. A longer production line also implies higher equipment cost, which can be minimized by the straightforward process flow of printed electronics. [43] The comparison between traditional electronics and printed electronics manufacturing is visualized in Figure 3.2.

Traditional manufacturing methods also include process steps that are not only energy-intensive, but also consume a lot of harsh chemicals, such as those involved in etching, which could be avoided with printing technologies. Environmental impact of electronics production is more easily lowered when material is deposited precisely where needed on the substrate, rather than etching away the excess material and therefore adding to the waste discharge of the production. [43]

While printed electronics have a smaller loss of raw materials, the environmental impact can be further reduced through careful material selection. Printing manufacturing typically uses relatively low temperatures, which enables the usage of plastic films, papers, or textiles. Greener manufacturing can therefore be achieved by opting for organic materials with good biodegradability. [43]

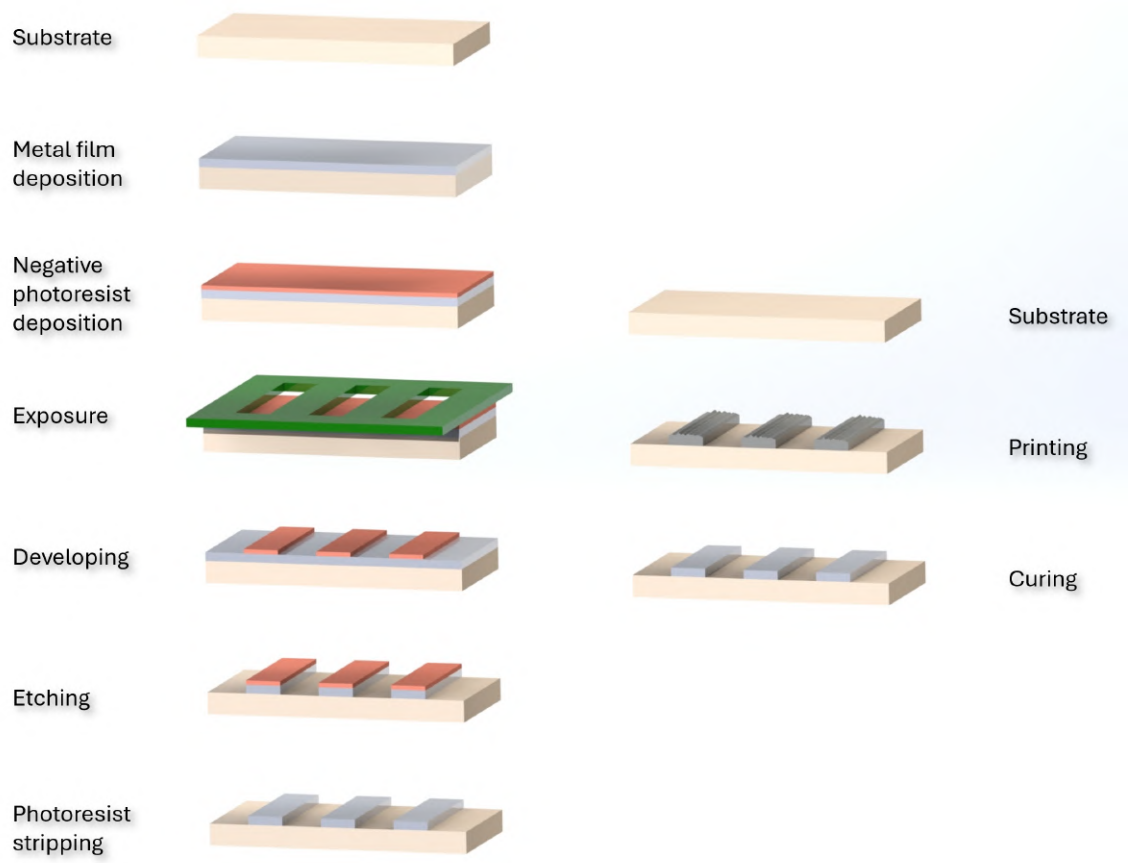

Figure 3.2. *A comparison of conventional electronics production and printed electronics. Printed electronics offer a significant reduction in the number of process steps, among other benefits.*

Overall, printed electronics offer numerous advantages: low cost, suitability for mass and large-scale production, environmentally friendly processes with less waste and the potential for biodegradable devices, the ability to create new applications with flexible electronics, as opposed to the rigid substrates used in traditional manufacturing. [43] However, like any technology, printed electronics also exhibit some disadvantages.

One downside of printed electronics is the relatively high resistivity of the inks, which can be hundreds or even thousands of times greater when compared to the values in traditional electronics. Even with the best conductive silver inks and optimized sintering of AgNPs, the achieved resistance values are approximately 2–5 times higher than those of bulk silver material [44]. This significant discrepancy causes the entire printed electronics circuit to behave like a resistor, which can lead to problems if not properly addressed. Therefore, the circuit design in printed electronics must take this problem into account and implement strategies to mitigate it. [43]

Additionally, silver paste, for instance, has challenges under high temperature and high

humidity, which accelerate metal ion transferring. Due to this phenomenon, the silver atoms can move from the anode to the cathode under an applied voltage potential. This causes poor insulation and short circuit failures, which are harder to avoid as the circuitry's gaps become smaller. This limits the miniaturization of devices. [43]

Printed electronics are still far from achieving the resolution and accuracy of traditional methods, as the resolution of most printing methods is 20–50 µm, and in the best cases close to 1 µm with optimized process. Hence, extensive research is still required in order to reach the nano-scale of silicon-based microelectronics. Although printed electronics is currently the main development direction of modern electronics, it will not replace traditional silicon-based counterparts anytime soon, but rather serve as a complementary technology [45]. It is showing the direction in transforming and upgrading the electronics manufacturing. [43] [46] Electronics are already being printed for various innovative applications, and this trend is likely to continue.

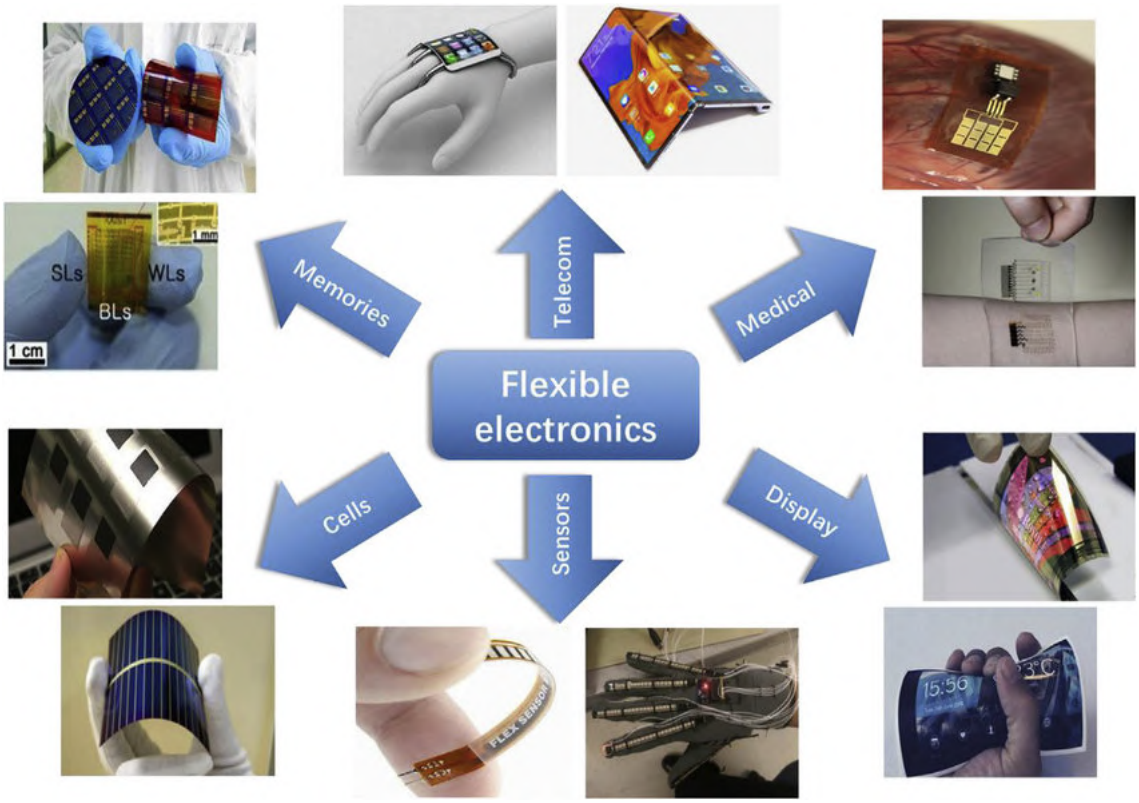

Figure 3.3. *Typical applications of flexible electronics which could be manufactured using printing technologies. Reproduced from [47] under the Creative Commons (CC) BY-NC-ND license.*

Printed electronics are applied across various fields, as illustrated in Figure 3.3, encompassing things like electrodes and conductive lines, lighting, sensors, displays, field-effect transistors (FETs), energy storage and harvest, smart packing, among other things. The technology of printed electronics is undergoing extensive research and it continues its journey towards reaching maturity and potentially replacing a significant number of tra-

ditional manufacturing methods. The rapid advancement is the consequence of huge investments from many well-known companies in the electrical industry, for instance, Intel, Siemens, Toshiba, Sony, Phillips, Motorola and Samsung. [43]

Lighting industry has been going through a drastic transformation and is expected to continue evolving in the future. This is important, especially in terms of energy consumption, as lighting is estimated to consume approximately 6% of the global electricity [48] [49]. When considering modern lighting consisting of LEDs, printed electronics has the potency of driving the field forwards, and to develop new revolutionary lighting products that could be applied to any shape on any surface, all while reducing the cost. [43]

Various energy devices have been developed and manufactured using printed electronics. This includes products such as traditional chemical batteries, organic photovoltaics (OPVs) and solar cells, and supercapacitors. The cost of solar cells and solar panels has dropped for various reasons over the past decades, and this trend is expected to continue further with advancement of printed electronics. This progress will likely drive forward the development of flexible solar cells. [43] These products are already being developed, for instance, by Finnish research center VTT. They describe the fabrication of roll-to-roll (R2R) printed organic photovoltaics, which were manufactured using gravure printing and rotary screen printing processes. Their OPV modules have achieved a maximum power conversion efficiency of 2.1%. [4] Although this solar cell has some ways to go in order to achieve the power efficiency of a conventional solar cell, being at 17–20% [50], printed OPVs have their advantages of being fully organic, lightweight, recyclable, and flexible. These OPVs could serve as integrated power supplies in many emerging wearable products. But for now, more extensive commercialization awaits for improvements in the efficiency and the reductions in the cost of functional inks. [43]

Another field well-suited for printed electronics is in displays, particularly in organic light-emitting diode (OLED) displays. In addition to a regular flat panel display, these OLED displays can be fabricated on flexible substrates, so that the glass is replaced with a plastic substrate. This innovation solves issues regarding the usage of brittle and heavy glass, thus achieving flexible displays with bending characteristics. [43]

As printed electronics becomes a key part of the electronics manufacturing, it will also be applied in smart integrated systems. These systems, as they are becoming one of the major development directions in printed electronics, include devices such as RFIDs, smart cards, motion sensing and health monitoring, smart fabrics and so on. Some of these devices are already introduced to the consumer markets. For instance, RFID antennas and smart tags are mass fabricated using the screen printing technology with conductive silver paste. These products can be used to achieve intelligent commodity management, where packaging products are monitored more efficiently enabling the advancements in large-scale logistics. [43]

3.2 Printing technologies and methods

In essence, printing is a replication process where the ink is transferred onto a substrate in a repeatable manner. This additive process requires a pattern carrier, either in analog or digital form, to define the layout for the transferred ink. [51] The inks used in printing consist of a functional component, as discussed earlier, along with solvents, binders, and additives. Solvents are utilized to dissolve the materials into a printable consistency, while binders help in the formation of homogeneous conductive path, and additives modify the ink properties such as wetting and rheology. [52] Typically, the added constituents reduce the final electrical properties compared to the pure material, but are necessary for the printing. This introduces trade-offs between maintaining the electrical performance and enhancing the printability. [51]

The properties of the substrate, such as purity, doping uniformity, surface morphology, also have an impact on the achieved printing quality and the final device performance. Before drying, the spontaneous movement of liquid ink can introduce changes to the dimensions of the printed structures. These dimensional changes can have an impact on the electrical performance of the device, and therefore, they should be addressed. [51]

Printing technologies can be divided into different categories as illustrated in Figure 3.4. One approach is to determine whether the method uses a physical template as a guiding pattern. This can include stencils, masks, molds, or engraved surfaces. Technologies, where the image formation is conducted using templates, are for instance: screen printing, gravure printing, offset printing, and letterpress printing. On the contrary, the template-free methods are jet printing and its various forms. Each method have their specific requirements for ink properties, such as viscosity and particle size. [51]

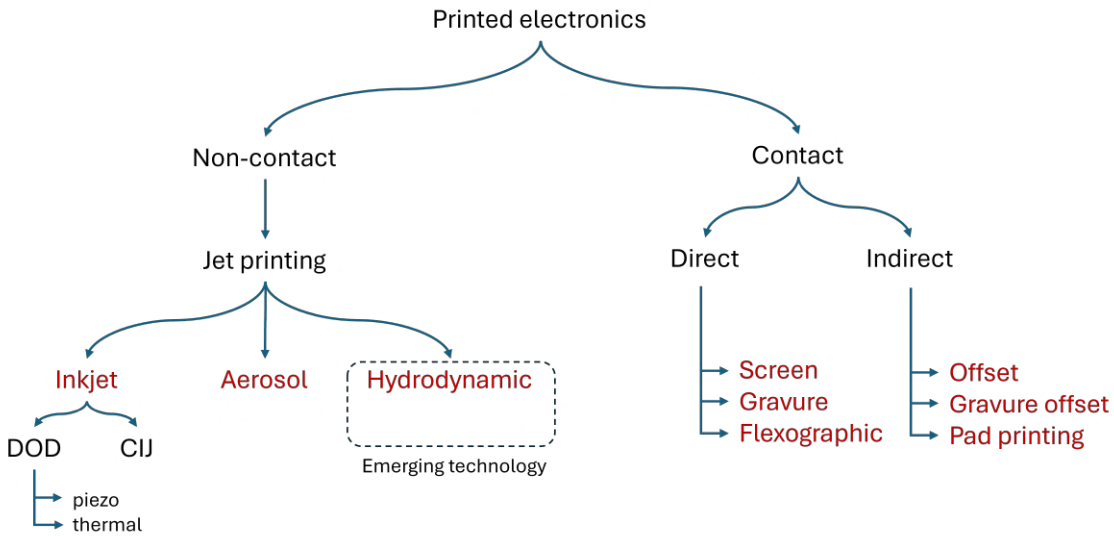

Figure 3.4. *Printed electronics technologies categorized according to their patterning techniques.*

3.2.1 Non-contact printing

Jet printing is broadly understood concept, since it incorporates the widely used inkjet printing technology, which is used in homes and offices for producing color images. Inkjet printing is a non-contact digital printing method where individual ink droplets are jetted out from a nozzle as illustrated in Figure 3.5. The formation of these droplets is precisely controlled by a computer, following a digital pattern of ink droplet matrix. Inkjet printing is categorized into continuous inkjet (CIJ) and drop-on-demand (DOD) inkjet, depending on the mode of operation. In CIJ operation, the ink droplets are continuously produced and ejected, and as the droplets are charged, their trajectory can be controlled using an electrostatic field. Thus, droplets are either deposited onto the substrate or deflected to an ink catcher for re-use. In DOD operation, the ink droplets are created and ejected only when needed. This is achieved by a voltage pulse that propels the ink out of the nozzle, either through the deformation of a piezoelectric material or by an increase of pressure caused by a heating element in thermal inkjet systems. In printed electronics, the most commonly used inkjet printers are based on piezoelectric DOD. [51]

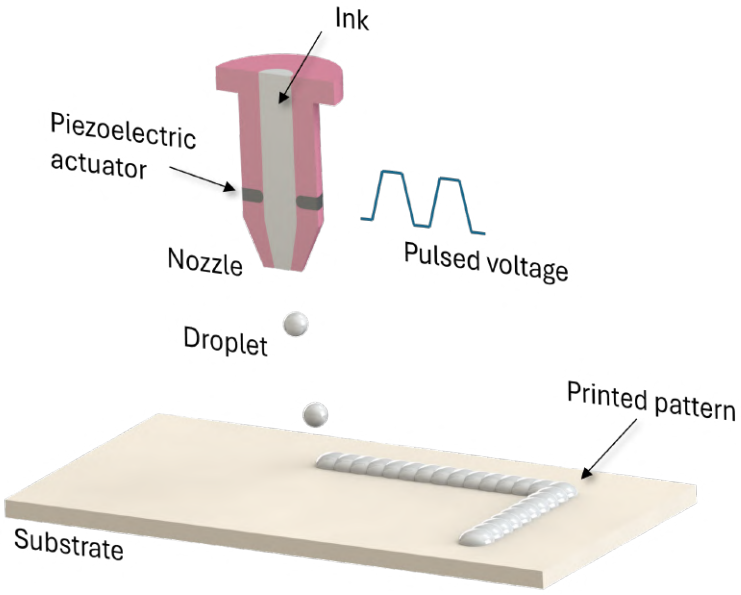

Figure 3.5. *A typical DOD inkjet printing system with piezoelectric actuator. Inspired by [53].*

Inkjet printing is extremely versatile due to its digital control and non-contact characteristics, and almost all electronic components can be manufactured using inkjet printing methods. However, some challenges remain, as the inks used in inkjet printing are difficult to formulate, as they must have low viscosity, small particle size, and low volatility to avoid nozzle clogging. Additionally, the resolution is relatively poor (greater than 20 µm), and the ink tends to spread after jetting because of its low viscosity. This can lead to a

phenomenon known as the "coffee ring effect", which occurs due to faster solvent evaporation at the edges causing the particles to flow and to accumulate towards the edges, resulting in non-uniform deposition. [51]

Another form of jet printing is aerosol jet printing, which operates based on a different principle than inkjet. In this method, a pneumatic or ultrasonic atomizer turns the ink into a dense aerosol containing droplets between 1–5 µm. These droplets are then carried by an air stream to the nozzle, from where the aerodynamically focused aerosol stream is sprayed onto a substrate. The continuous stream is stopped by a shutter at non-printed areas. [51]

Aerosol jet printer has a wide range of printable inks in terms of viscosity (0.7–2500 cP) and particle diameter, while also offering a high resolution. In these aspects, it can be seen as superior to inkjet printing, but aerosol jet printing also exhibits some challenges. While it relies on stable air flow, the printing parameter adjustment does not have an immediate effect, making the parameter optimization more complex. Additionally, aerosol jet printing is more expensive than inkjet printing, and while being less mature, its large-area printing is slower with lower throughput. [51]

In the area of emerging technologies, one could mention electrohydrodynamic jet printing. Since printing resolution is related to the ink droplet size and the printing nozzle, the resolution is difficult to improve in inkjet printing due to the risk of clogging the nozzle. In electrohydrodynamic jet printing this problem is solved applying a strong electric field between the nozzle and the substrate. By this approach, the ink droplet's surface tension can be overcome, achieving high printing resolution with 240 nm line width. [51]

All printing techniques that operate without templates are excellent for prototyping and suitable for research purposes. Their digital design patterns can be easily modified. Furthermore, the non-contact nature of the printing minimizes the risk of damaging or contaminating the substrate. Despite these advantages and the potential for increased throughput using parallel printing with multiple nozzles, these methods are not yet as mature for industrial large-scale production as traditional template-based methods [51].

3.2.2 Contact printing

In contrast to non-contact printing, replicate printing employs a template that carries the pattern. Once created, the template cannot be altered, making it therefore the most suitable for producing a large number of prints. Printing methods that utilize templates can be categorized into direct and indirect printing technologies based on whether the pattern-holding medium is in direct contact with the substrate. [51]

Gravure printing is a direct printing method that replicates an engraved pattern, as illustrated in Figure 3.6. The gravure cylinder has dented dots, also known as gravure cells,

which are loaded with ink and then transferred onto the substrate. Before transferring the pattern, any excess ink is removed using a doctor blade. While some gravure printers process singular sheets in a sheet-to-sheet manner, the most common method is R2R, known for its high speed and capacity for mass production. The primary disadvantages of gravure printing are the high cost of gravure plate manufacturing, and challenges of ink movement management, which is necessary to connect the individual disconnected cells into a homogeneous film. [51]

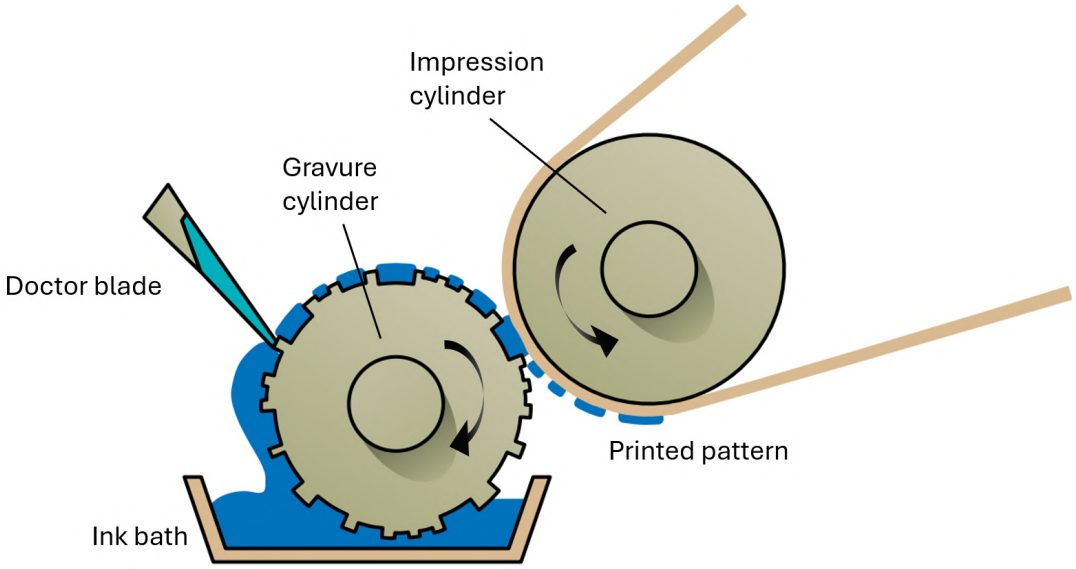

Figure 3.6. *Gravure printing process—adapted from an original illustration by Josh King-Farlow, with permission [54].*

Flexographic printing share similarities with gravure printing, but instead of directly transferring the pattern to the substrate, an additional plate cylinder is used. This cylinder is typically made from rubber or photopolymer that have the pattern areas protruding above the surrounding non-pattern areas. An anilox roller is used with its engraved dents to transfer the required amount of ink, similarly to the gravure printing. The raised pattern is then transferred onto the substrate. Although, flexographic printing plates are relatively easy and low cost to produce, they have a shorter service life when compared to gravure plates. Despite the fact that flexograph can handle a wide range of substrates and flexible materials, its printing process is more complex, and distortions may occur due to the printing plate's elastic nature. [51]

Flexographic printing is classified as a direct printing method because the pattern-holding plate cylinder is in direct contact with the substrate. On the contrary, offset printing is categorized as an indirect printing while there is no direct contact between the printing plate and the substrate. Offset printing works using an elastic intermediate carrier, which receives the pattern of the printing plate and transfers it onto the substrate. The print-

ing plate's pattern is created utilizing hydrophobic and hydrophilic printing areas. Offset printing is the most popular method in traditional printing industry, however, it has limited usage in printed electronics. The main reason lies in the high viscosity (40 000 cP) which is difficult to achieve for the inks used in printed electronics. [51]

While gravure printing is suitable for printed electronics, it cannot be directly applied to fragile substrates. Indirect gravure printing addresses this issue by using an intermediate blanket cylinder, which receives the printing pattern from the engraved cells of the gravure plate before transferring it onto the substrate. This methods allows for printing on a vast variety of substrates, while increasing printing complexity. [51]

Another indirect printing technology is so-called pad printing. It utilizes a special rubber stamp which carries the ink from the engraved gravure plate onto the substrate. Due to its nature, pad printing is able to print on uneven or rough surfaces, but it has its problems on pattern distortion stemming from the surface's topography and pad deformation. [51]

3.2.3 Screen printing

Screen printing is categorized alongside other contact printing methods; however, it is given its own subsection due to its significance in this work. Screen printing technology dates back to the early 20th century [55]. It has a simple working principle which has been extensively used within the industry. In this method, the ink is squeegeed through a mesh onto the underlying substrate using a metal or rubber squeegee. The mesh contains tiny threads and gaps that form the desired pattern. It is fabricated using optical lithography and light-sensitive material, whereas the mesh consists of plastic, natural silk, or metal fibers. The selection of the mesh parameters, stencil material, and deposition method are important, as they all have an impact on the final pattern and on its resolution. [51] The fabrication of the mesh includes filling the screen with an impervious emulsion so that the areas of printed patterns are kept open. The screen is glued to a frame under tension achieving a key part of the screen printing process. [55]

The mesh specifications such as mesh count and thread diameter, define important aspects like mesh opening and ink volume. Mesh count refers to the number of threads per centimeter or inch, while mesh opening corresponds to the distance between these threads. Ink volume can be interpreted as the amount of ink that gets squeegeed through the mesh in respect to the area. [56] The structure of the mesh with two different thread diameter and its impact on the ink volume is illustrated in Figure 3.7.

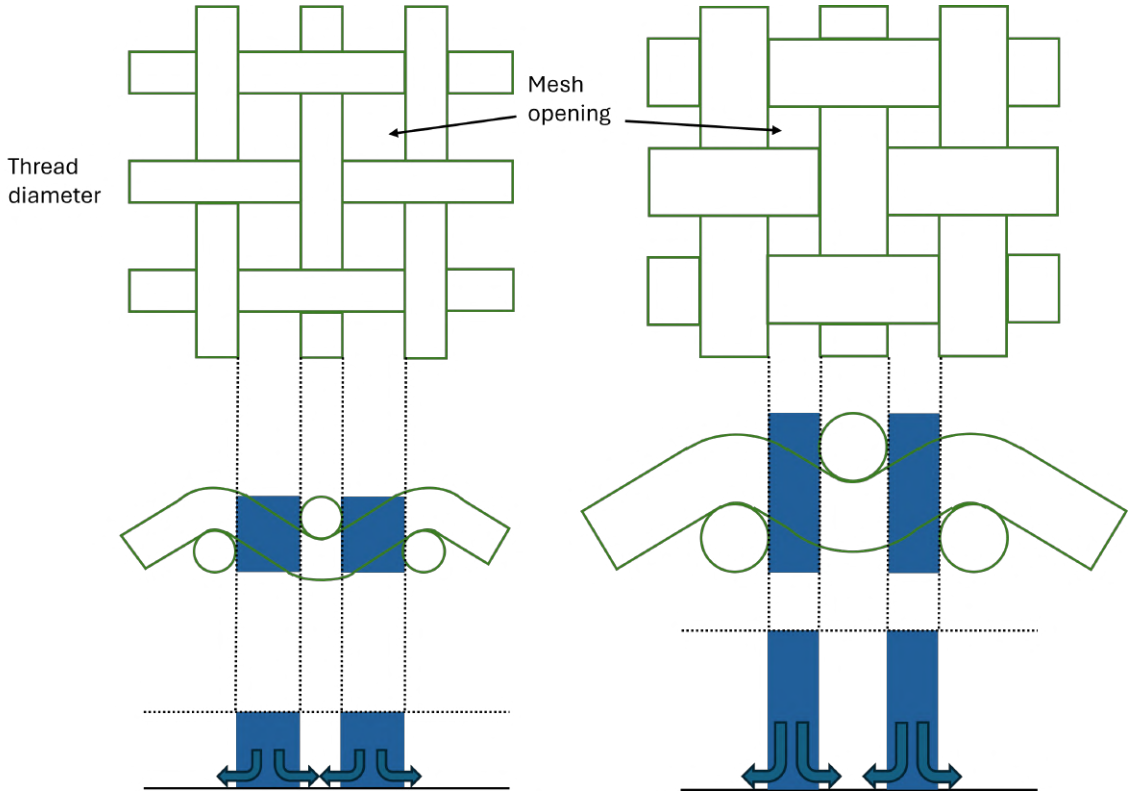

Figure 3.7. *A depiction of a screen printing mesh and the ink volume squeegeed through it. Inspired by [56].*

Ink volume *V* can be calculated as

$$Ink\ volume = \frac{Mesh\ opening^2 \cdot Mesh\ thickness}{(Mesh\ opening + Thread\ diameter)^2}, \tag{3.1}$$

where the unit is cm^3/m^2 and relates to the thickness of the ink layer [56]. The ink can be seen spreading on the substrate and filling the gaps between the mesh openings, resulting in a lower thickness compared to the thread diameter. This is referred to as the wet thickness d_{wet}, which can be used to calculate the final dry thickness of the print d_{dry} using the following equation

$$d_{dry} = d_{wet}\frac{\rho_{solid-\%}}{\rho} = Vk\frac{\rho_{solid-\%}}{\rho}, \tag{3.2}$$

where ρ is the ink's density, $\rho_{solid-\%}$ describes the solid material concentration in the ink, and *k* represents a unitless coverage efficiency factor accounting for non-ideal ink transfer through the mesh. [55] During the post-process, ink loses solvents and additives, leading to a reduction in thickness.

The ink utilized in screen printing must have high viscosity (1,000 – 10,000 mPa·s [57]) so that it won't leak through the gaps onto the substrate without the squeegee pressure.

High-viscous ink allows for better control of ink movement during printing, enabling thick print patterns, often greater than 10 µm. When a thick mesh is used, screen printing can achieve even 100 µm with a single print. However, thicker inks require more additives which have an impairing effect on the conductivity. [51] [42]

Screen printing can be divided into two technologies: flat-bed screen printing, as illustrated in Figure 3.8, and rotary screen printing, shown in Figure 3.9. Flat-bed printing is the most traditional method, where the screen and the substrate are flat, operating in a sheet-to-sheet manner. Compared to other printing methods, screen printing is cost-effective in terms of equipment and paste materials, but it possess lower resolution with rougher pattern surface, which limit its usage in devices with fine structures. [51]

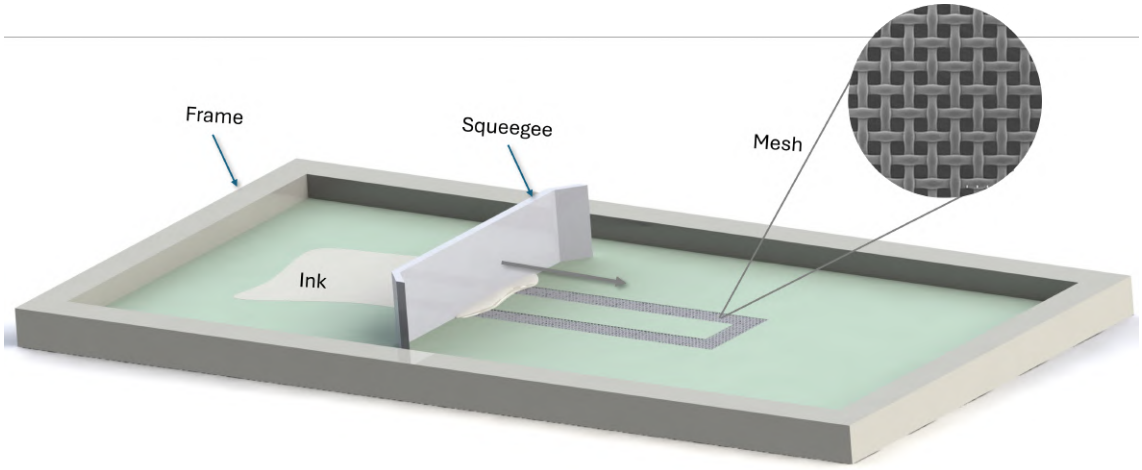

Figure 3.8. *A representation of flat-bed screen printing process and a magnification to the mesh structure. SEM image of the mesh obtained from [56]*

Screen printing is already widely used method for manufacturing various conventional electronic devices and components, including circuit boards, display boards, and membrane switches. It is likely to find more applications along the improvement of resolution and with new electronic pastes. [51] Rotary screen printing, in particular, can be utilized as a continuous R2R process, enabling higher throughput in large-scale manufacturing [55].

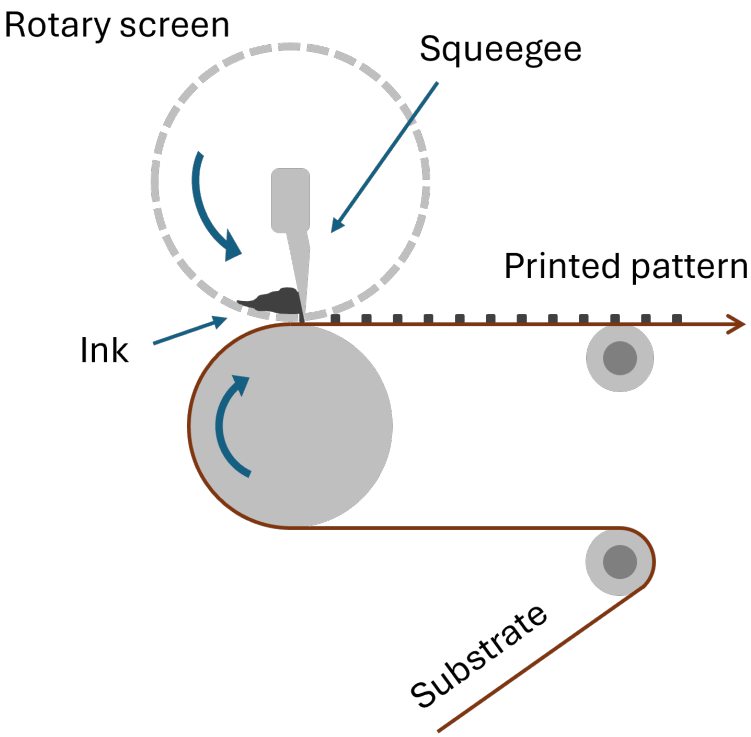

Figure 3.9. *An illustration of rotary screen printing. Inspired by [42].*

The screen is shaped as a cylinder with the squeegee positioned inside. The substrate is fed past the outside surface while transferring the rotary screen's pattern on it. This highly efficient process enables rapid production of complex patterns over large areas. [55] Having introduced the main printing methods, their characteristics are compared in Table 3.1.

Table 3.1. *Comparison of the main printed electronics technologies. [46] [52]*

Technology	Resolution [µm]	Cost	Material compatibility	Scalability	Speed
Screen printing	50–100	Low	High	High	Fast
Gravure printing	Sub-5	Medium-High	Limited	Very High	Very Fast
Flexography	20–50	Low	High	High	Very Fast
Inkjet printing	10–30	Medium	Limited	Medium	Slow

Screen printing was selected as the manufacturing method in this thesis. Its high material compatibility, low cost, and excellent scalability for large-scale production made it a great choice for the purpose of this thesis. Although screen printing does not exhibit the finest printing resolution, it is enough to produce conductive tracks for wearable electronics applications. Additionally, within our team, there is significant experience and know-how with screen printing, which further influenced the decision.

3.3 Pre- and post-printing processes

Regardless of the selected printing method, a printing pattern needs to be designed. Pattern distortions can occur due to ink movement, but the distortions can be mitigated to some extent through proper pattern design. For instance, in inkjet pattern, the pattern is composed of a matrix of dots, where the dot spacing and volume are pivotal for a successful print. Too large spacing might produce individual non-connecting drops, while too narrow spacing might lead to bulging of the printed lines. In gravure printing, the pattern design such as the structure of the cells and their width are determined while accounting factors like the ink properties, plate and substrate movement, and interactions between ink, plate, and substrate. [51]

With some materials, it may be necessary to modify the substrate's surface energy. This approach gives means to control the wettability and adhesion of the inks, hence, ensuring a better and more uniform print. The surface energy of the substrate also influences the printing resolution. Adjustments in the surface energy can be achieved, for instance, with chemical, plasma, or UV treatment. [51]

After printing, the printed materials undergo physical or chemical treatments which aim to enhance their properties. The ink is solidified and its residual solvent or additives are removed. Post-processing techniques, including sintering or curing, can also improve the morphology and microstructure of the print. [51]

Metal or oxide particles in the ink are typically bonded with organic materials, which are necessary for ink formulation, but due to their insulating nature they prevent electron movement between particles. The sintering process makes the particles loss their organic shell, allowing the particles to have a direct physical contact to one another. In sintering, the ink is heated so that the particles can fuse together, such as in silver NPs, thereby improving the electrical properties of particle-based inks. The most commonly used method is direct heating using a hot plate or oven, though this process can be time-consuming and may damage heat-sensitive substrate materials like plastics. Alternatively, UV, infrared, or laser can be employed for fast sintering and selective heating, which helps protect the substrate. [51]

In contrast to fusing the particles together, the curing process solidifies the printed ink through a polymerization process, forming connections between flakes without fusing the particles together. Thermal curing is the most common method, but UV-curing can also be used to rapidly solidify the printed ink, mitigating any spontaneous movement of the ink on the substrate. This helps to achieve prints with sharp edges without distortions. [51]

4. MATERIALS AND METHODS

In this chapter, the materials used are presented, encompassing various inks and substrates suitable for screen printing. These materials were selected by the project partners, so this thesis does not cover the selection process in detail. Additionally, although key values were sourced from material data sheets, specific material names cannot be disclosed due to project confidentiality requirements. This chapter also outlines the fabrication and characterization methods employed to produce the samples, followed by the techniques used to measure the necessary attributes. A more detailed account of these steps can be found in Chapter 5.

4.1 Materials

The chosen materials included 5 different inks and 7 substrates. Table 4.1 provides an overview of the most important properties of the used inks.

Table 4.1. *Used inks, their curing conditions, sheet resistances and type of non-volatile particles provided by data sheets. Specific names are under confidential agreement.*

Name	Curing condition	$\mathbf{R_{sh}}[\Omega/\square/25\mu\mathrm{m}]$	Content
Silver	10 min @ 120 °C	0.01	silver
Carbon A	15 min @ 120 °C	20	carbon
Carbon B	5 min @ 90 °C	50	carbon
Carbon C	5 min @ 120 °C	25	carbon
Carbon D	10 min @ 120 °C	40	carbon

Using carbon ink instead of silver is due to its reduced environmental impact and lower cost, although it suffers from lower conductivity. As mentioned earlier, silver ink is commonly used in printed electronics and was therefore selected here as a reference. The curing conditions and sheet resistances are acquired from the inks' data sheets.

The substrates used in this study included PET-75 µm, E-insulation paper, Paper smooth, sustainable packing material (SPM), PP white 60, PLA, and cellulose film. Due to data restrictions set by project partners, detailed information such as grammage and material composition could not be disclosed at this stage of the project.

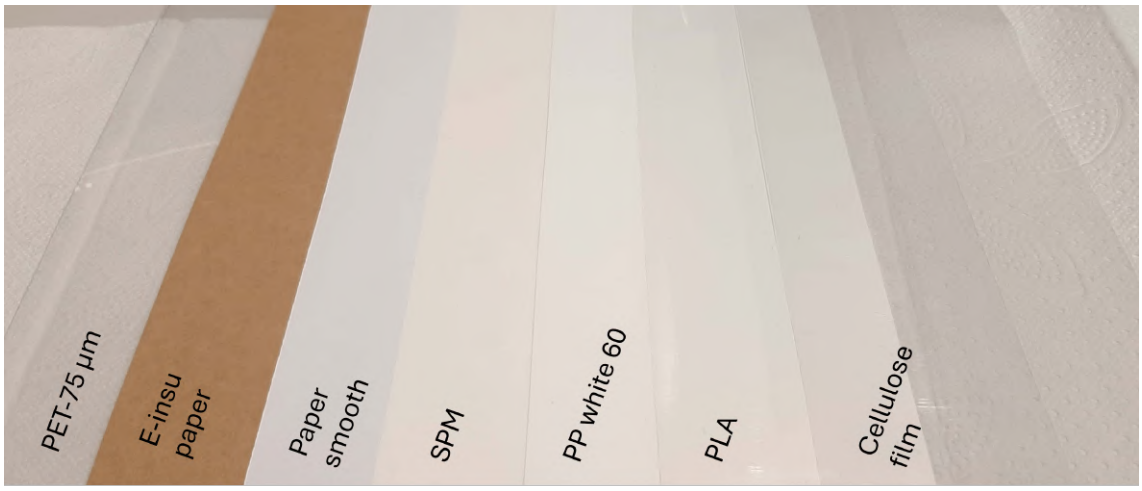

Figure 4.1. *All used substrates.*

The substrate materials selected for this thesis can be seen in Figure 4.1. PET-75 µm served as a reference for the other materials, as it is commonly used within the industry of printed electronics. The selection process was carried out by the project partners, who chose these substrates based on criteria such as their availability, biodegradability, and overall ecological impact. Each substrate was included to evaluate its performance under various bending conditions. The aim is to determine the most suitable substrate for the desired applications.

4.2 Fabrication methods

All samples were fabricated using a screen printing technique. More detailed explanation of this technique was presented in the chapter 3. The screen printer used in this thesis is fully-automatic Ekra X5 professional stencil printer. Its most relevant characteristics are presented in the table 4.2 and the whole system can be seen on the image 4.2.

Table 4.2. *Ekra X5 professional stencil printer characteristics. [58]*

Parameter	Value
Max frame size	740 x 740 mm
Max printing area	508 x 508 mm
Print material thickness	0.5 – 6 mm
Print speed	9 – 200 mm/s
Print pressure	10 – 250 N
Positioning	Fiducial recognition
Alignment repeatability	$\pm$ 12.5 µm @ 6 Sigma
Product changeover	< 2 min
Cycle time	8 s + print time

Figure 4.2. *Screen printing system of Ekra X5 professional stencil printer.*

The system consists of a vacuum table (left in the image 4.2) which is used to transport the substrate in and out of the printer, the stencil printer itself, and a computer that provides an interface to control the process.

In order to fabricate the samples, a mesh was designed with the desired pattern and a mesh count of 100/cm and thread diameter of 40 µm. The mesh parameters were selected within the recommended values of the screen printing inks. The mesh used in this thesis can be seen in Figure 4.3, and the specific pattern is shown in Figure 4.4.

The mesh consists of 10 print patterns, with 4 having wider tracks (width = 2 mm) and 6 having narrower tracks (width = 1 mm). Each one of them has 7 U-shaped loops that are easy to attach to a ZIF connector due to their 1.54 mm spacing.

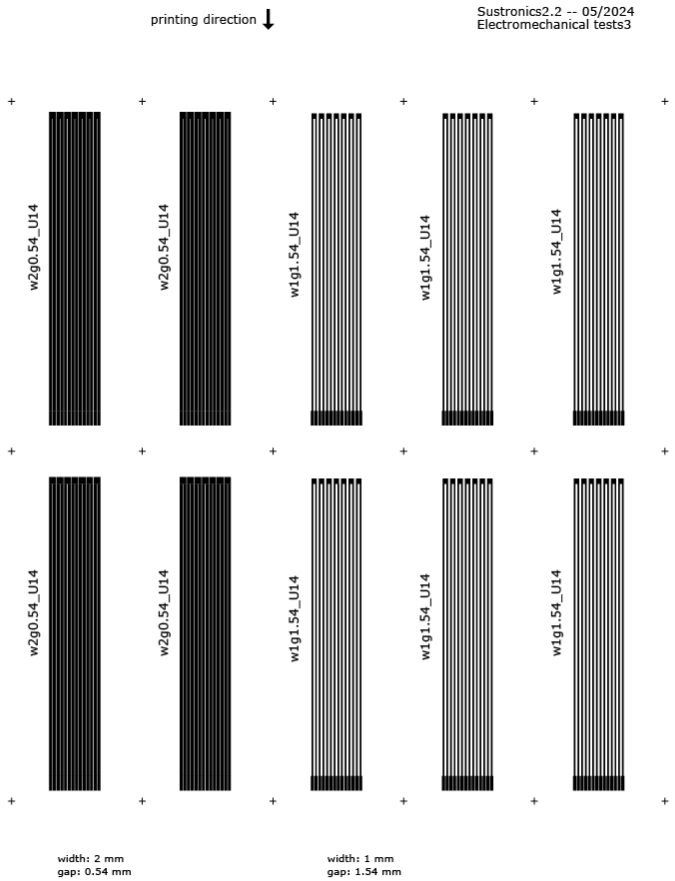

Figure 4.3. *Screen design that was used to print the samples. It has mesh count of 100 /cm and thread diameter of 40 µm.*

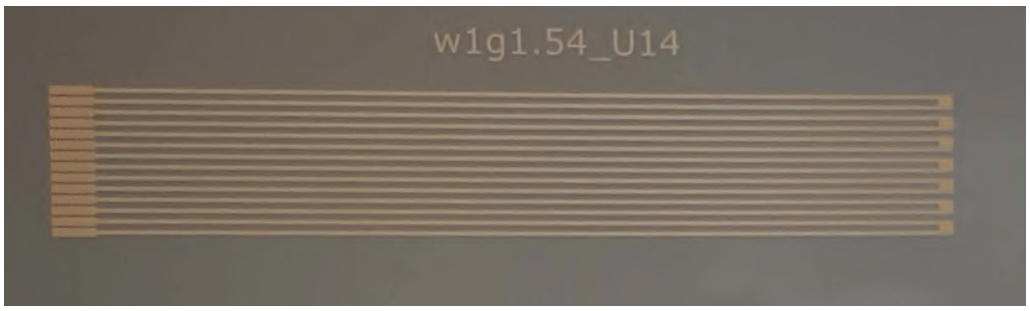

Figure 4.4. *Screen printing pattern. 7 U-shaped loops where track's width is 1 mm and gap 1.54 mm.*

After printing, the samples were cured in a Memmert box oven. The curing times and temperatures used are listed in Table 4.1, selected within the ranges recommended by the ink providers. Proper curing was ensured, as detailed in Chapter 5.

4.3 Characterization methods

The samples were characterized using two different bending setups to assess their electromechanical durability, as well as additional methods to measure their dimensions, including width and thickness, and to detect possible signs of failure. The sections are divided accordingly.

4.3.1 Bending between horizontal plates

All the substrate-ink combinations were characterized for their electromechanical properties. To achieve this, two prints at a time were attached to a self-made bending device, as illustrated in Figure 4.5. This device consists of two plates, with the bottom one stationary and the top one pneumatically driven back and forth, with a stroke length of 16 cm. The samples were affixed to the plates, allowing them to move with the upper plate and undergo partial bending. The movement of the top plate is managed by a control unit, which allows several parameter changes through its own user interface such as, cycle time, speed, and recoil of the plate. Bending could be selected to be continuous or alternatively to stop at a certain stage. Additionally, the bending radius can be controlled by changing the bottom plate to a thinner or thicker one, hence changing the gap between the plates. The same bending device was used by Halonen et al. to analyse bending of inkjet-printed conductors [59].

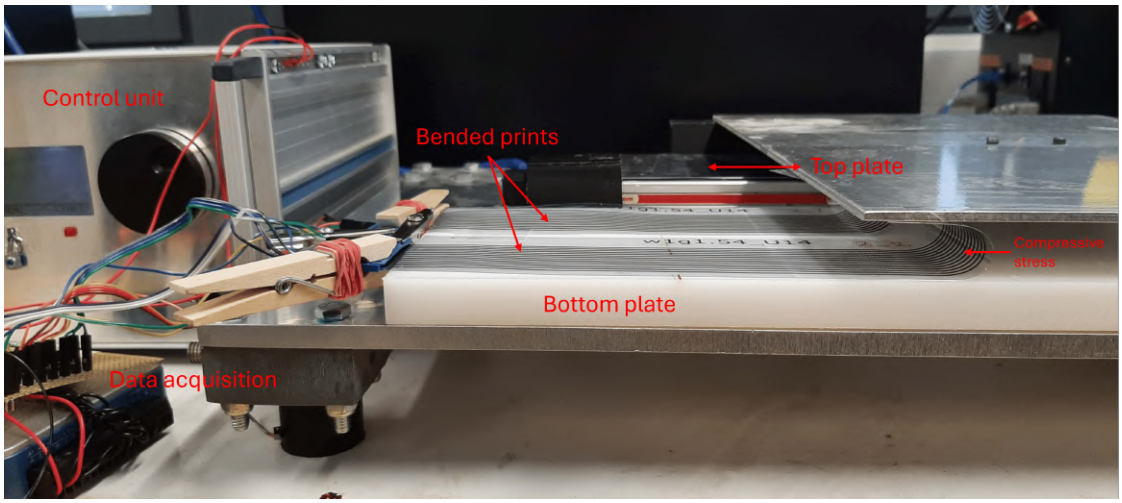

Figure 4.5. *Bending setup and its main parts.*

The National instruments (NI) USB-6003 was used for the data acquisition along a program written in LabVIEW. The NI-device consists of 8 analog inputs with an analog-to-digital converter (ADC) resolution of 16-bits. The absolute accuracy of analog input is typically 6 mV and maximum sample rate is 100 kS/s. The device's output power source was used to provide known voltage over the series connection of the track and known resistor as presented in Figure 4.6. The source's output voltage was +5 V $\pm$ 3 %, hence

one of the analog inputs (A0) was used to measure the output voltage to compensate for the variation. While the input impedance of the analog input is > 1 GΩ, it did not consume current. The power source can provide maximum current of 150 mA. [60]

Junction BD provides a connection to the control unit of the bending device. There is a potential of 25 V in respect to the ground when the sledge starts to move left. This information was utilized by the NI-device to determine when a new bend cycle starts, but before that, the voltage was lowered to 3.2 V by resistors R1 (680 kΩ) and R2 (100 kΩ). Lowered voltage was then sensed by digital input (PO), which is able to detect voltages within range -0.3 – 5.5 V with respect to digital ground. [60]

The tracks' resistances were determined based on voltage division and fixed known resistances, which could be easily switched between 1.2 kΩ and 82.5 kΩ. This made the test process easier as depending on the combination, a different voltage domain was required. For instance, tracks made of silver inks were in the range of 70–1400 Ω depending on the combination, so 1.2 kΩ reference was used. Conversely, carbon inks were within 35 kΩ – 160 kΩ, and the reference of 82.5 kΩ was utilized. The values of reference resistors were therefore selected to be within the same size of the measured tracks and also based on the available resistors. Although, these resistors exhibit 5 % tolerance, its effect can be ignored as the most accurate resistors were selected by measuring multiple resistors with a multimeter.

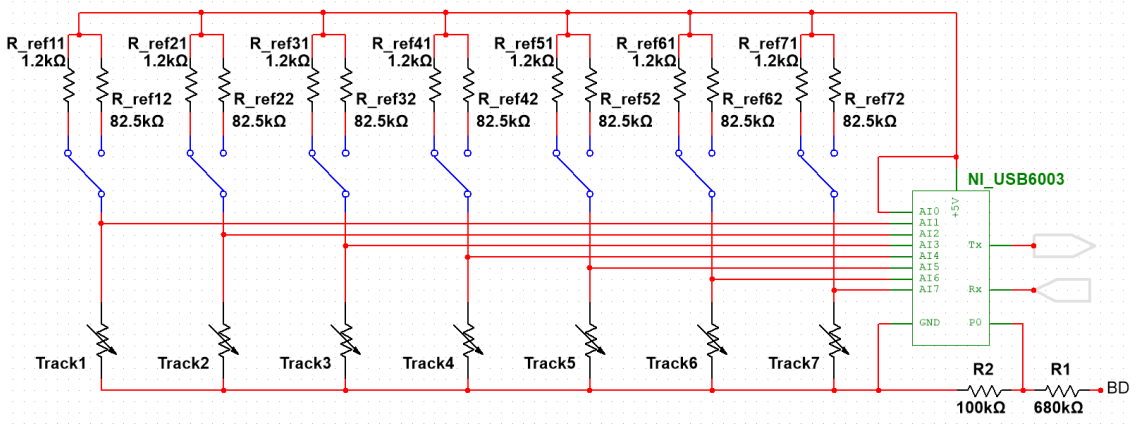

Figure 4.6. *Schematic of the measurement setup, where a voltage division between a track and a known resistor is measured by the NI-device.*

The presented setup is considered 2-wire measurement due to the common ground between power supply and voltage measurement. This causes inaccuracies because the measured resistance is influenced by the resistance of the wires. [61] 4-wire sensing could be implemented by using the differential analog inputs, but this would reduce the number of tracks that could be simultaneously measured, as the NI-device used has only 4 differential analog inputs [60]. Therefore, 2-wire measurement was considered adequate, when taking into account that the measured resistance values are relatively big

compared to possible extra few ohms from the wires and contacts, and also due to the fact that we are more interested in the change of resistance rather than absolute resistance.

NI-device's 16 bits can encode 65,536 possible values, representing a voltage step of 76 µV. ADC's integral non-linearity (INR) is $\pm$ 1.8 LSB, meaning least-significant bit, which converts to an error of 137 µV. However, this is more than an decade lower from the analog input's accuracy (6 mV) and is therefore ignored. This overall voltage accuracy sets the accuracy of measured resistance, which has different values depending how far the measured resistance is from the reference. This is a drawback of a constant voltage setup where the measured voltage changes non-linearly in respect to the sample's resistance. In the best scenario, track equals to the reference, giving an error of 0.5 %. If the track's resistance differs by one decade, the error would be 14 %. Considering that the best substrate-ink combination had initial resistance around 80 Ω, it would have been better to use smaller reference resistance, as the upper end had more margin. For example, 600 Ω would be better detecting the most conductive silver tracks and could still handle the more resistive ones even when their resistance increase during bending. The other reference used for the carbon prints, 82.5 kΩ, was well selected as all the combinations measured by it stayed within reasonable distance from the reference. Although, some measurements might lack accuracy, they can be improved by averaging and assuming that each measurement point varies randomly around the real value. Figure 4.7 displays the part of the program where NI-device is set to read values from each 8 analog inputs, and where these voltage values are converted to corresponding resistance values of the printed tracks based on Equation 4.1

$$R_{track} = \frac{V_{AI} R_{ref}}{V_{sup} - V_{AI}}, \tag{4.1}$$

where V_{AI}, V_{sup} and R_{ref} are measured voltage, supply voltage and reference resistance in respective order. [62] Full program can be found in Appendix A.

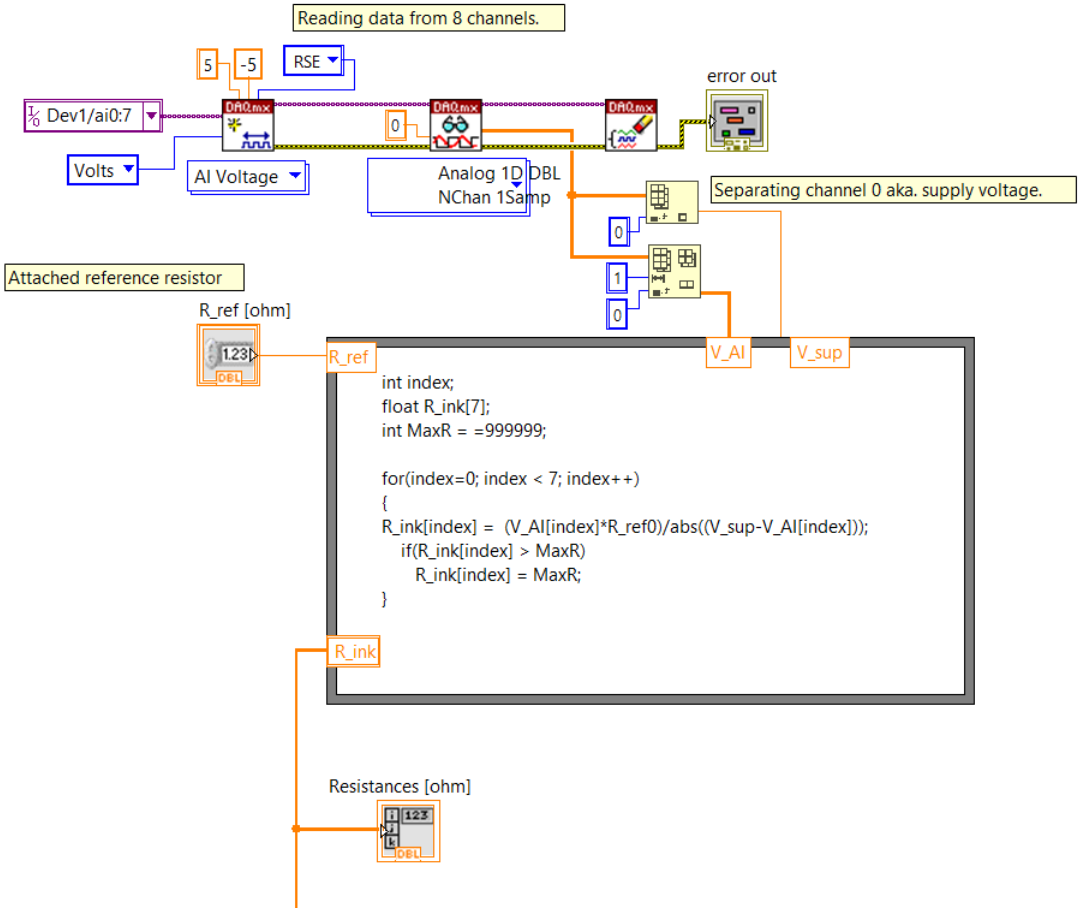

Figure 4.7. *Block diagram of the LabVIEW program that handles reading of the NI-device and calculates resistance based on the measured voltage.*

4.3.2 Bending using Mark-10

As later discussed in chapter 6, certain prints did not degrade during the bending tests. To expose them to even harsher bending conditions, they were subjected to another bending setup by attaching the samples to a Mark-10 ESM303. This arrangement consists of a forge test stand capable of producing up to 1.5 kN of tension or compression force [63]. The configuration used can be seen on Figure 4.8.

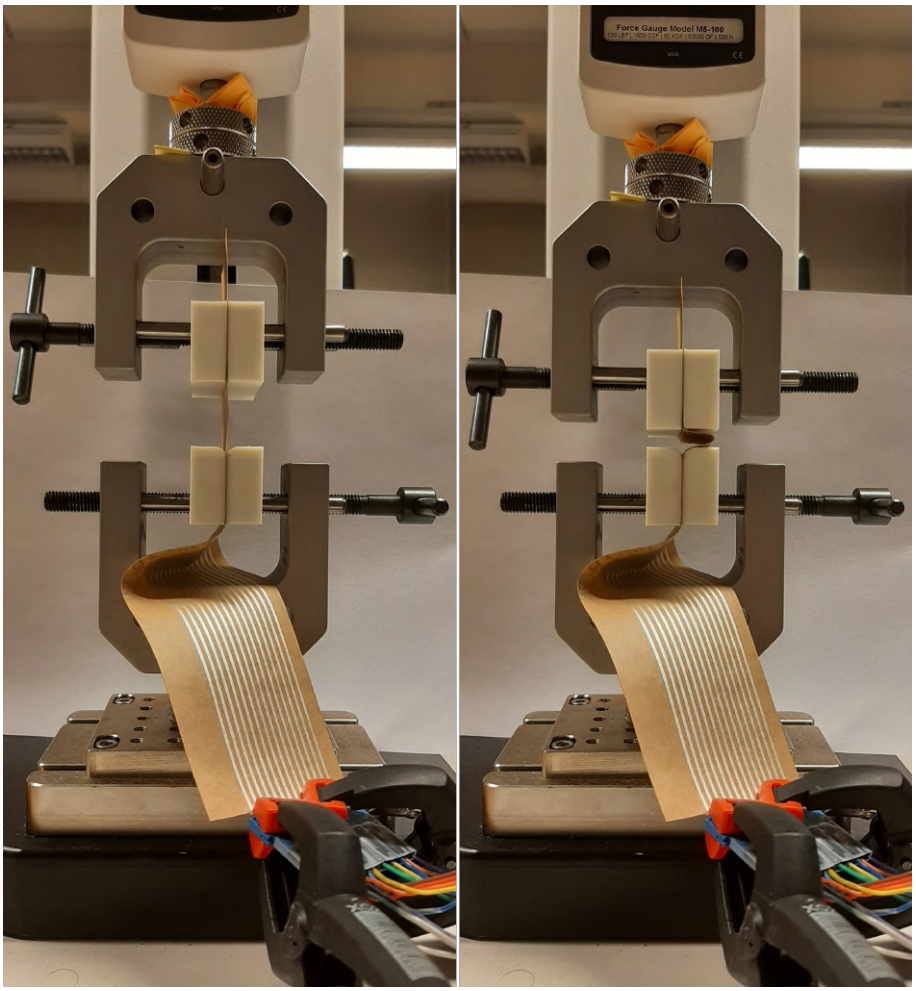

Figure 4.8. *Bending test conducted with Mark-10.*

The sample was affixed to the grips so that the lower grip was stationary , while the upper grip was able to move. LabVIEW program, found in Appendix B, was controlling and moving the grip, and bringing it down allowed the print to bend. Instead of having a fixed bending radius, this setup exposes the sample to a dynamic bending radius, which changes based on the position of the grip. While the previous bending setup exposed a big part of the sample to bending, in this test, only a one specific spot of the track is under the bending stress. The tracks' resistances were constantly measured using the NI device while increasing the bend-cycle count, similarly to the aforementioned bending setup. The program's user interface can be seen in Appendix C

Zhao et al. used a similar cyclic bending method for their printed flexible supercapacitors (SCs). By conducting a measurement system analysis (MSA), they found that the method was highly reliable and repeatable for evaluating printed flexible SC. The bending radius was subjected to a small variation between samples (< 9%) as well as a small variation between the cycles (in the range of 0.03 mm) during 500 bending cycles. The bending radius must be defined separately for every device as it may be different even under the same bending distance due to the different material properties. [64]

Although, MSA was not conducted for the samples in this thesis, and they differ from the tested SCs in terms of used materials and thicknesses, their study can be used to some extend assuring the reliability of the measurement setup. Different materials combinations are expected to behave slightly differently, affecting the bending radius between samples as well as between cycles. However, the latter can be ignored, as all the combinations are expected to have variation between cycles, which can be mitigated by averaging, and therefore the combinations can be compered. The variation between different combinations is more challenging as they might bend with different radii even with the same bending distance. However, its impact is ignored for now, as the main purpose of using this bending setup is to get some signs of degradation in the most durable combinations.

The samples did not perfectly fit into the bending setup and had to be slightly twisted to reach the measurement pads for the ZIF connector. This twisting introduced additional variables, but its effects were largely mitigated by using normalized resistance. Importantly, the twisted section remained stationary during the test, ensuring that only the part between the grips contributed to the increase in resistance. While the grip was in the upper position, the sample straightened and was free of bending stress. Conversely, when the grip was lowered to its down position, the sample was exposed to stress and bent accordingly, providing the necessary conditions to study the impact of cyclic bending on the material's electrical properties.

4.3.3 Other characterization methods

An optical microscope was used to verify that the track widths were correct, ensuring the printing process achieved the desired dimensions. The prints were also checked for their visual integrity, identifying any cracks that could lead to premature failure. After bending, the microscope was again utilized to detect new cracks or other signs of degradation. These observations were later used to identify the tracks' failure mechanisms.

Additionally, the thickness of some prints was measured using a DektakXT stylus profilometer. Its characteristics are presented in Table 4.3, and the device is depicted in Figure 4.9.

Table 4.3. *DektakXT stylus profilometer characteristics. [65]*

Parameter	Value
Measurement technique	Stylus profilometry (contact measurement)
Measurement capability	Two-dimensional surface profile measurements
Sample viewing	Digital magnification, 0.275 to 2.2 mm vertical FOV
Stylus force	1 to 15 mg with LIS 3 sensor
Scan length range	55 x 200 mm
Max. wafer size	200 mm
Max. sample thickness	50 mm
Vertical range	1 mm
Vertical resolution	1 Å max. (@ 6.55 µm range)
Step height repeatability	< 5 Å, 1 sigma on 0.1 µm step
Data points per scan	120 000 maximum

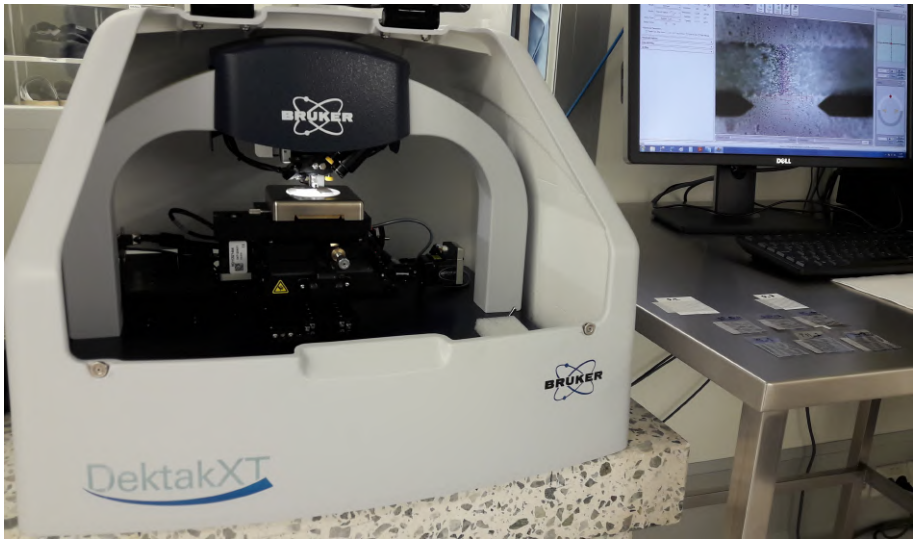

Figure 4.9. *DektakXT stylus profilometer.*

5. EXPERIMENTS

This chapter describes in detail the fabrication process of the samples, including the parameters used at each step. It also comprehensively covers all aspects related to the characterization.

The strategy of testing the electromechanical behaviour of various materials aims to evaluate substrates and inks separately. Firstly, combinations 1–5 include different inks printed on the same 75 µm PET substrate. Secondly, combinations 6–11 focus on different substrate when combined with the same silver ink. This approach helps in understanding how these materials perform under repeated mechanical stress. However, this strategy does not fully represent the final sustainable product, such as carbon ink combined with paper substrate. Nevertheless, the approach used in this thesis is designed to provide valuable insights into material performance, while keeping the number of combinations manageable.

All the tested substrate-ink combinations are listed in table 5.1. From each combination, at least six prints were made to ensure the reliability of the tests and the derived results. Some combinations required additional prints to address variations in the results. For instance, combination 11 had nine different prints.

Table 5.1. *Every tested substrate-ink combination.*

Combination	Substrate	Ink
1	PET-75 µm	Silver
2	PET-75 µm	Carbon A
3	PET-75 µm	Carbon B
4	PET-75 µm	Carbon C
5	PET-75 µm	Carbon D
6	E-insu paper	Silver
7	Paper smooth	Silver
8	SPM	Silver
9	PP white 60	Silver
10	PLA	Silver
11	Cellulose film	Silver

All samples were printed by Ekra X5 presented in Chapter 4. Prior to printing, the ink was stirred for 2 minutes to ensure homogeneity. Stirring was done manually in order to prevent the formation of air-bubbles. The substrates were cut to size 9 x 25 cm and cleaned with isopropyl alcohol (IPA). The mesh was placed in the printer and the substrate was transferred via a vacuum-table into the printer. A small amount of ink was added onto the mesh and the following printing parameters were set as shown in Table 5.2.

Table 5.2. *Screen printing parameters.*

Parameter	Value
Speed forward	100 mm/s
Speed reverse	100 mm/s
Pressure forward	200 N
Pressure reverse	200 N
Print cycles	1
Snap off	2.50 mm
Separation way	2.00 mm
Separation speed	0.50 mm/s

In every printing patch, the first print was discarded due to its higher resistance compared to the subsequent prints. This discrepancy is likely because, during the first run, the mesh is not fully saturated with ink, resulting in a thinner printed layer. Each print was produced in one cycle, except for the Paptic Sterna substrate. On this substrate, a single cycle seemed to produce very uneven and poorly conductive print therefore it was necessary to manufacture by two print cycles.

All the prints were cured in an oven under the conditions specified in Table 4.1. Proper curing was ensured by testing one sample. After the initial curing, the sample's resistance was measured, and then it was cured again. If the resistance remained within 5% of the initial measurement, the curing condition was deemed adequate.

The ink Carbon C turned out to be more challenging to print. It dried quickly, often clogging the mesh and blocking its openings. Consequently, it would have been necessary to clean the mesh between every individual print. Eventually, it was decided to exclude this ink due to the printing difficulties.

Before printing, the substrates were deliberately made slightly larger than necessary to ease the printing process and to eliminate the need of precise alignment. To accommodate the samples into the bending device, they were later cut to a size of 5.5 x 23.5 cm. Figure 5.1 illustrates all the different print combinations.

Figure 5.1. *All printed substrate-ink combinations.*

Two samples were placed to the bending device simultaneously and secured to its plates with tape. From each print, 3 tracks out of 7 were constantly measured during the bending process. The tracks were randomly selected in order to minimize potential bias. Additionally, both the initial and final resistance of each track from every print were measured with a multimeter. The parameters used for the bending test are listed in Table 5.3.

Table 5.3. *Parameters used in the bending test.*

Parameter	Value
Type of stress	Compressive
Bending radius [mm]	9
Distance travelled [mm]	160
Time per cycle [s]	4
Number of cycles	10,000
Total time per test [h]	11

The prints were located on the inner side of the bend, subjecting them to compressive stress. The bending radius was chosen based on the device's capabilities and considering the ease of placing the samples, and also taking into account the practical applications for these tracks. The distance travelled and the portion of the track being bend was determined by the length that the sledge could travel. The cycle time was initially set to 2 seconds. However, due to air leakage and pressure loss in the device, it was found to be more reliable to increase the time to 4 seconds, despite doubling the test time for each sample.

The failure criteria was chosen to be 1.7 times the initial resistance. This was evaluated to be a good measure to achieve clear differences between the combinations while keeping the number of required cycles within a reasonable range, which was initially estimated

to be around 10,000 cycles. However, as discussed later in this thesis, some substrates degraded in fewer cycles and did not require 11 hours of testing. Conversely, some substrates were more durable than anticipated and required additional test cycles.

In addition to this test setup, another series of tests was conducted. While all the aforementioned bending tests applied compressive strain, combinations 2, 6, 7, and 11 were tested with the print positioned on the outer side of the bend, subjecting them to tensile strain. This was done to gain insight into the effects of different types of stress on the printed conductor, and to either confirm or contradict the previous conclusion about the most durable substrate-ink combination.

As later shown in Chapter 6, some combinations lost their conductivity quickly; hence they were also tested with a larger bending radius. Additional tests were conducted for combinations 1, 6, 7 and 10 where the bending radius was increased from 9 to 17 mm. Increasing the radius reduces the stress applied to the prints, which is expected to slow their degradation. These tests aimed to assess the impact of the radius on the track's durability, and once more, to either validate or challenge the previous findings regarding the most durable combination.

While some combinations remained unaffected in the tests, they were subjected to more extreme bending to observe signs of degradation and decreased conductivity. This could not be done with the current test setup due to practical reasons. With a small radius, it became nearly impossible to attach the samples without damaging them. Therefore, another test configuration was planned using the Mark-10, as presented in Chapter 4. Utilizing a different setup also provides valuable insights for future projects when designing new testing procedures regarding bending.

The sample was secured between two grips, spaced 22 mm apart. The upper grip was lowered down so that the substrate was allowed to bend, while resistance measurements were taken simultaneously from all seven tracks. This was done using the same NI-device as in the previous tests, with slightly modified LabVIEW program to control the Mark-10.

Table 5.4. *Parameters used in Mark-10 bending tests.*

Parameter	**Value**
Type of stress	Compressive
Upper limit [mm]	22
Lower limit [mm]	6
Smallest radius [mm]	3
Speed [mm/min]	500
Cycles	10,000
Total time per test [h]	12

The combinations selected for this test were 2, 3, 5, 6, and 7. In order to determine the most appropriate testing parameters, combinations 6 and 7 were initially used to explore various conditions, so that the cycle time was sufficiently short and that the substrate bent with a consistently small radius in a repeatable manner. Based on these preliminary tests, the final testing parameters were established, as shown in Table 5.4

In summary, multiple different tests were conducted in order to determine the mechanical durability of screen printed conductors. All the tests are presented in Table 5.5. Due to the limited time, the number of replicate prints was relatively low. While this facilitates testing, it may compromise reliability.

Table 5.5. *An overview of the conducted tests.*

Type of test	Tested combinations	Number of replicates
Compressive bending (radius = 9 mm)	All	6–9
Tensile bending (radius = 9 mm)	2, 6, 7, 11	8
Compressive bending (radius = 17 mm)	1, 6, 7, 10	8
Mark-10 bending (radius = 3 mm)	2, 3, 5, 6, 7	8

For a more detailed analysis, the thickness of the prints was measured using DektakXT stylus profilometer, as described in Chapter 4. Before measuring, the stage was leveled with a glass plate and adjusted by rotating the stage-leveling knob. A scan was performed across three tracks from two replicates of each combination, resulting in six thickness measurements per combination. Selected measurement parameters can be seen in Table 5.6.

Table 5.6. *Parameters used in profilometer measurements.*

Parameter	Value
Scan type	Standard scan
Profile	Hills & Valleys
Stylus type	Radius: 2 µm
Stylus force	10 mg
Range	65.5 µm
Length	7 mm
Duration	180 s

The selected range was chosen as the closest available option that provided sufficient vertical range for these samples, along with an adequate vertical resolution of 1.0 nm. The scan length was determined based on the combined width of the three tracks and the gaps between them, plus an additional 1 mm margin. The scan duration was set to achieve a horizontal resolution of approximately 0.1 µm between data points.

In order to study the failure mechanisms of the prints, they were carefully examined under an optical microscope at 5x, 20x, and 50x magnifications. Cracks formed during bending suggested degradation and potential failure, likely contributing to the decrease in conductivity. The samples that were bent between the plates did not show clear visual signs of degradation, which could be due to the fact that big parts of the tracks were exposed to stress. The increase of resistance was caused by mild damage over a longer section, therefore making the damage more challenging to detect visually.

Samples that were tested with the Mark-10 had dynamically changing bending radius, where stress was concentrated in a small area. Within these samples, the bending-induced damage was slightly easier to identify. An extra light source was applied to the back of the prints, along with some efforts to roll the samples around a cylinder, to improve crack visibility. The results for each test, along with the observed failure mechanisms, are presented in the next Chapter 6.

6. RESULTS AND DISCUSSION

This chapter presents and discusses the obtained test results. It follows the same structure as the previous chapter: first, the prints' dimensions and sheet resistances are shown, followed by the findings from electromechanical tests in the order of compressive, tensile, larger radius, and Mark-10 tests. The significance of the results is then further analyzed, including the factors affecting mechanical durability. Finally, the failure mechanisms are illustrated with microscope images.

The initial sheet resistance was derived using Equation 2.10, where the number of squares was calculated based on the track's length and width, which were 400 mm and 1 mm, respectively. The track's dimensions were confirmed using an optical microscope, which can be seen in Figure 6.1. Furthermore, to account for the effective length added by the track's corners, one additional square was added, resulting in a total of 401 squares. Combination 4 does not have results; therefore, it is denoted as 'not available'. It was decided to exclude this combination from further analysis as the ink dried quickly, causing difficulties in the printing process.

Table 6.1. *Average initial sheet resistance, its standard deviation, and number of samples of each combination (n). Each sample contains 7 tracks from which an average is calculated for each sample. NA = not available*

Combination	Initial sheet R [$\Omega/\square$]	Standard deviation [$\Omega/\square$]	n
1	2.64	0.47	6
2	92.9	10.3	8
3	328	27.6	6
4	NA	NA	NA
5	191	3.85	6
6	0.75	0.09	8
7	1.13	0.06	8
8	0.31	0.05	6
9	1.38	0.15	7
10	0.74	0.21	6
11	0.19	0.03	9

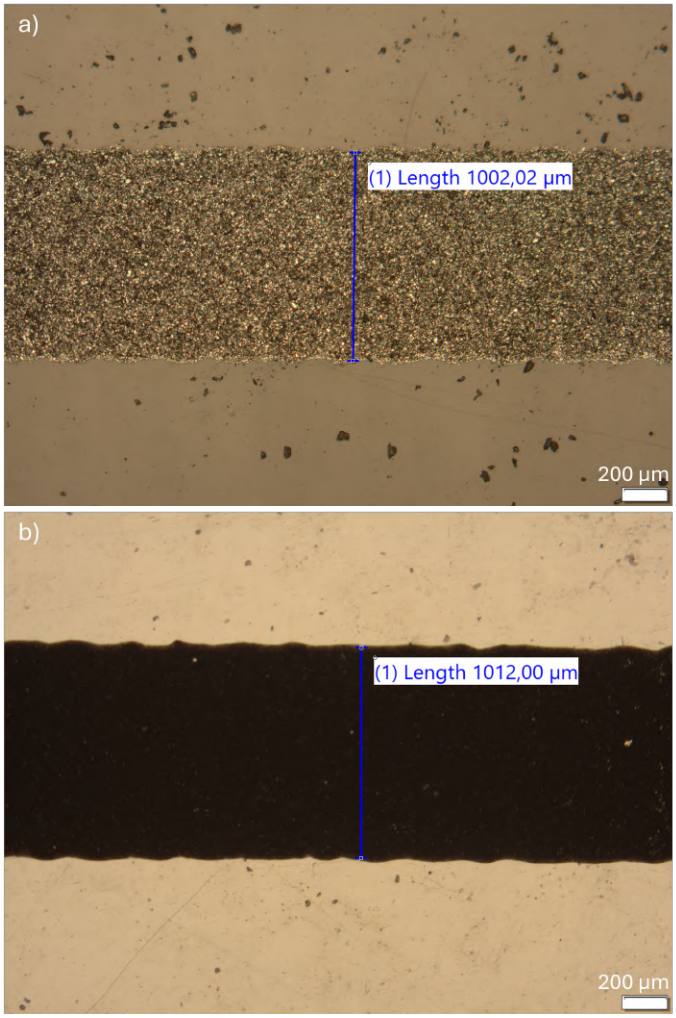

Figure 6.1. *Tracks' width measurements using an optical microscope, where a) combination 1 and b) combination 3.*

When comparing the achieved sheet resistances in Table 6.1 to their theoretical values given in Table 4.1, it is evident that the measured values are significantly higher. This difference arises from various factors. The first being the thickness of the track, as the theoretical sheet resistances provided in the datasheets are normalized to a thickness of 25 µm. The tracks printed for this thesis were in the range of 4–12 µm, hence resulting in a higher sheet resistance. A thickness measurement of combination 9 can be seen on Figure 6.2. Theoretical ink volume given by Equation 3.1 is approximately 20.4 cm^3/m^2, when mesh opening, mesh thickness, and thread diameter are 56 µm, 60 µm, and 40 µm respectively. The print's wet thickness calculated using equation 3.2 is 10.2–20.4 µm when the unknown coverage efficiency factor is 0.5–1. As indicated in the datasheet of the silver ink (specific details restricted by project agreements), the ink has a density of 2.08 kg/l and VOC-density (volatile organic compound) of 703.8 g/l. These values give solid content of 66% and dry thickness of 6.8–13.5 µm based on Equation 3.2 when k is 0.5–1. Achieved silver print thickness on PET-substrate was approximately 5.9 µm, suggesting low coverage efficiency factor, which can be expected with high-viscous inks

and non-optimal print settings.

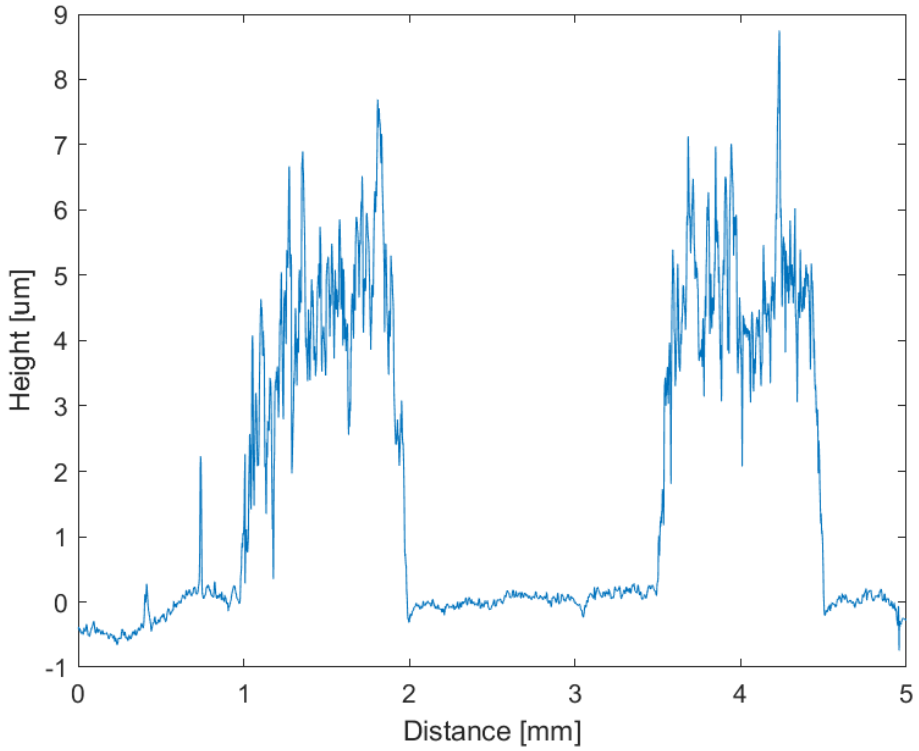

Figure 6.2. *Combination 9 measured with DektakXT. The print's surface is very rough and uneven, thus affecting the measured sheet resistance. Notice the different scale on the axis.*

The second factor concerns the printing parameters. To achieve lower resistance values, the printing parameters such as pressure, speed, snap-off as well as the mesh characteristics need to be optimized separately for each substrate-ink combination. This process can be very time-consuming and was therefore not conducted within the scope of this thesis. Consequently, with non-optimized parameters, the obtained conductivity is lower. Provided that the prints were conductive and intact under visual inspection, they were evaluated to produce legitimate results for the electromechanical testing.

By measuring the required cycles to reach the 1.7 threshold, the first set of bending tests yielded the results presented in Table 6.2. All the substrate-ink combinations could be grouped into three categories based on how they withstand mechanical stress. Group 1 corresponds to combinations that show a rapid degradation when the print is subjected to mechanical stress. Conversely, combinations that show very slow and gradual degradation belong to group 2, and finally combinations within the group 3 showed no signs of degradation when bent. Their resistances remained unchanged throughout these tests, and are also denoted as 'TNR' due to not reaching the threshold. Moreover, the standard deviation of combination 11 is notably large, as later discussed.

Table 6.2. *Average number of cycles until degradation for each combination, including standard deviation, number of samples (n), and group based on the observed behaviour. TNR = threshold not reached*

Combination	Cycles	Standard deviation	n	Group
1	67	8.2	6	1
2	TNR	TNR	8	3
3	TNR	TNR	6	3
5	TNR	TNR	6	3
6	55	8.3	8	1
7	1,098	386	8	2
8	35	9.7	6	1
9	193	64	7	1
10	157	29	6	1
11	13,084	11720	9	2

Figure 6.3 illustrates the normalized resistance plotted against the cycle count and presents two of these categories: fast degradation of combination 6 from group 1, and in contrast, durable combination 11 belonging to group 2.

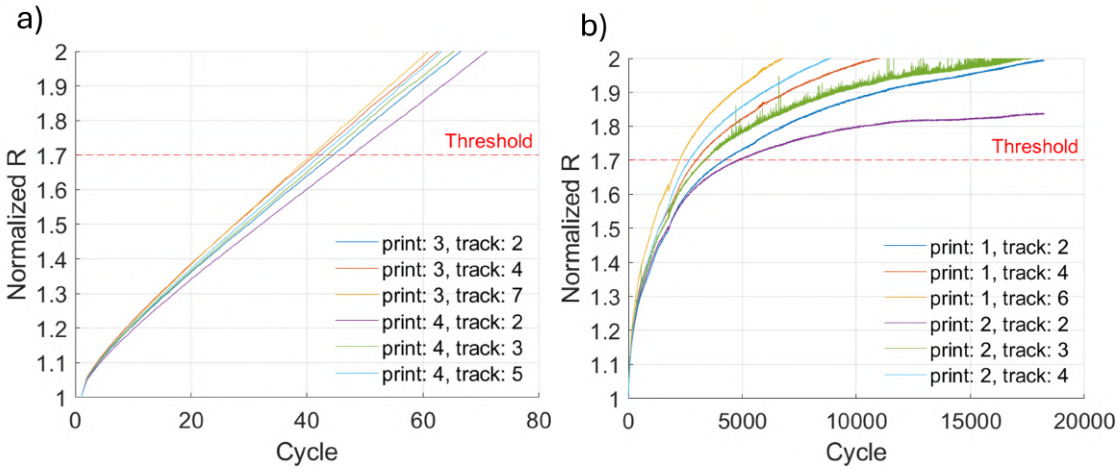

Figure 6.3. *Bending tests of a) combination 6 and b) combination 11. A fast and slow degradation of the prints.*

Tracks' resistances are normalized by their initial resistance values to more easily observe the change as a function of cycle count. Figure 6.4 gives an example of the third category, where the normalized resistance remains almost unchanged.

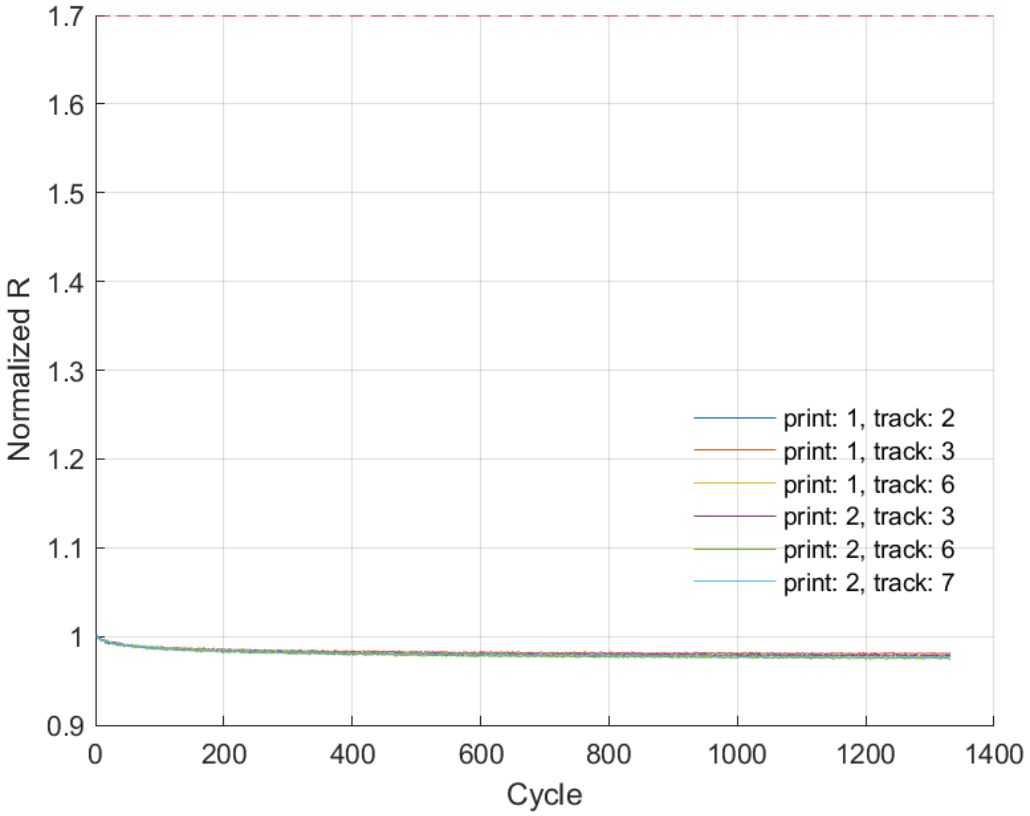

Figure 6.4. *Bending test of combination 2. No signs of degradation.*

The bending results are furthermore presented in Figure 6.5 as a box-chart to clarify the differences between the combinations and to show the variation in the results. A box-chart provides a visual representation of various statistical values. The red horizontal line indicates the median of the dataset. The upper and lower edges of the box represent the upper and lower quartiles (25–75 %), respectively, defining the interquartile range (IQR). Whether a value is more than 1.5 times the IQR away from the top or bottom edge of the box, it is considered an outlier and marked with a red 'x'. Additionally, the whiskers show the maximum and the minimum data values that are not outliers.

Carbon inks (combinations 2–5) are excluded as they never reached the set threshold. To be precise, the cycle number represents the fifth cycle count that surpassed the 1.7 threshold, and print's cycle number is an average of the three simultaneously measured tracks. This was done to minimize erroneous readings. The normalized resistance did not always increase smoothly; hence by taking the fifth value, it was possible to ensure that the track's resistance was undoubtedly over the set limit. By adopting the same measure for all the prints, comparable results were achieved.

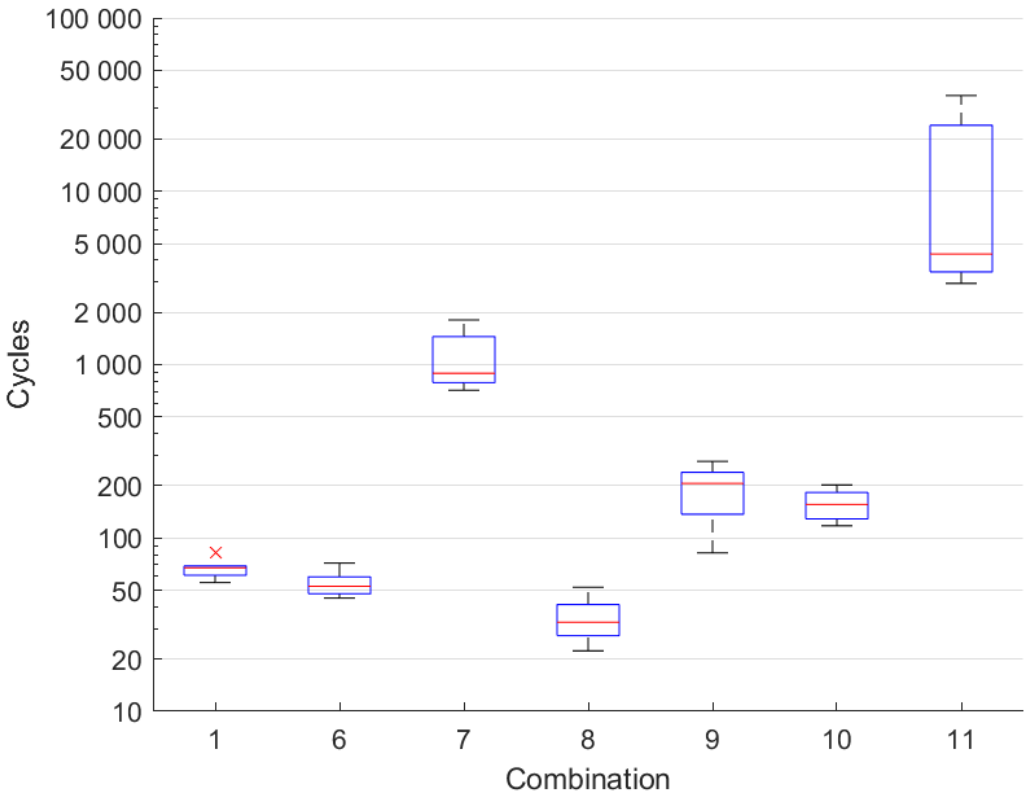

Figure 6.5. *A comparison of different substrate-ink combinations under mechanical stress. The number of cycles represents the point at which the normalized resistance exceeded 1.7.*

The failure rates of the samples are presented in Figure 6.6 as a cumulative failure. Data points are plotted based on the number of cycles when the samples failed, or in this case, when the samples reached the threshold defined as 1.7 times the original resistance. Weibull's cumulative distribution function was then fitted to the data set as explained in Chapter 2. The shape parameters, presented in Table 6.3 with their confidence interval (CI), were greater than one for every curve, indicating a wear-out type failure, as could be expected considering the nature of these samples. The fitted CDF for combination 11 did not closely follow its data points, and therefore it was split into two different groups: A and B, with their own plots. The high standard deviation of combination 11, as shown earlier, indicates some anomalies within the results. The data suggest that something changed during the processing, as the samples in A and B were fabricated at different times. It was concluded that samples in group A were not properly cleaned with IPA and therefore had lower durability than the samples in group B. Nevertheless, the curves and data points of combination 11 are above the adjacent ones by relatively great margin, meaning that the derived conclusion should remain clear.

Table 6.3. *Weibull parameters with their 95% confidence interval. Combination 11 is split into two groups.*

Combination	α	CI (α)	β	CI (β)
1	71.3	66.7 – 76.2	7.4	5.2 – 10.5
6	58.6	54.4 – 63.1	5.8	4.3 – 7.7
7	1,234	1,067 – 1,426	2.9	2.2 – 3.9
8	38.5	33.7 – 44.1	3.6	2.6 – 5.1
9	214	185 – 248	3.2	2.2 – 4.5
10	167	151 – 184	4.8	3.4 – 6.9
11A	3,827	3,444 – 4,253	5.1	3.4 – 7.6
11B	28,095	22,840 – 34,560	3.0	1.9 – 4.7

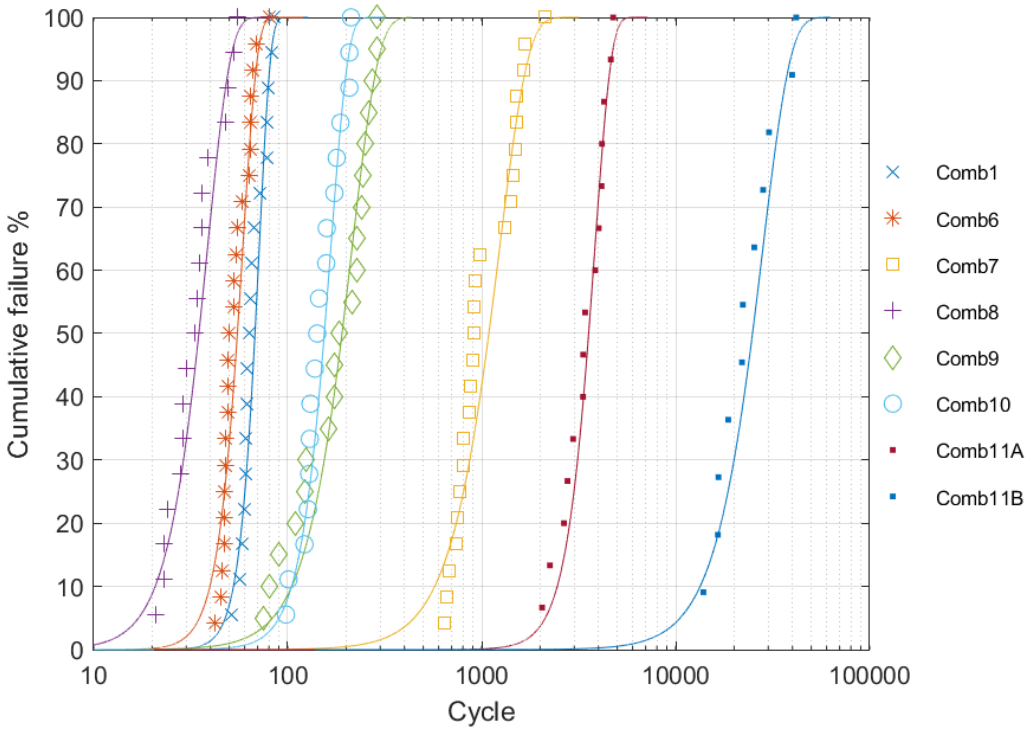

Figure 6.6. *Cumulative failure of different substrate-ink combinations under mechanical stress. A symbol corresponds to a data point while the line illustrates a Weibull's CDF fitted for the data set.*

Based on the first test setup, the tested carbon inks tolerated mechanical stress the most. Following these, the combinations 7 and 11 were able to withstand thousands of cycles. The remaining combinations (1, 6, 8, 9, and 10) were the weakest, with the number of cycles ranging from a few hundred to as low as 30 cycles. While the original tests provided comparable and clear results between different combinations, the legitimacy of the results was further explored with a different setup. It was important to conduct tests with modified settings and see whether the same conclusions would be derived.

In the tensile strain tests, the carbon ink of combination 2 showed no degradation as observed in the previous tests. The other tested combinations (6, 7, and 11) showed higher tolerance compared to the original setup. Figure 6.7 illustrates this effect while Figure 6.8 and Figure 6.9 compare these three combinations in both compressive and tensile bending based on measured data and Weibull parameters presented in Table 6.4.

Table 6.4. *Weibull parameters with their 95% confidence interval, in compressive and tensile stress. Compressive of combination 11 includes only samples from group B.*

Combination	α	**CI (α)**	β	**CI (β)**
6C	58.6	54.4 – 63.1	5.8	4.3 – 7.7
6T	83.9	73.4 – 96.0	3.2	2.4 – 4.2
7C	1,234	1,067 – 1,426	2.9	2.2 – 3.9
7T	3,882	3,110 – 4,844	1.9	1.4 – 2.6
11C (only B)	28,095	22,840 – 34,560	3.0	1.9 – 4.7
11T	45,109	36,530 – 55,704	2.3	1.6 – 3.4

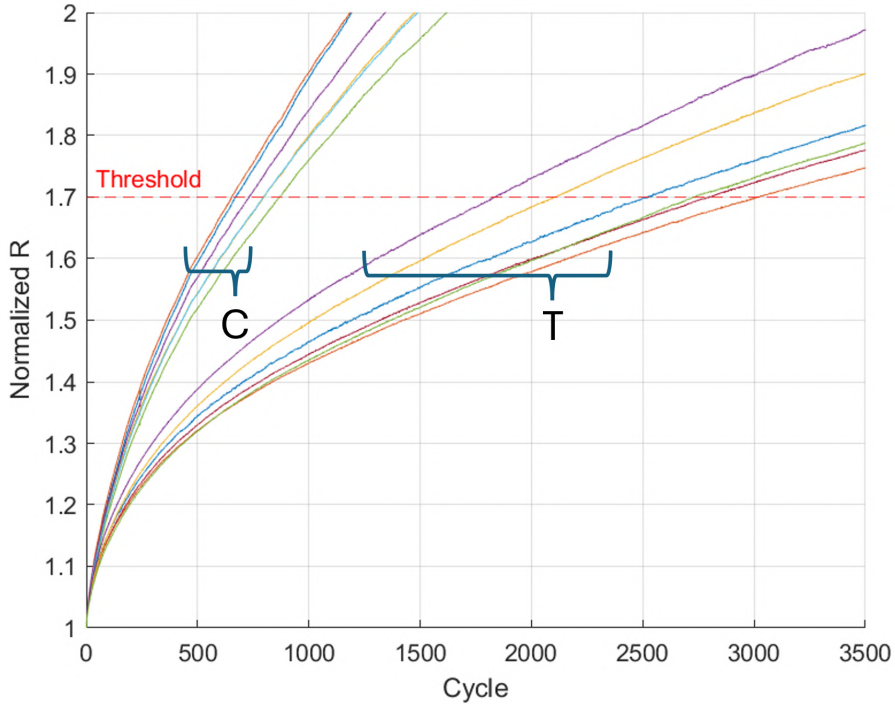

Figure 6.7. *Bending test of combination 7 in both compressive (C) and tensile (T) stress.*

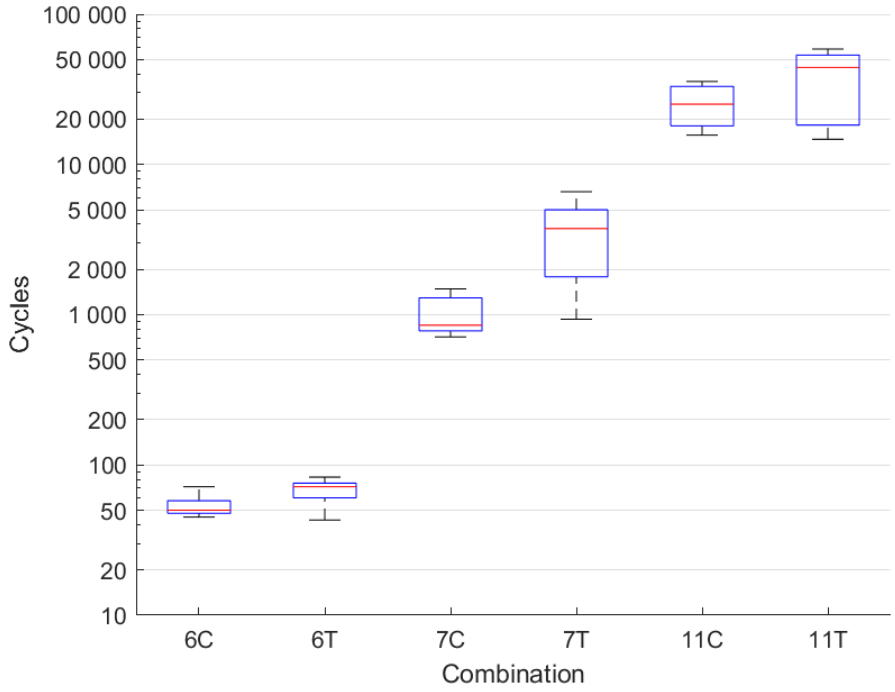

Figure 6.8. *Box chart of combinations 6, 7, and 11 in both compressive (C) and tensile (T) stress. Combination 11 includes only samples from group B.*

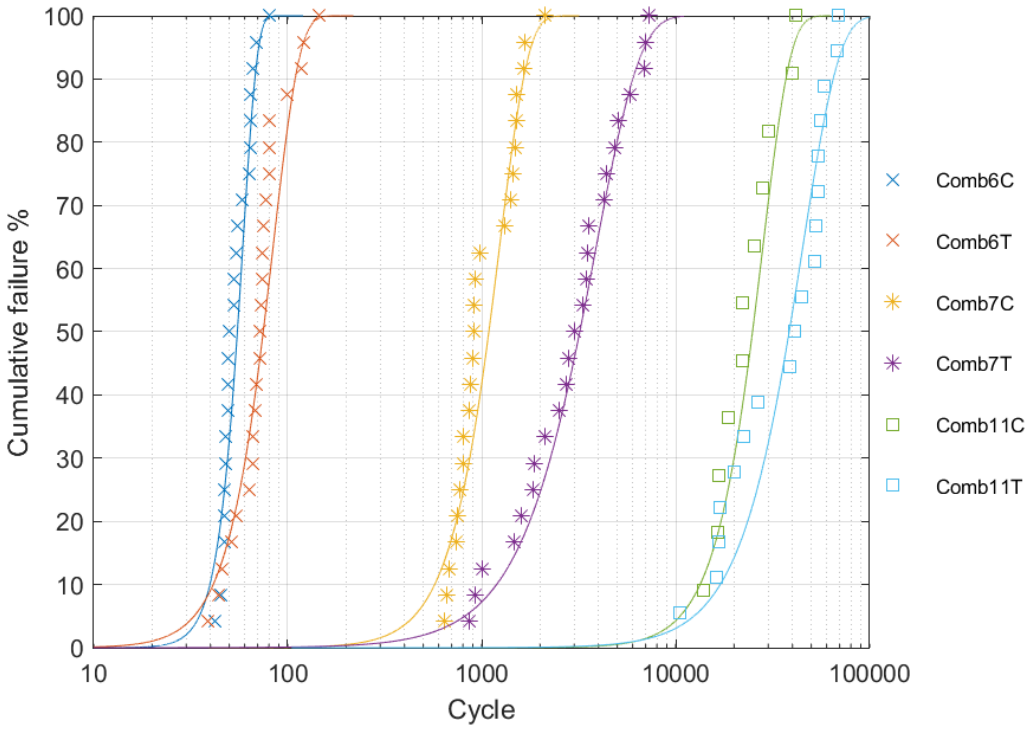

Figure 6.9. *Cumulative failure and fitted CDF of combinations 6, 7 and 11 in both compressive (C) and tensile (T) stress. Combination 11 includes only samples from group B.*

Based on the obtained result, it seems that the effect is similar across all these substrates: they are more durable under tensile stress, and the order of durability remains unchanged. While this observation appears to be correct, more combinations and a larger number of samples should be tested to confirm this finding. This is important, as some of the boxes and whiskers overlap each other, meaning that some samples could also behave as they were part of the other population. For instance, 11C and 11T in Figure 6.8 demonstrate notable overlapping, likely due to the measurement setup. For more durable samples, withstanding over 20,000 cycles, testing was not conducted until they fully reached the threshold, but rather stopped at a certain point, and the data were extrapolated as if the samples would continue to deteriorate at a similar rate. Although this approach saves time, it introduces additional uncertainty into the results.

Similar conclusions regarding the bending stress can be derived from Weibull's CDF. The samples tested in tensile bending failed later, with a greater number of cycles; hence, the fitted curves are shifted further to the right in Figure 6.9. As with the box chart, some data points could be interpreted as specimens from adjacent populations, and therefore, more tests should be conducted. Furthermore, lot-to-lot variation is noticeable in 7C, where data points shift suddenly, likely due to minor changes in the fabrication process.

The combinations (1, 6, 7, and 10), that were also tested with a larger bending radius, clearly demonstrates the expected result regarding the effect of radius on the stress and failure. Figures 6.11, 6.10 and 6.12 illustrate the effect of the bending radius, and Table 6.5 presents the Weibull parameters.

Table 6.5. *Weibull parameters with their 95% confidence interval. Combinations 1, 6, 7, and 10 with two different radius (r = 0.9 cm, R = 1.7 cm).*

Combination	α	**CI (α)**	β	**CI (β)**
1r	71.3	66.7 – 76.2	7.4	5.2 – 10.5
1R	540	488 – 596	4.3	3.2 – 5.6
6r	58.6	54.4 – 63.1	5.8	4.3 – 7.7
6R	304	274 – 337	4.1	2.9 – 5.6
7r	1,234	1,067 – 1,426	2.9	2.2 – 3.9
7R	34,942	29,278 – 41,701	2.4	1.8 – 3.2
10r	167	151 – 184	4.8	3.4 – 6.9
10R	930	834 – 1038	3.9	2.9 – 5.1

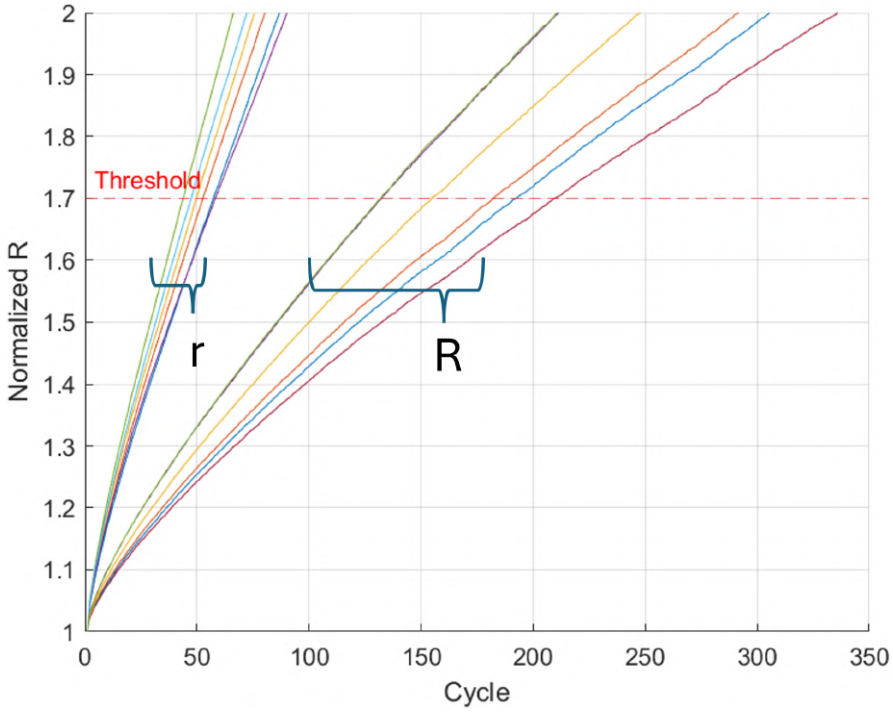

Figure 6.10. *Bending test of combination 6 with two different radius (r = 0.9 cm, R = 1.7 cm).*

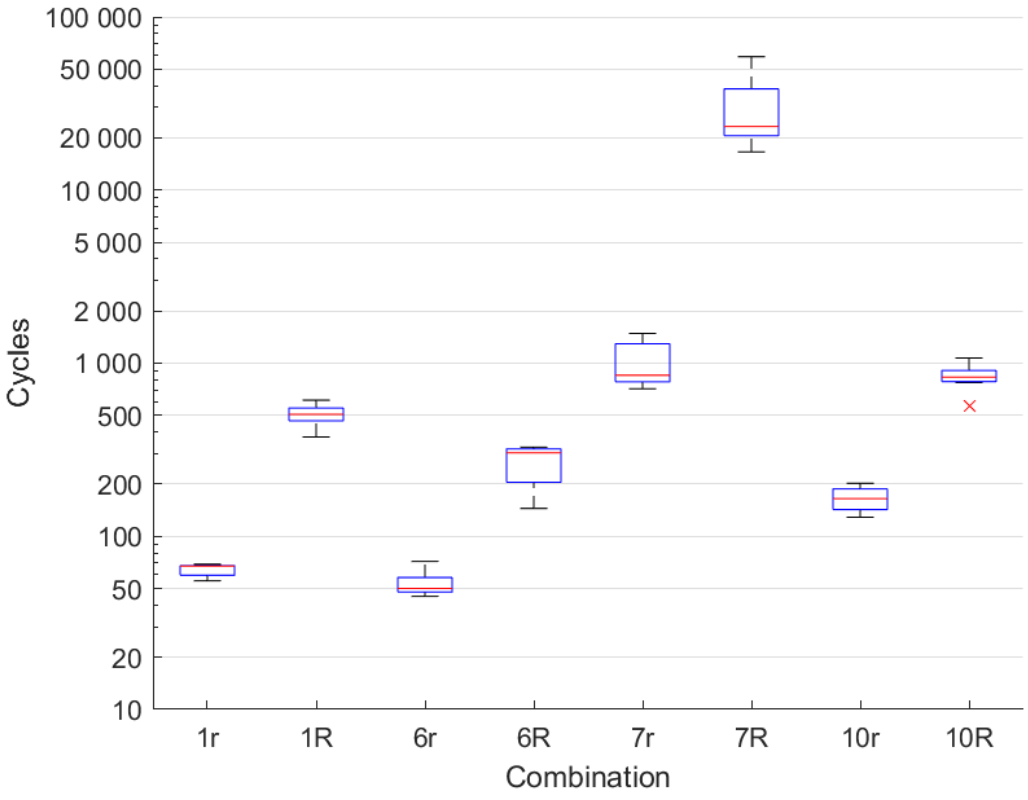

Figure 6.11. *Bending test of combinations 1, 6, 7, and 10 with two different radius (r = 0.9 cm, R = 1.7 cm).*

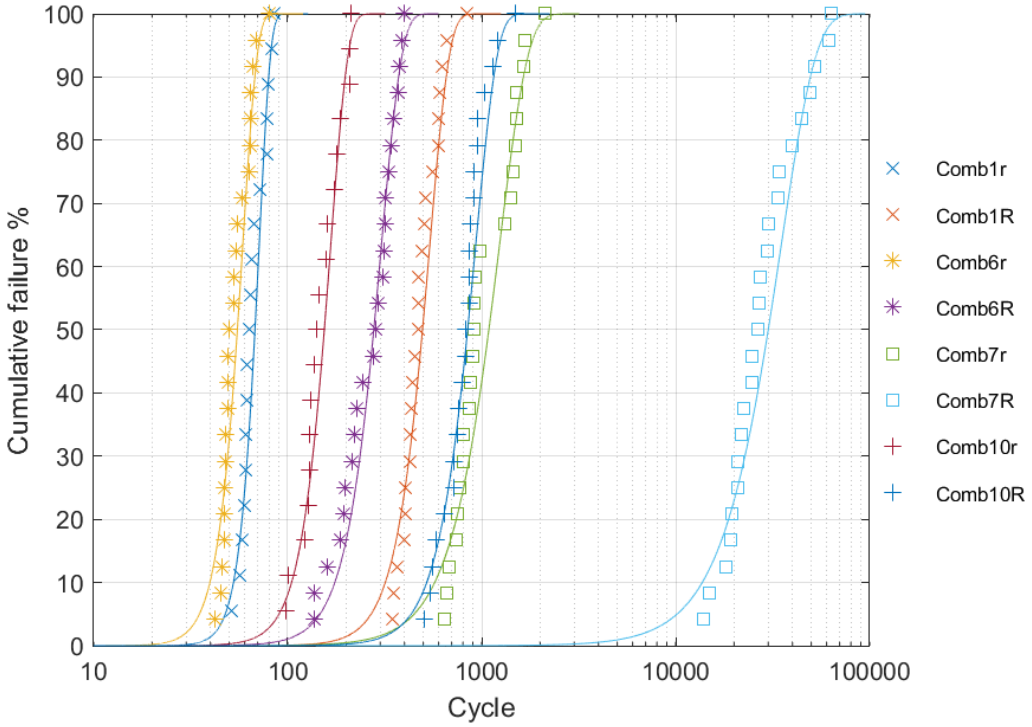

Figure 6.12. *Cumulative failure of the specimens and fitted CDF of combinations 1, 6, 7, and 10 with two different bending radius (r = 0.9 cm, R = 1.7 cm).*

As the bending radius was increased, the stress on the prints decreased allowing them to withstand a higher number of bending cycles. This effect is important to note, as in practical applications, the actual bend radius could be much larger. Therefore, some substrate-ink combinations may perform well in practice even if they were evaluated as weak in these tests. Yet again, when observing Figure 6.11 and Figure 6.12 they indicate that the order of the durability remains among these combinations. This once more reinforces the conclusion regarding how these combinations should be rated.

When switching to the other bending setup, as introduced in previous chapters, Mark-10 bending tests revealed initially a slight improvement by applying greater bending-induced stress than the horizontal plate device. This reflected into accelerated degradation of combination 6 samples, which exceeded the threshold within an average of 49 cycles–a reduction of approximately 10% in the cycle count required. However, this outcome was lower than anticipated, likely due to the cyclic stress being concentrated within a narrow region rather than over a larger area, as with the horizontal plates. This localized stress caused rapid deterioration in specific areas on the specimen, quickly reaching maximum degradation while the rest of the sample remained intact, leading to resistance stabilization. For instance, combination 7 exhibited rapid initial degradation, but additional cycles had almost no further impact on its resistance. Meanwhile, carbon inks demonstrated no signs of degradation, prompting the decision to discard this setup, as it failed to produce the desired differentiation for carbon ink combinations.

While all the results mentioned above utilize normalized resistance to compare proportional changes, it is important to acknowledge the practical applications where absolute resistance values play a significant roles. Whether it's a conductive track connecting different parts of a circuit or a sensor measuring strain and elongation, the resistance of the print must remain within a specific range, not exceeding a resistance value that would make the circuit non-functional. Different combinations are presented in Figure 6.13 as their absolute resistance in respect to the compressive bending cycle. A representative sample is selected for each combination, and a moving average is applied to reduce noise.

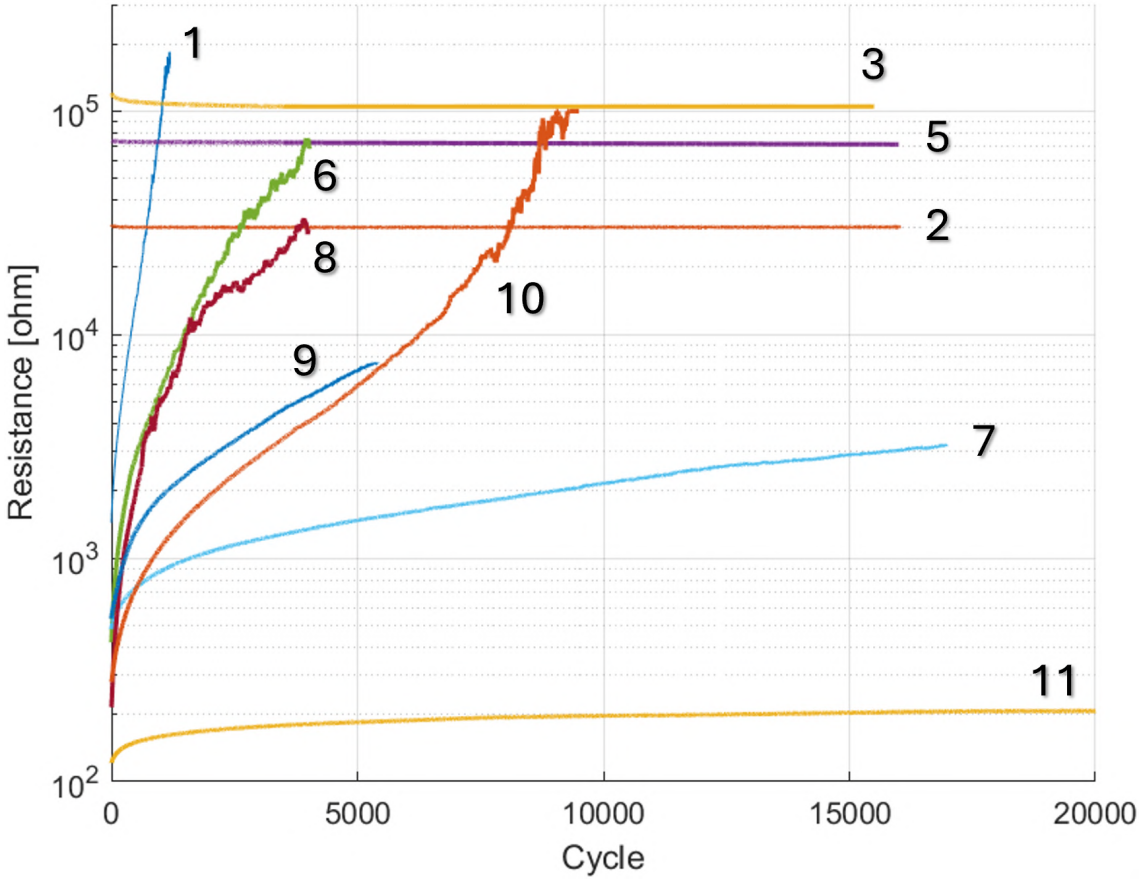

Figure 6.13. *The absolute resistance of the tracks as a function of bending cycles for each combination.*

Analysis based on absolute resistance does not provide as clear insights into material breakage as normalized resistance does, but it helps to identify how the materials would perform as part of a real electronic circuit. The graph suggests that, although carbon inks (combinations 2, 3, and 5) did not degrade under bending, their resistance remains substantially higher compared to most other combinations. For instance, the resistance of combination 11 seems to saturate, and thus it would never exceed the carbon inks resistance under these bending circumstances.

In order to understand why some combinations were more durable than others, a more

thorough analysis was performed. The thickness of the substrates and prints were measured and are presented in Table 6.6. Combinations are numbered as before, with the addition of number 12, which uses silver ink on a 125 µm PET substrate. This combination was included to further examine the effect of substrate thickness. The surface features of combinations 6, 7, and 8 were coarse and uneven as shown in Figure 6.14, hence the print thickness was not measurable using the DektakXT profilometer. Instead, it was obtained by a rough estimate based on the other combinations. Furthermore, the thickness are presented in Figure 6.15, where the shown substrate thicknesses are divided by two to represent the distance from the neutral axis when the substrate is bent.

Table 6.6. *Ink and substrate thickness of each combination, including their relative standard deviation. Thickness values are an average of 6–9 measurements.*

Combination	Print thickness [µm]	RSD [%]	Substrate thickness [µm]	RSD [%]
1	5.94	22.8	76.3	1.1
2	4.33	9.8	76.3	1.1
3	6.83	10.2	76.3	1.1
5	3.83	11.4	76.3	1.1
6	5.32	NA	95.7	7.6
7	5.32	NA	48.2	5.4
8	5.32	NA	129	5.2
9	5.70	7.6	45.8	2.1
10	4.26	15.5	89.0	5.1
11	6.38	14.4	42.9	2.4
12	5.94	22.8	126	0.7

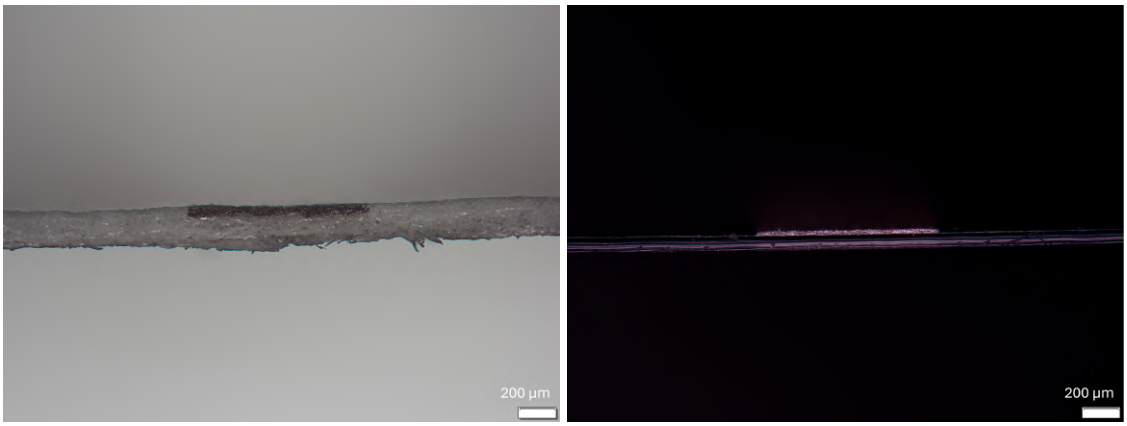

Figure 6.14. *Cross-sectional views of combinations 8 and 1, respectively. The ink in combination 8 partially penetrates into the rough substrate, while the smoother surface of combination 1 results in better print quality. Magnification: 5x.*

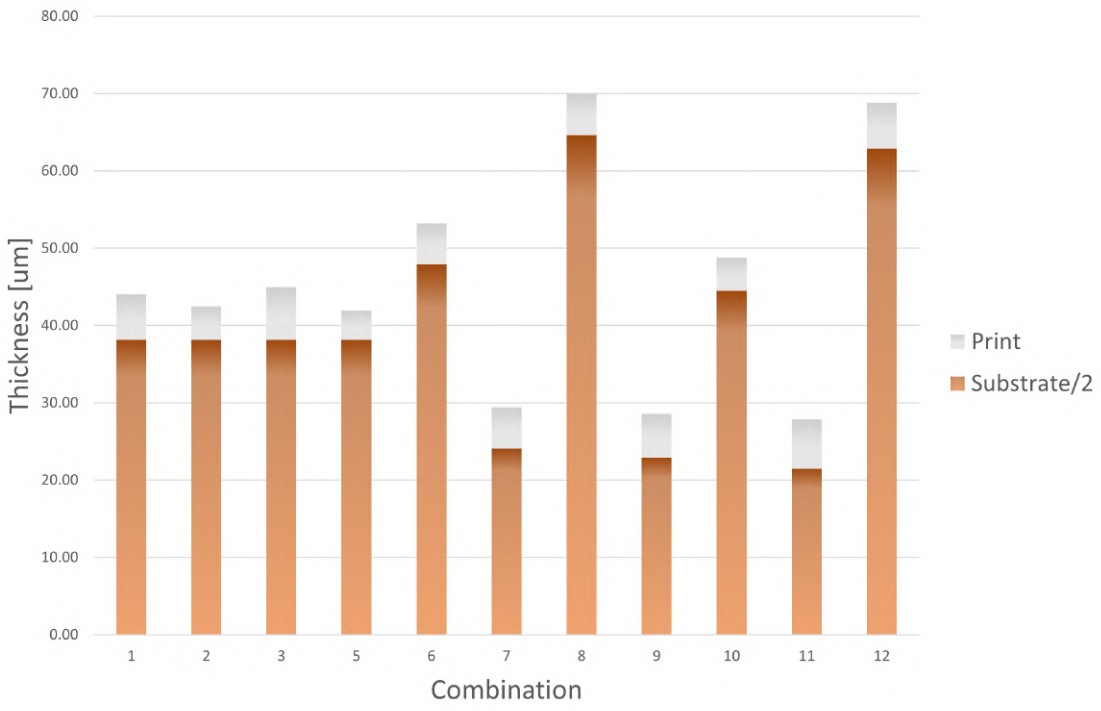

Figure 6.15. *Bar chart showing the print and substrate thicknesses for each combination. Here substrate thicknesses are half of their actual thickness as the neutral axis of bending is assumed going through middle of the substrate, corresponding to y=0.*

As depicted in the chart, the ink thickness exhibit relatively low variation compared to the substrates, suggesting that the greatest impact on the strain variation comes from the substrate used. The strain on the print was calculated using Equation 2.6, considering both substrate and ink thicknesses. However, this equation does not take into consideration material properties like the elastic modulus, making it less accurate than Equation 2.7. If the elastic modulus of the print were greater than that the substrate, the neutral axis would shift closer the top surface, reducing strain on the print, as explained in Chapter 2. Unfortunately, due to limited data, this effect could not be accounted for, and similar elasticity was assumed between substrate and print, resulting in a simplified model. However, it is important to note that the printed layer does not fully cover the substrate's surface, which may mitigate the effect of differing elastic moduli, aligning more closely with the simplified equation's results. The results for different bending radii, along with the roughness of the substrate, can be found in Table 6.7. The roughness values for the substrates, provided by the project partners, were used as given, and their legitimacy is assumed based on partner-provided data; the specific measurement methods are therefore not discussed further.

Table 6.7. *Strain on the top surface of the print for different bending radii, along with substrate roughness.*

Combination	Height [µm]	Strain-%			Substrate
		r = 17	r = 9	r = 3	roughness [µm]
1	44.06	0.259	0.490	1.469	2.27
2	42.45	0.250	0.472	1.415	2.27
3	44.95	0.264	0.499	1.498	2.27
5	41.96	0.247	0.466	1.399	2.27
6	53.19	0.313	0.591	1.773	2.53
7	29.40	0.173	0.327	0.980	2.47
8	69.97	0.412	0.777	2.332	3.05
9	28.58	0.168	0.318	0.953	NA
10	48.76	0.287	0.542	1.625	2.18
11	27.84	0.164	0.309	0.928	2.01
12	68.81	0.405	0.765	2.294	2.27

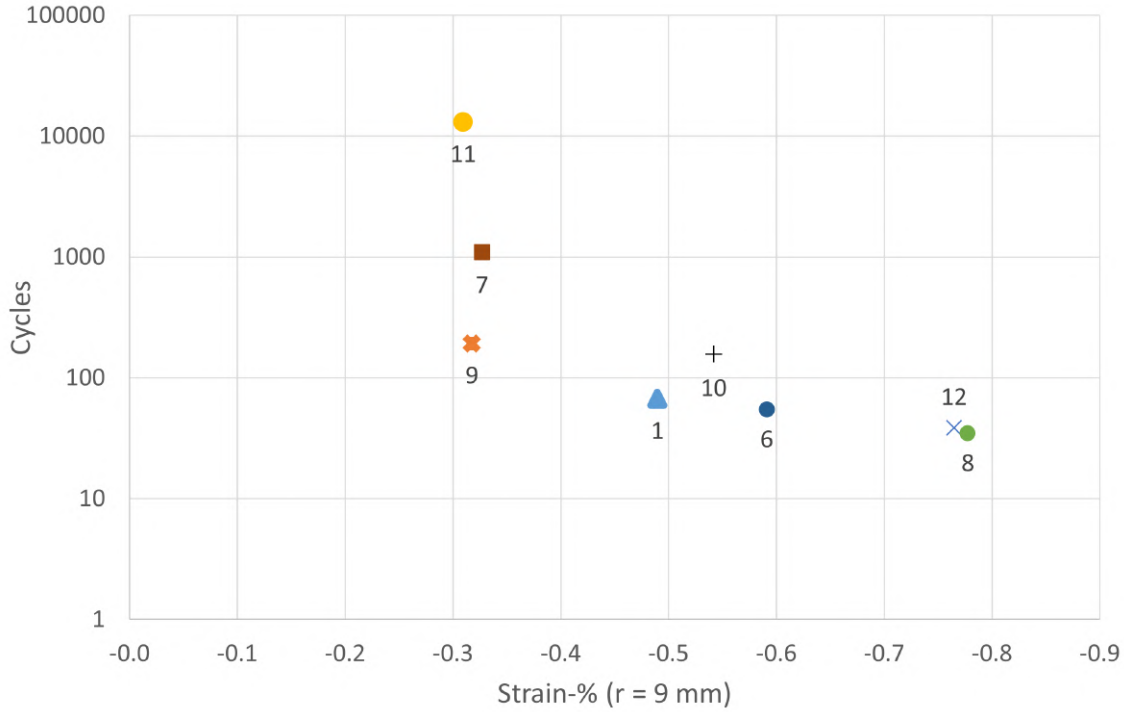

Figure 6.16. *Number of cycles as a function of strain-% for a bending radius of 9 mm.*

Figure 6.16 depicts the relation between the number of cycles and the strain on the print, with each data point representing an average for each respective combination. The samples were subjected to compressive strain, resulting in negative strain values. Happonen et al. investigated the cyclic bending reliability of screen-printed silver traces and reported

that the tracks' thickness significantly impacted their durability under repeated stress cycles [66]. While here the thickness – and strain derived from it – appears to correlate with the specimen's lifetime and durability, no definitive conclusions can be drawn solely based on thickness.

To further analyze the connection between material properties and electromechanical durability, the height and substrate roughness were multiplied to examine their combined influence. Materials with higher surface roughness were shown to fail earlier in three-point bending tests, as presented by Sneddon et al., who demonstrated a decrease in failure strain with increased average surface roughness (Ra) in a titanium alloy beams. [67] While this finding does not directly apply to cases involving two distinct materials, for instance, a substrate and an ink, it offers insight into potential outcomes with uneven surfaces. A rough substrate may create localized stress concentrations at the peaks and valleys, while the substrate thickness impacts the overall strain. Due to these effects, the product of height and roughness could serve as a measure of stress contributing to the failure of the print, as demonstrated in Figure 6.17.

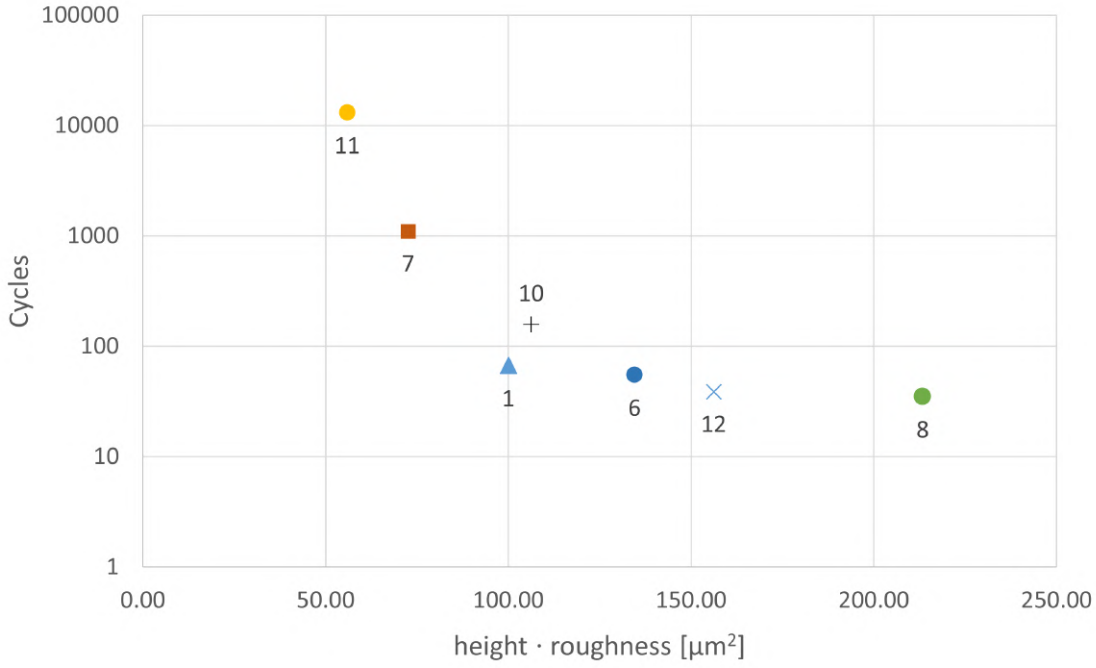

Figure 6.17. *Number of cycles as a function of the product between height and roughness.*

It can be interpreted that a thicker and rougher substrate is amplifying the stress concentrations, leading to earlier breakage. Conversely, a substrate such that used in combination 11, is both thin and relatively smooth, thus being able to withstand numerous bending cycles more effectively. This aligns with research conducted by Zhang et al., who studied the impact of surface roughness on the cracking of sprayed coating. In their film/substrate system, cracks propagated towards a valley's localized stress concentrations. [68]

After bending, the samples were examined under a microscope, and the cracks formed during cyclic bending were photographed, as in Figure 6.18 and Figure 6.19.

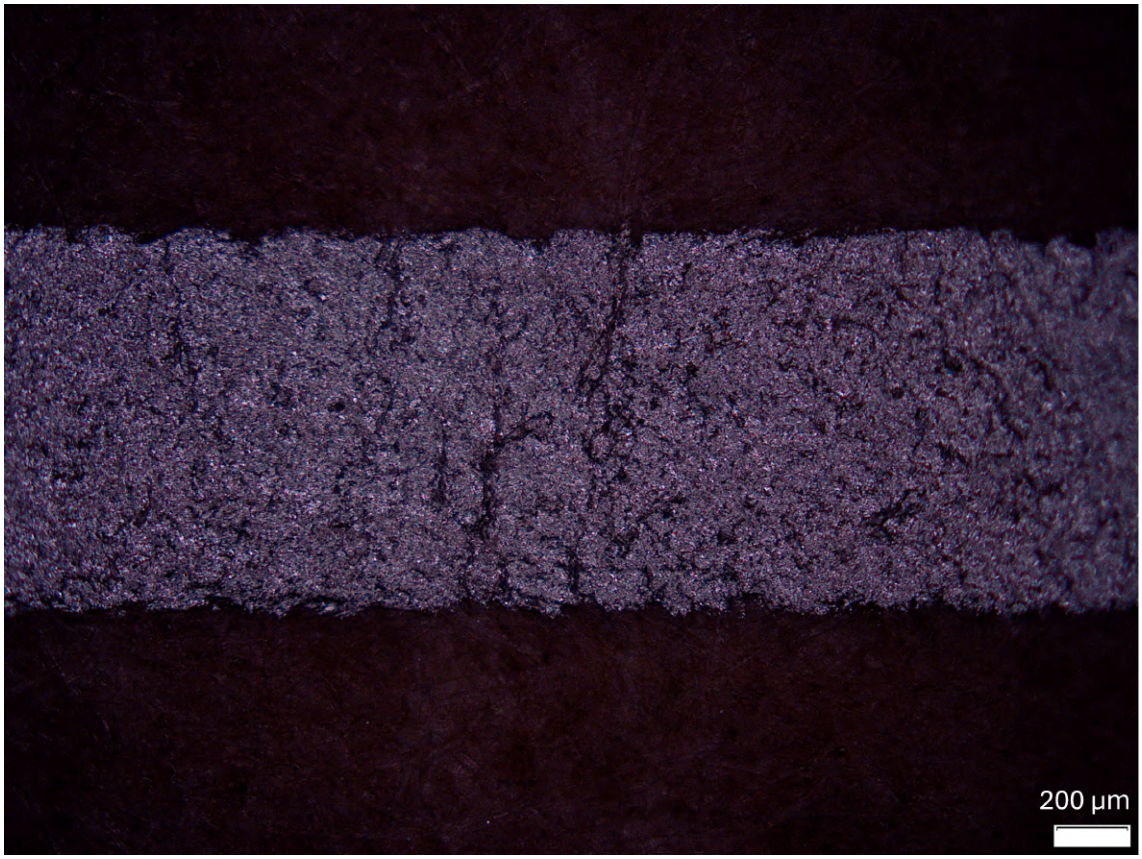

Figure 6.18. *Cracks induced by cyclic bending in combination 6. Magnification: 5x.*

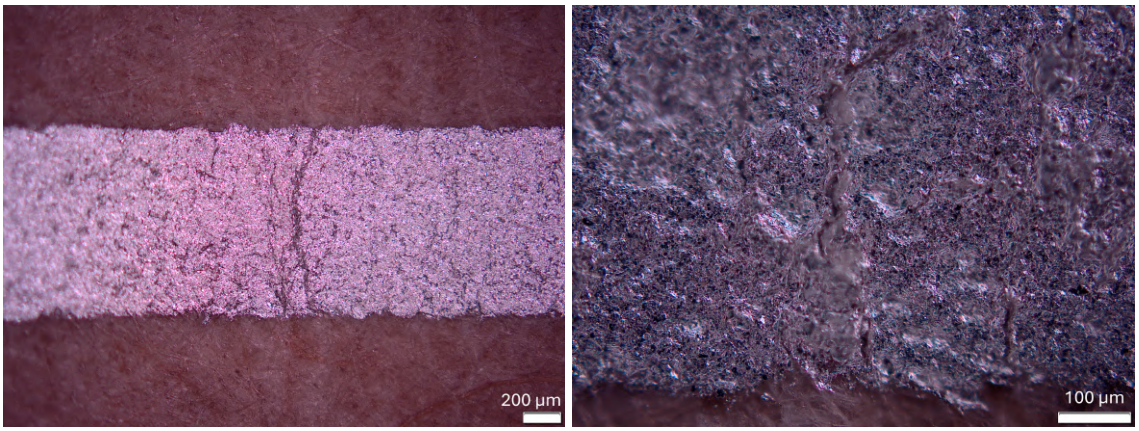

Figure 6.19. *A crack that has propagated through the entire track width. Magnification: 5x and 20x.*

Figure 6.18 shows several crack initiations disturbing the linear conductive path, leading to an increase in resistance. Figure 6.19 presents a fully propagated crack splitting the printed track into separate parts, resulting in a complete loss of conductivity.

7. CONCLUSION

The purpose of this thesis was to investigate the electromechanical behavior of printed tracks made with sustainable materials. The samples were fabricated using screen printing, and were tested under various bending conditions to evaluate their durability. The study focused on understanding how these sustainable materials perform under mechanical stress.

The work also involved designing and constructing a measurement setup compatible with two different bending devices. The setup consisted of a data acquisition device from National Instruments, a resistance measurement system across seven channels, and a program written in LabVIEW handling the measured data. An additional program was developed to control a Mark-10 device, which served as the second bending apparatus, while the first one was a pneumatic horizontal plate system.

All the materials were selected by the project partners of Sustronics, emphasizing availability, biodegradability, and overall ecological impact. In total, seven different substrate materials and four inks were tested. Table 7.1 summarizes the performance ratings of each combination, presenting the average number of bending cycles required for the resistance to increase by 1.7 times its initial value, thus addressing the first research question.

Table 7.1. *Combinations rated based on their durability under bending.*

	Combination	**Materials**	**Cycles**
Best	2, 3, 5	PET – Carbon inks	No degradation
	11	Cellulose film – Silver ink	13,084
	7	Paper smooth – Silver ink	1,098
	9	PP white 60 – Silver ink	193
	10	PLA – Silver ink	157
	1	PET – Silver ink	67
	6	E-insu paper – Silver ink	55
Worst	8	SPM – Silver ink	35

Analysis of different bending stresses revealed that all tested combinations (6, 7, and 11) endured significantly more cycles (38–212% more) under tensile strain than com-

pressive strain, thereby addressing the third research question. Additionally, tests with different bending radii highlighted the correlation between radius, strain experienced, and its impact on the number of cycles, which was found to be similar across all tested combinations. However, it is important to note that only a limited number of combinations were tested under both compressive versus tensile conditions, as well as with varying bending radii. This limits the strength of conclusions that can be drawn. Future studies could benefit conducting these tests to all combinations, especially regarding the former one, to see wether all samples would be more durable under tensile bending regardless of the selected materials. Previous studies have shown that specimens are more vulnerable in tensile bending-mode due to the pulling apart of conductive particles, which disrupts the conductive network more easily than compressive bending-mode, where particles are pushed together [69]. Chen et al. observed that their screen-printed silver conductors exhibited a larger relative resistance change per cycle under tensile stress compared to compressive stress [70]. These findings contradict those in the current thesis, suggesting the need for further exploration with additional material combinations.

Overall, based on the conducted tests, the combinations containing carbon inks were undoubtedly the most durable under bending. A study by Liao et al. demonstrated that their carbon-based conductive ink could withstand over 2,000 folding cycles, with the flexible circuit's resistance increasing by only 11%, indicating excellent mechanical stability due to the carbon nanotube network [71]. In this thesis, these carbon-based combinations exhibited the least increase in normalized resistance over bending cycles. However, this may not directly translate to real-life applications, as the absolute resistance of carbon inks remained significantly higher than most other combinations, even after several thousand bending cycles, as was observed with combinations 7, 9, 10, and 11.

In addition, the relation between material properties and observed durability under bending was investigated, providing insights relevant to the second research question. Due to limited material data, the strain experienced by the print was roughly estimated by assuming an identical Young's moduli for the print and the substrate. With more material data in the future, this estimate could be refined for greater accuracy. Nevertheless, the effects of material thickness and surface roughness on print durability were studied, and it was found that the product of these two values could serve as a measure of stress contributing to print failure. Substrate thickness influenced the overall strain, while surface roughness impacted stress concentration. Experimental data supported this conclusion: thin, smooth substrates led to durable substrate-ink combinations, whereas thick, rough surfaces caused the prints to fail prematurely.

While this thesis succeeded answering the research questions, and evaluating the impact of different substrate materials on the electromechanical durability, it was unable to draw distinct conclusions regarding the differences among the inks. All three tested carbon inks demonstrated superior electromechanical durability when considering the conducted

bending tests. Even when the carbon inks were subjected to the most extreme bending condition, using the Mark-10 device with a 3 mm bending radius, the tracks showed no signs of degradation. In order to achieve comparable differences between the carbon inks, a new bending setup would be needed, allowing a small radius to be applied over a larger sample area.

Moreover, it would be beneficial to observe the performance of these carbon inks on other substrates. Testing was initially limited to applying carbon inks on PET, and using silver ink on various other substrates to manage the number of combinations. With more time and resources, carbon inks should be deposited on these sustainable substrate materials to see if they yet again exhibit superior durability. Furthermore, this approach would better align with the final goal of the project, where the entire product is made of environmentally friendly materials.

Expanding from single-factor testing to more comprehensive hybrid testing could yield more realistic results, as devices are often subjected to several factors that collectively influence their lifespan. For instance, a wearable device attached to the human body might experience mechanical deformation across multiple axes while also enduring rubbing and exposure to moisture. While a test that accounts for all these factors simultaneously would be complex, it represents an intriguing approach for future studies.

REFERENCES

[1] Yue Zhao, Aeree Kim, Guanxiang Wan, and Benjamin C. K. Tee. “Design and applications of stretchable and self-healable conductors for soft electronics”. *Nano Convergence* 6.1 (Aug. 2019), p. 25. ISSN: 2196-5404. DOI: 10.1186/s40580-019-0195-0. URL: https://doi.org/10.1186/s40580-019-0195-0.

[2] Benjamin Iñiguez. “Flexible and Printed Electronics”. *More-than-Moore Devices and Integration for Semiconductors*. Ed. by Francesca Iacopi and Francis Balestra. Cham: Springer International Publishing, 2023, pp. 105–125. ISBN: 978-3-031-21610-7. DOI: 10.1007/978-3-031-21610-7_3. URL: https://doi.org/10.1007/978-3-031-21610-7_3.

[3] Mohammad N. Nassajfar, Ivan Deviatkin, Ville Leminen, and Mika Horttanainen. “Alternative Materials for Printed Circuit Board Production: An Environmental Perspective”. *Sustainability* 13.21 (2021). ISSN: 2071-1050. DOI: 10.3390/su132112126.

[4] M. Välimäki, P. Apilo, R. Po, E. Jansson, A. Bernardi, M. Ylikunnari, M. Vilkman, G. Corso, J. Puustinen, J. Tuominen, and J. Hast. “R2R-printed inverted OPV modules – towards arbitrary patterned designs”. en. *Nanoscale* 7.21 (May 2015). Publisher: The Royal Society of Chemistry, pp. 9570–9580. ISSN: 2040-3372. DOI: 10.1039/C5NR00204D. URL: https://pubs.rsc.org/en/content/articlelanding/2015/nr/c5nr00204d.

[5] *Sustronics*. en-US. URL: https://sustronics.eu/ (visited on 09/20/2024).

[6] André Canal Marques, José-María Cabrera, and Célia de Fraga Malfatti. “Printed circuit boards: A review on the perspective of sustainability”. *Journal of Environmental Management* 131 (Dec. 2013), pp. 298–306. ISSN: 0301-4797. DOI: 10.1016/j.jenvman.2013.10.003. URL: https://www.sciencedirect.com/science/article/pii/S030147971300649X.

[7] Martin H. Sadd. *Elasticity: theory, applications, and numerics*. eng. Third edition. Amsterdam: Elsevier, 2014. ISBN: 978-0-12-410432-7.

[8] *Understanding Young’s Modulus*. en-US. Nov. 2020. URL: https://efficientengineer.com/youngs-modulus/ (visited on 03/06/2024).

[9] Vadim Silberschmidt and Valery Matveenko. *Mechanics of Advanced Materials: Analysis of Properties and Performance*. Jan. 2015. ISBN: 978-3-319-17117-3. DOI: 10.1007/978-3-319-17118-0.

[10] K. E. Evans and A. Alderson. “Auxetic Materials: Functional Materials and Structures from Lateral Thinking”. *Advanced materials (Weinheim)* 12.9 (2000). Place:

Weinheim Publisher: WILEY-VCH Verlag GmbH, pp. 617–628. ISSN: 0935-9648. DOI: 10.1002/(SICI)1521-4095(200005)12:9<617::AID-ADMA617>3.0.CO;2-3.

[11] Tuomas Happonen. “Reliability studies on printed conductors on flexible substrates under cyclic bending”. eng. Accepted: 2023-05-12T05:21:35Z ISBN: 9789526212425. PhD. University of Oulu, May 2016. URL: https://oulurepo.oulu.fi/handle/10024/35884.

[12] Arthur P Boresi and Richard J Schmidt. *Advanced Mechanics of Materials*. 6th ed. John Wiley & Sons, 2003. ISBN: 978-0-471-43881-6.

[13] Y. Wyser, C. Pelletier, and J. Lange. “Predicting and determining the bending stiffness of thin films and laminates”. *Packaging technology & science* 14.3 (2001). Place: Chichester, UK Publisher: John Wiley & Sons, Ltd, pp. 97–108. ISSN: 0894-3214. DOI: 10.1002/pts.540.

[14] Z. Suo, E. Y. Ma, H. Gleskova, and S. Wagner. “Mechanics of rollable and foldable film-on-foil electronics”. *Applied physics letters* 74.8 (1999), pp. 1177–1179. ISSN: 0003-6951. DOI: 10.1063/1.123478.

[15] A. Goswami. *Thin film fundamentals*. 1st Edition. New Delhi, India: New Age International Publisher, 1996. ISBN: 81-224-0858-3.

[16] Liam Gillan, Jussi Hiltunen, Mohammad H. Behfar, and Kari Rönkä. “Advances in design and manufacture of stretchable electronics”. en. *Japanese Journal of Applied Physics* 61.SE (Apr. 2022). Publisher: IOP Publishing, SE0804. ISSN: 1347-4065. DOI: 10.35848/1347-4065/ac586f. URL: https://iopscience.iop.org/article/10.35848/1347-4065/ac586f/meta.

[17] Yvan Bonnassieux, Christoph J Brabec, Yong Cao, Tricia Breen Carmichael, Michael L Chabinyc, Kwang-Ting Cheng, Gyoujin Cho, Anjung Chung, Corie L Cobb, Andreas Distler, Hans-Joachim Egelhaaf, Gerd Grau, Xiaojun Guo, Ghazaleh Haghiashtiani, Tsung-Ching Huang, Muhammad M Hussain, Benjamin Iniguez, Taik-Min Lee, Ling Li, Yuguang Ma, Dongge Ma, Michael C McAlpine, Tse Nga Ng, Ronald Österbacka, Shrayesh N Patel, Junbiao Peng, Huisheng Peng, Jonathan Rivnay, Leilai Shao, Daniel Steingart, Robert A Street, Vivek Subramanian, Luisa Torsi, and Yunyun Wu. “The 2021 flexible and printed electronics roadmap”. *Flexible and Printed Electronics* 6.2 (May 2021). Publisher: IOP Publishing, p. 023001. ISSN: 2058-8585. DOI: 10.1088/2058-8585/abf986. URL: https://dx.doi.org/10.1088/2058-8585/abf986.

[18] Roberto Nisticò. “Polyethylene terephthalate (PET) in the packaging industry”. *Polymer Testing* 90 (Oct. 2020), p. 106707. ISSN: 0142-9418. DOI: 10.1016/j.polymertesting.2020.106707. URL: https://www.sciencedirect.com/science/article/pii/S0142941820310333.

[19] Muhammad Irsyad Suhaimi, Anis Nurashikin Nordin, Aliza Aini Md Ralib, Ioana Voiculescu, Wing Cheung Mak, Lim Lai Ming, and Zambri Samsudin. “Mechanical durability of screen-printed flexible silver traces for wearable devices”. *Sensing and*

Bio-Sensing Research 38 (2022). Publisher: Elsevier B.V, p. 100537. ISSN: 2214-1804. DOI: 10.1016/j.sbsr.2022.100537.

[20] Muhammad Usman Ali Khan, Raad Raad, Faisel Tubbal, Panagiotis Ioannis Theoharis, Sining Liu, and Javad Foroughi. “Bending analysis of polymer-based flexible antennas for wearable, general iot applications: A review”. *Polymers* 13.3 (2021). Place: Switzerland Publisher: MDPI, pp. 1–34. ISSN: 2073-4360. DOI: 10.3390/polym13030357.

[21] Takao Someya. *Stretchable Electronics*. 1. Aufl. Newark: Wiley-VCH, 2012. ISBN: 3-527-32978-1. DOI: 10.1002/9783527646982.

[22] Michael Szycher. *Szycher's Handbook of Polyurethanes*. 2nd edition. Milton: CRC Press, 2013. ISBN: 1-4398-3958-1. DOI: 10.1201/b12343.

[23] R.A. Auras, B. Harte, S. Selke, and R. Hernandez. “Mechanical, physical, and barrier properties of poly(lactide) films”. *Journal of Plastic Film and Sheeting* 19.2 (2003), pp. 123–135. DOI: 10.1177/8756087903039702.

[24] A. Géczy, A. Csiszár, E. Rozs, I. Hajdu, B. Medgyes, O. Krammer, D. Straubinger, and L. Gál. “Novel PLA/Flax Based Biodegradable Printed Circuit Boards”. *2022 45th International Spring Seminar on Electronics Technology (ISSE)*. May 2022, pp. 1–6. ISBN: 2161-2536. DOI: 10.1109/ISSE54558.2022.9812827.

[25] L. -T. Lim, R. Auras, and M. Rubino. “Processing technologies for poly(lactic acid)”. *Progress in Polymer Science* 33.8 (Aug. 2008), pp. 820–852. ISSN: 0079-6700. DOI: 10.1016/j.progpolymsci.2008.05.004. URL: https://www.sciencedirect.com/science/article/pii/S0079670008000373.

[26] Elina Jansson, Johanna Lyytikäinen, Panu Tanninen, Kim Eiroma, Ville Leminen, Kirsi Immonen, and Liisa Hakola. “Suitability of Paper-Based Substrates for Printed Electronics”. *Materials* 15.3 (2022). Place: Switzerland Publisher: MDPI AG, p. 957. ISSN: 1996-1944. DOI: 10.3390/ma15030957.

[27] Zhenan Bao and Xiaodong Chen. “Flexible and Stretchable Devices”. *Advanced materials (Weinheim)* 28.22 (2016). Place: Germany Publisher: Blackwell Publishing Ltd, pp. 4177–4179. ISSN: 0935-9648. DOI: 10.1002/adma.201601422.

[28] Samuli Tuominen. *Printed Temporary Transfer Tattoos for Skin-Mounted Electronics*. MSc thesis. Tampere University, 2018. URL: https://urn.fi/URN:NBN:fi:tty-201810032362.

[29] Zhao Fu. “Mechanical Reliability and Failure Mechanisms of Printed Flexible & Stretchable Electronics”. PhD. Tampere University, 2024. URL: https://urn.fi/URN:ISBN:978-952-03-3500-7.

[30] Novarials. *Silver Nanowires A70 (70nm×50µm)*. URL: https://www.novarials-store.com/products/silver-nanowires-70nm (visited on 07/22/2024).

[31] Wanli Li, Qingqing Sun, Lingying Li, Jinting Jiu, Xu-Ying Liu, Masayuki Kanehara, Takeo Minari, and Katsuaki Suganuma. “The rise of conductive copper inks: chal-

lenges and perspectives". *Applied materials today* 18 (2020). Publisher: Elsevier Ltd, p. 100451. ISSN: 2352-9407. DOI: 10.1016/j.apmt.2019.100451.

[32] Tuan Sang Tran, Naba Kumar Dutta, and Namita Roy Choudhury. "Graphene inks for printed flexible electronics: Graphene dispersions, ink formulations, printing techniques and applications". *Advances in colloid and interface science* 261 (2018). Place: Netherlands Publisher: Elsevier B.V, pp. 41–61. ISSN: 0001-8686. DOI: 10.1016/j.cis.2018.09.003.

[33] Kamna Chaturvedi, Vaishnavi Hada, Sriparna Paul, Bibek Sarma, Deeksha Malvi, Manish Dhangar, Harsh Bajpai, Anju Singhwane, Avanish Kumar Srivastava, and Sarika Verma. "The Rise of MXene: A Wonder 2D Material, from Its Synthesis and Properties to Its Versatile Applications—A Comprehensive Review". *Topics in Current Chemistry* 381.2 (Mar. 2023), p. 11. ISSN: 2364-8961. DOI: 10.1007/s41061-023-00420-1. URL: https://doi.org/10.1007/s41061-023-00420-1.

[34] Wenting Dang, Vincenzo Vinciguerra, Leandro Lorenzelli, and Ravinder Dahiya. "Printable stretchable interconnects". *Flexible and Printed Electronics* 2.1 (Mar. 2017). Publisher: IOP Publishing, p. 013003. ISSN: 2058-8585. DOI: 10.1088/2058-8585/aa5ab2. URL: https://dx.doi.org/10.1088/2058-8585/aa5ab2.

[35] Milton Ohring. "Chapter 4 - The Mathematics of Failure and Reliability". *Reliability and Failure of Electronic Materials and Devices*. Ed. by Milton Ohring. San Diego: Academic Press, Jan. 1998, pp. 175–236. ISBN: 978-0-12-524985-0. DOI: 10.1016/B978-012524985-0/50005-2. URL: https://www.sciencedirect.com/science/article/pii/B9780125249850500052.

[36] F Ellyin. *Fatigue Damage, Crack Growth and Life Prediction*. 1st ed. Dordrecht: Springer Netherlands, 1996. ISBN: 0-412-59600-8. DOI: 10.1007/978-94-009-1509-1.

[37] J A Collins. *Failure of Materials in Mechanical Design: Analysis, Prediction, Prevention. Second Edition*. Pages: 6546 x 9 in. 1993. ISBN: 0-471-55891-5.

[38] Zhehui Zhao, Haoran Fu, Ruitao Tang, Bocheng Zhang, Yunmin Chen, and Jianqun Jiang. "Failure mechanisms in flexible electronics". *International journal of smart and nano materials* 14.4 (2023). Place: Abingdon Publisher: Taylor & Francis Ltd, pp. 510–565. ISSN: 1947-5411. DOI: 10.1080/19475411.2023.2261775.

[39] Longchao Dai, Yin Huang, Hang Chen, Xue Feng, and Daining Fang. "Transition among failure modes of the bending system with a stiff film on a soft substrate". *Applied physics letters* 106.2 (2015). Place: Melville Publisher: American Institute of Physics. ISSN: 0003-6951. DOI: 10.1063/1.4905697.

[40] Sari Merilampi, Toni Björninen, Veikko Haukka, Pekka Ruuskanen, Leena Ukkonen, and Lauri Sydänheimo. "Analysis of electrically conductive silver ink on stretchable substrates under tensile load". *Microelectronics and reliability* 50.12 (2010). Place: Kidlington Publisher: Elsevier Ltd, pp. 2001–2011. ISSN: 0026-2714. DOI: 10.1016/j.microrel.2010.06.011.

[41] *Flexible Electronics Market Size, Share, Growth Report, 2030*. en. Tech. rep. 978-1-68038-838-1. Grand View Research, Sept. 2023, p. 120. URL: https://www.grandviewresearch.com/industry-analysis/flexible-electronics-market.

[42] Katsuaki Suganuma. “Printing Technology”. *Introduction to Printed Electronics*. Ed. by Katsuaki Suganuma. New York, NY: Springer New York, 2014, pp. 23–48. ISBN: 978-1-4614-9625-0. DOI: 10.1007/978-1-4614-9625-0_2. URL: https://doi.org/10.1007/978-1-4614-9625-0_2.

[43] Wei Wu. *Printed Electronics Technologies*. The Royal Society of Chemistry, July 2022. ISBN: 978-1-78801-415-1. DOI: 10.1039/9781788019699. URL: https://doi.org/10.1039/9781788019699.

[44] Lixin Mo, Zhenxin Guo, Li Yang, Qingqing Zhang, Yi Fang, Zhiqing Xin, Zheng Chen, Kun Hu, Lu Han, and Luhai Li. “Silver Nanoparticles Based Ink with Moderate Sintering in Flexible and Printed Electronics”. *International Journal of Molecular Sciences* 20.9 (2019). ISSN: 1422-0067. DOI: 10.3390/ijms20092124.

[45] J. Chang, T. Ge, and E. Sanchez-Sinencio. “Challenges of printed electronics on flexible substrates”. *2012 IEEE 55th International Midwest Symposium on Circuits and Systems (MWSCAS)*. Aug. 2012, pp. 582–585. ISBN: 1558-3899. DOI: 10.1109/MWSCAS.2012.6292087.

[46] Tessy Theres Baby, Gabriel Cadilha Marques, Felix Neuper, Surya Abhishek Singaraju, Suresh Garlapati, Falk von Seggern, Robert Kruk, Subho Dasgupta, Benedikt Sykora, Ben Breitung, Parvathy Anitha Sukkurji, Uwe Bog, Ravi Kumar, Harald Fuchs, Timo Reinheimer, Morten Mikolajek, Joachim R. Binder, Michael Hirtz, Martin Ungerer, Liane Koker, Ulrich Gengenbach, Nilesha Mishra, Patric Gruber, Mehdi Tahoori, Jasmin Aghassi Hagmann, Heinz von Seggern, and Horst Hahn. “Printing Technologies for Integration of Electronic Devices and Sensors”. *Functional Nanostructures and Sensors for CBRN Defence and Environmental Safety and Security*. Ed. by Anatolie Sidorenko and Horst Hahn. Dordrecht: Springer Netherlands, 2020, pp. 1–34. ISBN: 978-94-024-1909-2.

[47] Wenxiu Gao, Yi Zhu, Yaojin Wang, Guoliang Yuan, and Jun-Ming Liu. “A review of flexible perovskite oxide ferroelectric films and their application”. *Journal of Materiomics* 6 (Nov. 2019). DOI: 10.1016/j.jmat.2019.11.001.

[48] *Electricity consumption – Electricity Information: Overview – Analysis*. en-GB. URL: https://www.iea.org/reports/electricity-information-overview/electricity-consumption (visited on 08/13/2024).

[49] *Global electricity consumption in lighting in the Net Zero Scenario, 2010-2030 – Charts – Data & Statistics*. en-GB. URL: https://www.iea.org/data-and-statistics/charts/global-electricity-consumption-in-lighting-in-the-net-zero-scenario-2010-2030 (visited on 08/13/2024).

[50] *Photovoltaic Energy Factsheet*. en. URL: https://css.umich.edu/publications/factsheets/energy/photovoltaic-energy-factsheet (visited on 08/14/2024).

[51] Zheng Cui and Chunshan Zhou. *Printed electronics : materials, technologies and applications*. 1st ed. Singapore: Wiley, 2016. ISBN: 1-118-92095-3.

[52] Jenny Wiklund, Alp Karakoç, Toni Palko, Hüseyin Yiğitler, Kalle Ruttik, Riku Jäntti, and Jouni Paltakari. “A Review on Printed Electronics: Fabrication Methods, Inks, Substrates, Applications and Environmental Impacts”. *Journal of Manufacturing and Materials Processing* 5.3 (2021). ISSN: 2504-4494. DOI: 10.3390/jmmp5030089.

[53] Elahe Jabari, Farzad Liravi, and Ehsan Toyserkani. “2D printing of graphene: a review”. *2D Materials* (Aug. 2019). DOI: 10.1088/2053-1583/ab29b2/meta.

[54] Josh King-Farlow. *Print process diagrams*. en. URL: https://www.king-farlow.com/print-process-diagrams/ (visited on 08/23/2024).

[55] Frederik C. Krebs. “Fabrication and processing of polymer solar cells: A review of printing and coating techniques”. *Processing and Preparation of Polymer and Organic Solar Cells* 93.4 (Apr. 2009), pp. 394–412. ISSN: 0927-0248. DOI: 10.1016/j.solmat.2008.10.004. URL: https://www.sciencedirect.com/science/article/pii/S0927024808003486.

[56] Nittoku. *Screen Printing Mesh Business|Screen Specifications*. URL: https://www.nt-jp.com/en/products/screen/screen-spec.php (visited on 11/07/2024).

[57] Thomas Öhlund. “Metal Films for Printed Electronics : Ink-substrate Interactions and Sintering”. PhD. Mid Sweden University, Dec. 2014.

[58] Ekra. *SERIO X5 Professional Fully-Automatic*. URL: https://www.scanditron.com/equipment/ekra-x5-professional-stencil-printer/ (visited on 06/24/2024).

[59] E. Halonen, A. Halme, T. Karinsalo, P. Iso-Ketola, M. Mäntysalo, and R. Mäkinen. “Dynamic bending test analysis of inkjet-printed conductors on flexible substrates”. *2012 IEEE 62nd Electronic Components and Technology Conference*. June 2012, pp. 80–85. ISBN: 2377-5726. DOI: 10.1109/ECTC.2012.6248810.

[60] National instruments. *USB-6003*. URL: https://www.ni.com/fi-fi/shop/model/usb-6003.html?srsltid=AfmBOoqKuJAxzbx-zCIE5kI9ERNHEJgi8IvcGTyzXjBhJKLWJCfftWD8 (visited on 10/15/2024).

[61] Keysight. *How to Measure Resistance Using Four-Wire Measurement*. en. URL: https://www.keysight.com/us/en/solutions/measure-resistance-using-four-wire-measurement.html (visited on 10/16/2024).

[62] Heinz. Schmidt-Walter and Ralf. Kories. *Electrical engineering : a pocket reference*. 1st ed. Boston: Artech House, 2007. ISBN: 1-59693-245-7.

[63] Mark-10. *Models ESM303 & ESM303H FORCE TEST FRAMES, User’s guide*. URL: https://mark-10.com/downloads/product-downloads/manualESM303.pdf (visited on 06/27/2024).

[64] Zhao Fu, Aarne Jauho, Kaisa-Leena Väisänen, Marja Välimäki, Jari Keskinen, and Matti Mäntysalo. “Assessment of a Cyclic Bending Test Method for Printed Flexible Supercapacitor”. (2022). Publisher: IEEE.

[65] Bruker Nano Surfaces Division. *DektakXT*. URL: https://mmrc.caltech.edu/DektakXT/Manuals/DektakXT%20specifications.pdf (visited on 06/25/2024).

[66] T. Happonen, J. -V. Voutilainen, J. Häkkinen, and T. Fabritius. "The Effect of Width and Thickness on Cyclic Bending Reliability of Screen-Printed Silver Traces on a Plastic Substrate". *IEEE Transactions on Components, Packaging and Manufacturing Technology* 6.5 (May 2016), pp. 722–728. ISSN: 2156-3985. DOI: 10.1109/TCPMT.2016.2544441.

[67] Scott Sneddon, Yang Xu, Mark Dixon, David Rugg, Peifeng Li, and Daniel M. Mulvihill. "Sensitivity of material failure to surface roughness: A study on titanium alloys Ti64 and Ti407". *Materials & Design* 200 (Feb. 2021), p. 109438. ISSN: 0264-1275. DOI: 10.1016/j.matdes.2020.109438. URL: https://www.sciencedirect.com/science/article/pii/S0264127520309746.

[68] W.X. Zhang, X.L. Fan, and T.J. Wang. "The surface cracking behavior in air plasma sprayed thermal barrier coating system incorporating interface roughness effect". *Applied Surface Science* 258.2 (Nov. 2011), pp. 811–817. ISSN: 0169-4332. DOI: 10.1016/j.apsusc.2011.08.103. URL: https://www.sciencedirect.com/science/article/pii/S0169433211013511.

[69] Tuomas Happonen, Tapio Ritvonen, Pentti Korhonen, Juha Häkkinen, and Tapio Fabritius. "Bending reliability of printed conductors deposited on plastic foil with various silver pastes". *The International Journal of Advanced Manufacturing Technology* 82.9 (Feb. 2016), pp. 1663–1673. ISSN: 1433-3015. DOI: 10.1007/s00170-015-7403-9. URL: https://doi.org/10.1007/s00170-015-7403-9.

[70] R. Chen, J. H. Chow, Y. Zhou, J. S. Meth, and S. K. Sitaraman. "Cyclic Bending Effects on Resistance of Screen-Printed Silver Conductors". *IEEE Transactions on Components, Packaging and Manufacturing Technology* 11.11 (Nov. 2021), pp. 1877–1888. ISSN: 2156-3985. DOI: 10.1109/TCPMT.2021.3108491.

[71] Yu Liao, Rui Zhang, Hongxia Wang, Shuangli Ye, Yihua Zhou, Taolin Ma, Junqing Zhu, Lisa D Pfefferle, and Jun Qian. "Highly conductive carbon-based aqueous inks toward electroluminescent devices, printed capacitive sensors and flexible wearable electronics". *RSC advances* 9.27 (2019). Place: England Publisher: The Royal Society of Chemistry, pp. 15184–15189. ISSN: 2046-2069. DOI: 10.1039/c9ra01721f.

APPENDIX A: FULL LABVIEW PROGRAM USED IN HORIZONTAL PLATE BENDING.

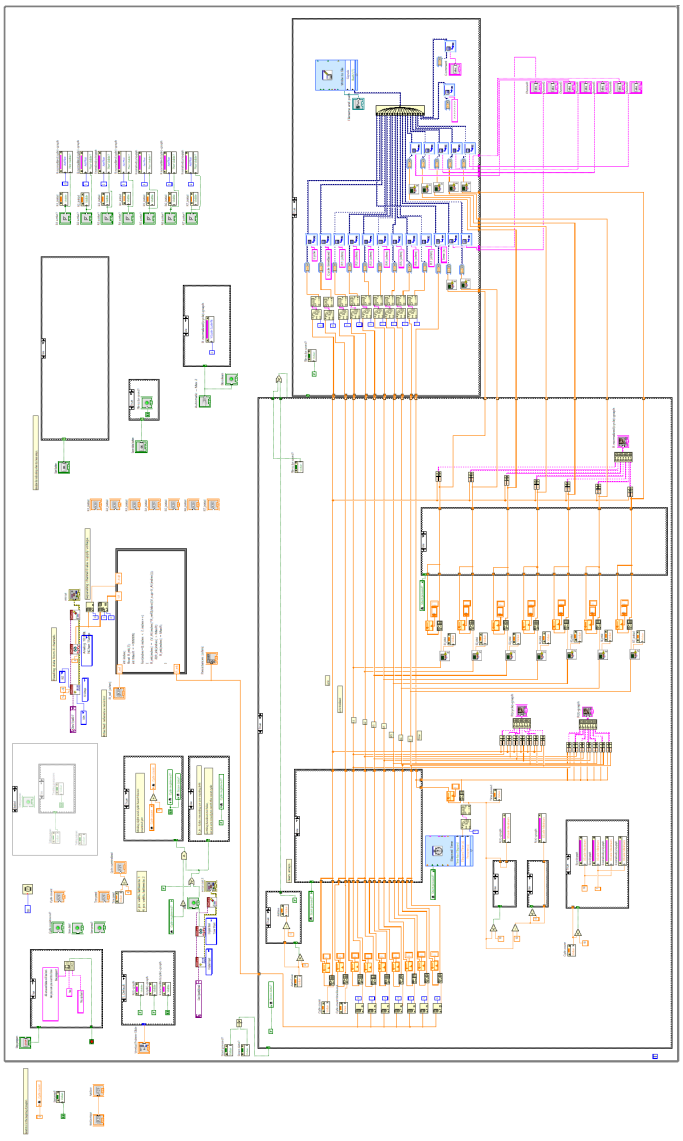

Figure A.1. *LabVIEW program used with NI-device to measure resistance values of the tracks and to save data.*

APPENDIX B: PROGRAM FOR MARK-10

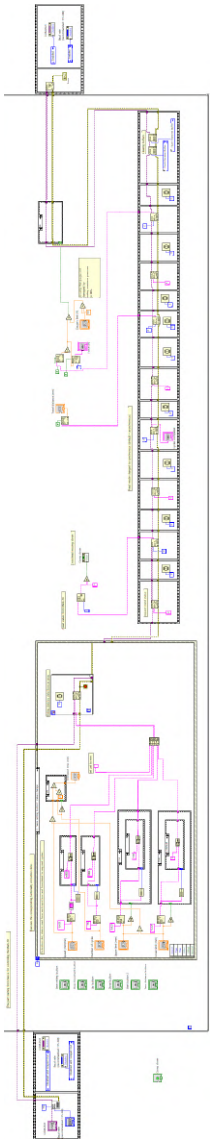

Figure B.1. *LabVIEW program used for controlling Mark-10. This was used along the previous program during bending tests with Mark-10.*

APPENDIX C: LABVIEW FRONT PANEL

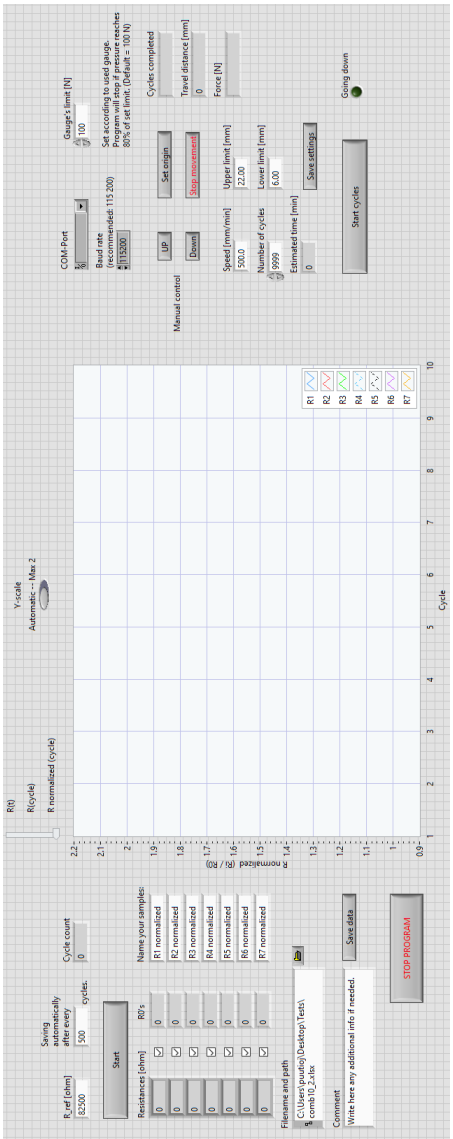

Figure C.1. *Front panel of the LabVIEW program working as a user interface during testing.*